

**APPLICATION OF RADARSAT-2 POLARIMETRIC DATA FOR LAND USE
AND LAND COVER CLASSIFICATION AND CROP MONITORING IN
SOUTHWESTERN ONTARIO**

(Spine title: Mapping and Agricultural Application Using RADARSAT-2 Data)

(Thesis format: Integrated Article)

by

«Qin Ma»

Graduate Program in Geography

A thesis submitted in partial fulfillment
of the requirements for the degree of
Master of Science

The School of Graduate and Postdoctoral Studies
The University of Western Ontario
London, Ontario, Canada

© Qin Ma 2013

THE UNIVERSITY OF WESTERN ONTARIO
School of Graduate and Postdoctoral Studies

CERTIFICATE OF EXAMINATION

Supervisor

Examiners

Dr. Jinfei Wang

Dr. Phil Stooke

Supervisory Committee

Dr. Micha Pazner

Dr. William Church

The thesis by

Ma Qin

entitled:

**Application of RADARSAT-2 Polarimetric Data for Land Use and
Land Cover Classification and Crop monitoring in Southwestern
Ontario**

is accepted in partial fulfillment of the
requirements for the degree of
Master of Science

Date

Chair of the Thesis Examination Board

Abstract

Timely and accurate information of land surfaces is desirable for land change detection and crop condition monitoring. Optical data have been widely used in Land Use and Land Cover (LU/LC) mapping and crop condition monitoring. However, due to unfavorable weather conditions, optical images of high quality are not always available. Synthetic Aperture Radar (SAR) sensors, such as RADARSAT-2, are able to transmit microwaves through cloud cover and light rain, and thus offer an alternative data source.

Chapter 2 investigates the potential of multi-temporal Quadpol RADARSAT-2 data for LU/LC classification in the urban rural fringe areas of London, Ontario. Nine LU/LC classes were identified at the highest overall accuracy of 91.0%.

Chapter 3 explores the sensitivity of polarimetric RADARSAT-2 parameters to crop growing conditions. Strong correlations are found between the polarimetric parameters and Normalized Difference Vegetation Index (NDVI) of corn and soybeans. In addition, some polarimetric parameters proved to be sensitive to crop height.

Keywords

Remote Sensing, Land Use and Land Cover Classification, Crop, Multi-temporal, Polarimetric RADARSAT-2, Normalized Difference Vegetation Index

Acknowledgments

First, I would like to thank my supervisor, Dr. Jinfei Wang. She helped me from the very beginning with developing the research topic, looking for the data and software for the project, planning and conducting the field work to the final thesis writing. I benefit a lot from the useful teaching in Remote Sensing courses, her thoughtful advice and constructive criticism in study, and great encouragement and tender care in life. Her passion in research and education, as well as her humble and nice template to people inspired me to be a better researcher.

Second, thank Dr. Jiali Shang from the Agriculture and Agri-food Canada for her support of providing the RapidEye images and RADARSAT-2 data for this research. Without her suggestions of research design and valuable comments about paper writing, my research would not be completed.

I would also like to thank all the people in our lab, Chuiqing Zeng, Ting Zhao, Nicholas Lantz, Autumn Gambles, and Francisco Flores de Santiago for supporting and encouraging me in the two years' study and research. The visitor professor Wen Dou from Southeastern University, China gave me helpful suggestions and encouragement when I encounter some problems in my research. It was those inspiring and intelligent chatting with him and his family that helped me get through the hard time. Also, thank Dr. Peng Wang from Chinese Academy of Sciences, who is my primary teacher of microwave. Peng Wang taught me a lot about basic knowledge of microwave and SAR data processing. In addition, thank Kathy Tang for driving us out to the fields in the hot summer of 2012.

Finally, I would like to thank my family and boyfriend for their support and encouragement throughout my study in the foreign country. Their endless cares about my study and life from home country bring me with great warmth and hope, which makes me feel no more lonely or afraid. I am very grateful to have such wonderful people in my life. Without your love I would not accomplish what I have.

Table of Contents

CERTIFICATE OF EXAMINATION	ii
Abstract	ii
Acknowledgments	iii
Table of Contents	iv
List of Tables	viii
List of Figures	x
Chapter 1	1
1 Introduction	1
1.1 Research Content	1
1.2 Research Objectives	4
1.3 Study Area and Study Data	5
1.4 Thesis Format	9
1.5 References	10
Chapter 2	15
2 Assessment of Multi-temporal Polarimetric RADARSAT-2 data for Land Use and Land Cover classification in an Urban/Rural Fringe Area	15
2.1 Introduction	15
2.1.1 Background	15
2.1.2 Previous Studies	16
2.1.3 Objectives	18
2.2 Study Area and Data Description	18
2.2.1 Study Area	18
2.2.2 The Optical Data	19
2.2.3 Field Data Collection	20

2.3	Methodology	21
2.3.1	RADARSAT-2 Data Pre-processing	21
2.3.2	Classification Scheme and Training Samples	29
2.3.3	RADARSAT-2 Data Classification	30
2.3.4	Post- classification Processing	32
2.3.5	Classification Accuracy Assessment	33
2.4	Results Analysis and Discussions	35
2.4.1	Training Data Analysis	38
2.4.2	Classification Results Using Gaussian and Wishart	41
2.4.3	Classification Results Using Different Polarimetric SAR Parameters	41
2.4.4	Classification Results Using Different Time Combinations	43
2.4.5	Classification Results Using Different Post-classification Processing Methods.....	47
2.5	Conclusions	48
2.6	Reference	51
Chapter 3.....		56
3	Sensitivity of RADARSAT-2 Polarimetric SAR Data to Normalized Difference Vegetation Index and Crops Height.....	56
3.1	Introduction.....	56
3.1.1	Background	56
3.1.2	Previous Studies	57
3.1.3	Objectives.....	59
3.2	Study Areas and Data Description.....	59
3.2.1	Study Area.....	59
3.2.2	Satellite Data	60
3.2.3	Field Work	61

3.3 Methodology	62
3.3.1 Polarimetric Data Processing	63
3.3.2 NDVI Calculation	66
3.3.3 Correlation Analysis	67
3.4 Results and Discussion	67
3.4.1 Field Data Collection	68
3.4.2 Correlation Analysis between RADARSAT-2 Polarimetric SAR Data and Crop Height	70
3.4.3 Correlation Analysis between RADARSAT-2 Polarimetric SAR Data and Crop NDVI	76
3.5 Conclusion	85
3.5 References	86
Chapter 4	89
4 Conclusion	89
4.1 Summary	89
4.2 Conclusions	90
4.3 Contributions of This Research	91
4.3.1 Technical Contribution	91
4.3.2 4. 3. 2 Application Contribution	91
4.4 Possible Future Research	92
4.4.1 Texture Analysis and Object Classification	92
4.4.2 Correlation Analysis with Other Agricultural Parameters	92
Appendices	93
A Polarimetric Decomposition Theorem and Results	93
A1 H/Alpha/A Decomposition and Pedestal Height	93
A 2 Freeman Decomposition	94

B Reference Data and Samples	95
B1 Optical Images.....	96
B2 Training Samples and Testing Samples	98
B3 LU/LC Classes and Field Work Pictures	100
B 4 Crop Height Measurements.....	102
C Classification Results	107
C.1 Gaussian MLC and Wishart MLC	107
C.2 PolSAR Parameters	109
C.3 Time Combinations	117
C.4 Post-classification Processing	127
Curriculum Vitae.....	133

List of Tables

Table 1.1 RADARSAT-2 data parameters	8
Table 1.2 The parameters of RapidEye data	9
Table 1.3: To ensure your tables update automatically in the List of Tables, right click your table and select "Insert Caption."	错误!未定义书签。
Table 2.1 RADARSAT-2 and RapidEye imagery	20
Table 2.2 Number of the plots and pixels selected for each LU/LC class in the training groups.....	35
Table 2.3 Number of the plots and pixels selected for five crop types in the testing samples.....	37
Table 2.4 Number and percentage of pixels selected for the testing samples of all LU/LC classes.....	37
Table 2.5 The classification results from four-date data by different combinations	45
Table 2.6 The classification results from three-date data by different combinations	47
Table 3.1 Summarizing of Satellite images and acquiring dates	61
Table 3.2 The correlation between crop height and SAR parameters	71
Table 3.3 Sampling segmentation results for soybean and corn fields superimposed on the June 7th (a), July 16th and 24th (b), August 5th (c), and August 25th (d) 2012, NDVI maps.	77
Table 3.4 The correlation between soybean and corn NDVI to basic polarimetric parameters in FQ7 and FQ21	78
Table 3.5 the ranking of correlation coefficients between polarimetric parameters and NDVI for soybeans	84

Table 3.6 The ranking of correlation coefficients between polarimetric parameters and NDVI for corn	84
Table C.7 Error matrix for Gaussian MLC using all T3 elements from 504, 528 , 621,715 images	109

List of Figures

Figure 1.1 Study Area	6
Figure 1.2 The boundaries of RapidEye images (Red), RADARSAT-2 images (Yellow), and study areas (Green).....	7
Figure 2.1 The location of London, Ontario, and the RapidEye image of the study area	19
Figure 2.2 Flow chart of data processing methodology.....	21
Figure 2.3 An overview of the preprocessing of RADARSAT-2 images	22
Figure 2.4 RGB composition images presenting different polarimetric decomposition methods.	25
Figure 2.5 Filtered Pauli RGB images using different speckle filtering methods	26
Figure 2.6 Pauli RGB image before(a) and after(b) geometric correction using MapReady	28
Figure 2.7 Data distributions of wheat from the raw Pauli parameters (blue), logarithm Pauli parameters (red), and simulated normal curve (black) at T11 (a), T22 (b) and T33 (c). (d) Comparison of fitted normal curves and logarithm Pauli parameters histogram curve.....	31
Figure 2.8 An overview of the comparisons among various classification strategies	36
Figure 2.9 Temporal profiles of Pauli decomposition parameters value for various crop types in PauliT11 single bounce (a), PauliT22 double bounce (b), and PauliT33 volume scattering(c).....	39
Figure 2.10 H/Alpha/A (a, T11, T22, T33 scattering value in dB) and Freeman decomposition parameters (b, Double Volume and Odd scattering value in Db.) from ten LU/LC classes.	40

Figure 2.11 the classification result using different time combination ranking by classification OA from highest to lowest.	44
Figure 2.12 Accuracy statistics using different post-classification processing methods ..	48
Figure 2.13 LU/LC map of the study area generated by five-date image after sieve filtering.....	49
Figure 3.1 Study fields presented on the true color combined RapidEye image	60
Figure 3.2 The methodology of the data processing and Analyzing	62
Figure 3.3 Flowchart showing the polarimetric RADARSAT-2 datasets processing	65
Figure 3.4 Key crop growing stages for corn and soybeans during the growing season..	69
Figure 3.5 Key crop growing stages for wheat and field Peas during the growing season	70
Figure 3.6 Temporal evolution of the SAR responses over corn and soybean. SAR parameters are presented together with crop height and precipitation amounts.	73
Figure 3.7 Temporal evolution of the SAR response over wheat (a) and peas (b). SAR parameters presented together with crop height and precipitation amount	75
Figure 3.8 Correlation between the HV, HH-VV for the RADARSAT-2 FQ7 and FQ21 acquisitions and NDVI for corn and soybean	80

Chapter 1

1 Introduction

1.1 Research Content

Canada is one of the largest agricultural producers and exporters in the world.

Agriculture is an important element of the Canadian economy. However, the proportion of the population and GDP devoted to agriculture has fallen dramatically over the past few decades.

In Ontario, due to the rapid urban development, the depression of agricultural economy is even more obvious. In the decade from 1981 to 1990, the total net farm income in the Ontario was 6,812 million CAD, which was 23% of the total net income in Canada.

While in the decade of 2001 to 2010 the number decreased to 2,891 million CAD, which occupied merely 11% of the total net farm income in the whole country (Statistics Canada, 2012). The decrease in number of farms and total farm area from 2006 to 2011 was also reported by Statistics Canada (Statistics Canada, 2012). During the six years, the number of farms decreased by 9.2%, and meanwhile, the total area occupied by farms also dropped by 4.8%.

In Southern Ontario alone, thousands of acres of productive agricultural land are lost due to the rapid sprawl and farmland severances each year. Take the Greater Toronto Area for example, over 2,000 farms and 130,000 acres of farmland were converted to urban purposes in the two decades between 1976 and 1996.

The rapid loss of agricultural areas to urban land use in the urban/rural fringe, such as the case in Southern Ontario, has raised great concern. Increasing research has focused on assessing the impacts of urban expansion on agricultural and forest ecosystems (Lombard et al. 2003; Pellizzeri 2003; Pellizzeri et al. 2003; Niu and Ban 2010; Zhang et al. 2010; Zhu et al.2011).

Remote Sensing offers an effective solution to detect changes to land surfaces. With their wide area coverage and repetitive characteristics, satellite sensors are able to collect up-to-date and reliable information about the current state of land surfaces, and further facilitate the Land Use and Land Cover (LU/LC) changes detection, as well as monitoring agricultural plants.

The complexity of urban/rural fringe environments, which are composed of a wide variety of LU/LC classes, makes LU/LC mapping challenging. However, benefiting from the rich informational content of the multispectral data, optical images have been proven to be a promising data source. The application of optical remote sensing data in LU/LC mapping has a long history, ever since the launch of Landsat optical satellites. Over the last few years, with the advent of advanced optical satellite sensors (i.e. Quickbird, Ikonos, SPOT, Worldview, and RapidEye), the spectral and spatial resolution of images have been highly improved (Corbane et al., 2008). More sophisticated methods, such as object-based classification, have been developed to improve the classification accuracy (Geneletti & Gorte, 2003; Gao et al., 2006; Li et al., 2008; Li et al., 2009; Watts et al., 2009).

Multi-temporal Remote Sensing information is particularly useful in agricultural applications, such as annual crop inventory and crop condition monitoring (Defries & Townshend, 1994; Friedl et al., 2010; Gopal et al., 1999; Guerschman et al., 2003; Hansen et al., 2000; Tucker et al., 1985; Wolter et al., 1995). The bio-physical characteristics of vegetation, such as pigmentation, internal leaf structure and moisture, vary from crop to crop and from time to time. The changes in the biophysical characteristics can be directly reflected by the amount of visible and infrared (V-IR) energy recorded on the satellite images (Reese et al., 2002; Guerschman et al., 2003; Turker and Arikian, 2005; Fiset et al., 2005). A large number of vegetation indices (i.e. the normalized difference vegetation index (NDVI), the optimized soil adjusted vegetation index, the enhanced vegetation index, and the modified triangular vegetation index) are derived from the multispectral optical data to track the temporal changes in biophysical characteristics of different vegetation types (Andrés et al., 2011).

LU/LC change detection and crop condition monitoring using optical images are successful only when images can be acquired frequently over the whole growing period. However, due to the existence of haze and cloud, high quality optical data are not always available in unfavorable weather conditions. Therefore, when time and area gaps in data acquisitions occur, the applications of optical images are often limited (McNairn et. al., 2009). Microwaves are able to transmit through most cloud and haze, hence, the backscattering signals are less influenced by weather conditions. The SAR system, which transmits and receives microwave signals, provides complementary information for remote sensing. Besides, the backscattering signals are sensitive to the architecture and dielectric properties of land surfaces, such as plant canopy, built-ups and soils (McNairn et. al., 2009).

The advantages of **SAR images** over optical data are more obvious in agricultural applications because crops change rapidly during their growing seasons. The SAR signals are primarily a function of the canopy structures such as the size, shape and orientation of leaves, stalks and fruit, the water contents of the crop canopy and soil. However, the structure and water content varies from crop to crop and changes among different stages. Therefore, SAR images have the potential not only to distinguish different crop types, but also to monitor the crops' growing conditions. For the past few years, many studies have proved the capabilities of SAR data for crops' condition monitoring and biophysical parameter retrieval (Blaes et al., 2005; Chakraborty et al., 2005; Moran et al., 1997; Nicolas et al., 2009; Shao et al., 2001).

Studies show that the sensitivities of SAR backscattering to crops' conditions also depend on the **SAR sensor parameters** (wavelength, incidence angles, and polarization). Generally, short SAR wavelengths, such as X-band (~3cm) and C-band (~6cm), are less capable to penetrate through the canopy, and therefore mainly interact with the top part of the canopy layers, while longer wavelengths such as L-band(~20cm) and P-band (~100cm) can penetrate into the vegetation cover and even reach the soil (Ulaby et al., 1987). Specifically, the penetration depth depends on the biophysical parameters of the scatters within a vegetation layer (e.g., water content, size and geometry of the scatterers), which might enhance or attenuate the interaction between microwaves and scatterers.

In addition to exploring the **frequency** dimension of the SAR system, some researchers have investigated the polarimetric properties of SAR data in LU/LC classification and vegetation monitoring. (Pierce et al., 1994; Du & Lee, 1996; Lee et al., 2001; Freitas et al., 2008). Results prove that, by utilizing polarimetric SAR instead of single polarization data, higher accuracy can be achieved in both LU/LC mapping and crop monitoring. Ever since the recent launch of radar satellites, such as ENVISAT ASAR, ALOS PALSAR, RADARSAT-2 and TERRASAR-X, more polarimetric SAR data are becoming available. In the meantime, some polarimetric decomposition theorems have been developed and applied (Cloude & Pottier, 1996; Freeman & Durden, 1998; Yang et al., 1998; Cameron & Rais, 2006), which provide additional information for LU/LC classification and crops monitoring. The decomposition parameters extracted from the polarimetric SAR data are related to the physical properties of land surfaces, and thus are sensitive to the structures of different LU/LC types and crops in various stages. However, the potential of polarimetric decomposition parameters in LU/LC classification and change detection, especially in crops growing conditions monitoring, is not fully explored in the previous research.

1.2 Research Objectives

The objectives of this research is to evaluate the multi-temporal Quadpol RADARSAT-2 dataset in LU/LC mapping and crop monitoring in Southwestern Ontario. As mentioned above, rapid urban sprawl has greatly influenced the agricultural economy and productivity in this area. However, multitemporal polarimetric SAR data have seldom been used in this agricultural area before. The newly available RADARSAT-2 data provide a great opportunity to study the impacts of urban development on ~~the~~ agriculture in Southwestern Ontario.

The research in this thesis will seek to provide the answers to the following questions:

1. How accurately can LU/LC be classified in ~~this~~ urban/rural fringe area ~~using the~~ fine beam multi-temporal polarimetric RADARSAT-2 satellite images?

2. What is the suitable classification method for LU/LC classification in urban/rural fringe areas using polarimetric RADARSAT-2 satellite images?
3. What is the suitable multi-date combination of the polarimetric RADARSAT-2 images in LU/LC classification?
4. What is the potential of polarimetric RADARSAT-2 data in monitoring crop height change?
5. How sensitive is the RADARSAT-2 polarimetric parameters to the crop biophysical parameter NDVI?

The studies presented in Chapter 2 and Chapter 3 answer these questions by addressing these research objectives:

1. To assess the potential of polarimetric RADARSAT-2 data in LU/LC classification in urban/rural fringe areas.
2. To analyze the sensitivity of different RADARSAT-2 polarimetric parameters to the temporal changes of crop height and NDVI.

1.3 Study Area and Study Data

The study area is located in the urban/rural fringe area of London, Ontario (Figure 1.1). ~~This area is in the midst of the Great Lake region.~~ The city London is ~~within the~~ Middlesex County right at the forks of the non-navigable Thames River. London is well-known for its ~~high coverage of forests,~~ and is named the “forest city” ~~after that.~~ Economically, it is situated along the Quebec City-Windsor Corridor, approximately halfway between Toronto, Ontario and Detroit, Michigan. In 2011, there were approximately 366,151 residents in the city with an area of 420.57 km² (Statistics Canada, 2012). The city’s economy is dominated by ~~high education,~~ medical research, insurance, and information technology. In addition, London is a center of life science and biotechnology-related research; much of ~~this~~ is conducted or supported by the University of Western Ontario. ~~The main land use in the city is institutional, commercial and industrial areas, residential areas, roads, forests, grasses, and water bodies. In the land use in the rural areas are mainly~~

agricultures. ~~The main crops growing in this area are~~ wheat, corn, soybeans, hay, and field peas.

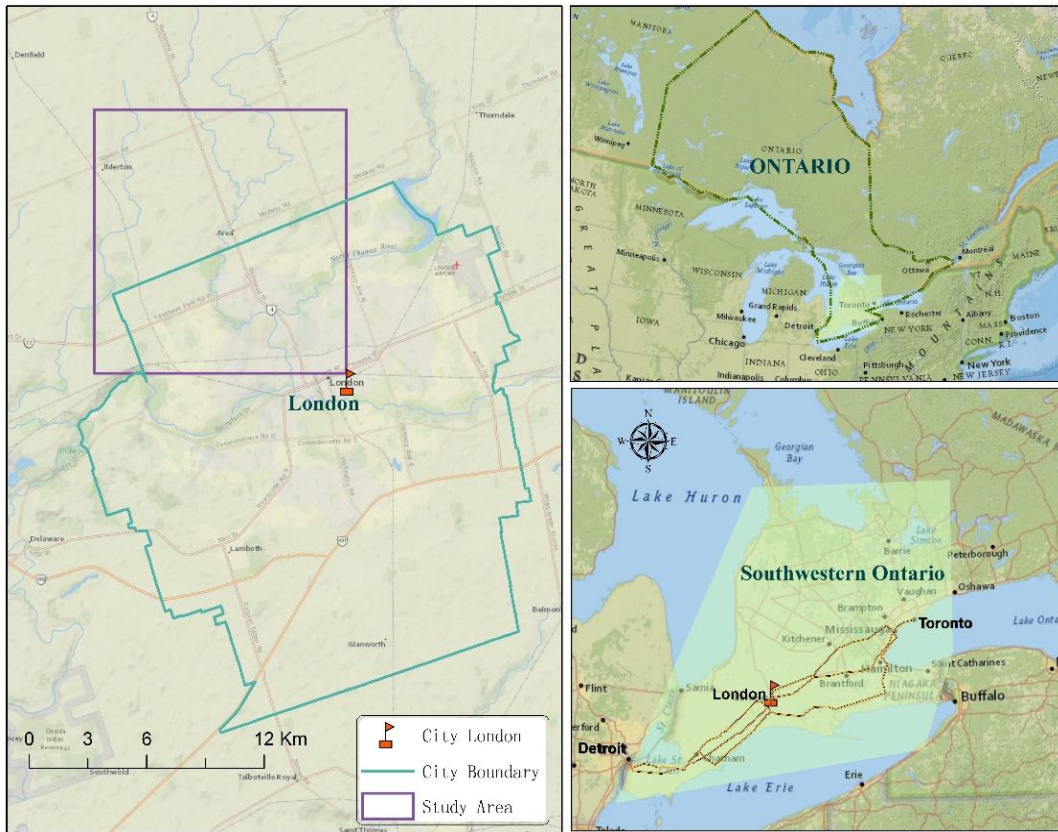


Figure 1.1 Study Area

The satellite images used in the research include RADARSAT-2 SAR images and RapidEye optical images. The boundaries of satellite images and study areas are displayed in Figure 1.2 Other ancillary data, such as images from Google earth, and air photo images are also used to facilitate the research.

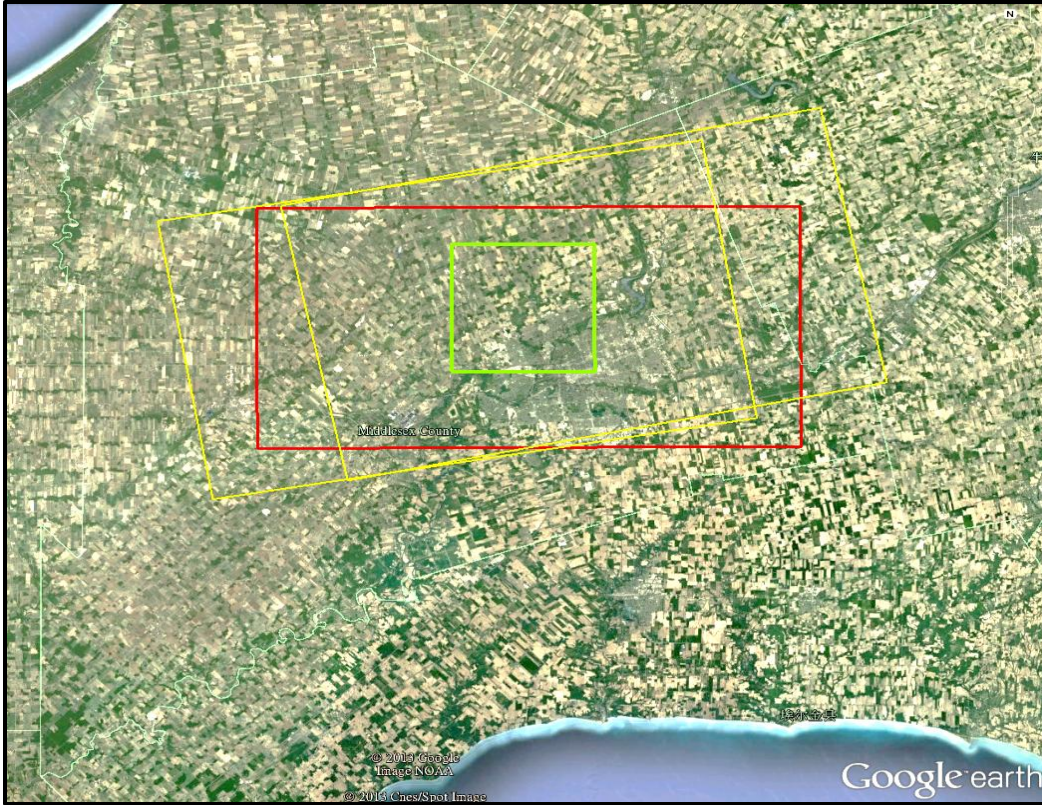


Figure 1.2 The boundaries of RapidEye images (Red), RADARSAT-2 images (Yellow), and study areas (Green)

The RADARSAT-2 is a radar observation satellite that was successfully launched on December 14th, 2007 by MacDonald Dettwiler & Associates (MDA) and Canadian Space Agency. RADARSAT-2 is a follow-up to RADARSAT-1, in order to enhance the SAR systems' applications in sea ice mapping, iceberg detection, marine surveillance for ships and pollution detection, geological mapping, wetlands mapping, topographic mapping, land use land cover mapping, and agricultural crop monitoring.

Two sets of wide fine beam Quadpol RADARSAT-2 data were acquired for this research (Table 1.1). One set was taken at the steeper incidence angle, between 25 °to 28 °, while the other set of data were taken in a shallower incidence angle, between 40 °to 42 °. Both data sets have similar pixel spacing, around 5 meters, and wide coverage of 50km by 25km. All the images were taken from early May to September, 2012 over the whole study area.

Table 1.1 RADARSAT-2 data parameters

Name	Pixel spacing Pixel×Line	Coverage (km)	Incidence Near edge	Incidence Far edge	Dates (mdd2012)
Wide Fine Quadpol7	4.7m×4.7m	50X50	24.9°	28.3°	504, 528, 621, 715, 901
Wide Fine Quadpol21	4.7m×5.1m	50X50	40.2°	41.6°	507, 624, 718, 811, 904, 928

The RapidEye is a commercial optical satellite developed by TÜV NORD of Germany, MDA, and RapidEye AG. The RapidEye system contains five independent satellites, which enables observation of Earth’s surface in high-resolution over large areas. The RapidEye images can be used to provide valuable information on field areas, crop conditions.

The nadir resolution for these satellite images are 6.5 meters, and the swath width is 77 kilometers. To facilitate the agricultural applications, the red edge and near infrared spectral bands, which are most sensitive to vegetation conditions, are designed. Many Vegetation Indices have been derived from the multispectral bands to capture the vegetation characteristics (Andrés et al., 2011).

Although RapidEye seems to be a perfect data source for agricultural applications, it is limited by weather conditions. In this study, five scenes of RapidEye images were acquired over the crop growing season (Table 1.2). During that season, however, many days are cloudy or rainy. Each complete RapidEye dataset were combined by two scenes, one in the west and the other in the east. In order to get a cloud free image in the mid of July of the whole study area, we have to subset and combine part of images taken on the July 16th and July 24th together. The poor qualities of some images make it difficult to interpret complete and useful information from them.

Table 1.2 The parameters of RapidEye data

Spectral Band	Blue	Green	Red	Red Edge	Near Infrared
Wavelength(nm)	440-510	520-590	630-685	690-730	760-850
Dates(m_dd_yyy)	6_07_2012	7_16_2012	7_24_2012	8_05_2012	8_25_2012
Scene Location	West&East	West	East	West&East	West&East

1.4 Thesis Format

This research is presented in an integrated-article format. Chapter 1 gives a brief review of the literature on the research problem, the objectives of the research, and the study area and data used in the research.

The focus of the thesis is to investigate the potential of Quadpol RADARSAT-2 SAR data in LU/LC information extraction and crop condition monitoring. To achieve this goal, different imagery sources and processing methods were used. Chapter 2 focuses on assessing the potential of RADARSAT-2 polarimetric image LU/LC classification. Chapter 3 analyzed the sensitivities of polarimetric parameters to the NDVI index and crop height.

1.5 References

- Andrés Viña, Anatoly A. Gitelson, Anthony L. Nguy-Robertson, Yi Peng, Comparison of different vegetation indices for the remote assessment of green leaf area index of crops, *Remote Sensing of Environment*, Volume 115, Issue 12, 15 December 2011, Pages 3468-3478, ISSN 0034-4257, 10.1016/j.rse.2011.08.010.
- Blaes, X., Vanhalle, L., & Defourny, P. (2005). Efficiency of crop identification based on optical and SAR image time series. *Remote Sensing of Environment*, 96, 52–365.
- Cameron, W. L., & Rais, H. (2006). Conservative polarimetric scatterers and their role in incorrect extensions of the Cameron decomposition. *IEEE Transactions on Geoscience and Remote Sensing*, 44, 3506–3516.
- Chakraborty, M., Manjunath, K. R., Panigrahy, S., Kundu, N., & Parihar, J. S. (2005). Rice crop parameter retrieval using multi-temporal, multi-incidence angle RADARSAT SAR data. *ISPRS Journal of Photogrammetry & Remote Sensing*, 59, 310–322.
- Cloude, S. R., & Pottier, E. (1996). A review of target decomposition theorems in radar polarimetry. *IEEE Transactions on Geoscience and Remote Sensing*, 34, 498–18.
- Corbane C, Faure J-F, Baghdadi N, Villeneuve N, Petit M. Rapid Urban Mapping Using SAR/Optical Imagery Synergy (2008). *Sensors*. 8(11):7125-7143.
- Defries, R. S., & Townshend, J. R. G. (1994). NDVI-derived land cover classification at global scale. *International Journal of Remote Sensing*, 15(17), 3567–3586.
- Du, L., & Lee, J. S. (1996). Fuzzy classification of earth terrain covers using complex polarimetric SAR data. *International Journal of Remote Sensing*, 17, 809–826.
- Fisette, T., Maloley, M., Chenier, R., White, L., Huffman, T., Ogston, R., Pacheco, A., Gasser, P. Y., 2005. Towards a national agricultural land cover classification evaluating decision tree approach. In: 26th Canadian Symposium on Remote Sensing, Wolfville, Nova Scotia, June 14–16 (on CD-ROM).

- Freeman, A., & Durden, S. L. (1998). A three-component scattering model for polarimetric SAR data. *IEEE Transactions on Geoscience and Remote Sensing*, 36, 963–973.
- Freitas, C. D., Soler, L. D., Anna, S. J. S. S., Dutra, L. V., dos Santos, J. R., Mura, J. C., & Correia, A. H. (2008). Land use and land cover mapping in the Brazilian Amazon using polarimetric airborne p-band SAR data. *IEEE Transactions on Geoscience and Remote Sensing*, 46, 2956–2970.
- Friedl, M. A., Menashe, D. S., Tan, B., Schneider, A., Ramankutty, N., Sibley, A., et al. (2010). MODIS collection 5 global land cover: Algorithm refinements and characterization of new datasets. *Remote Sensing of Environment*, 114, 168–182.
- Gao, Y., Mas, J. F., Maathuis, B. H. P., Zhang, X. M., & Van Dijk, P. M. (2006). Comparison of pixel-based and object-oriented image classification approaches — A case study in a coal fire area, Wuda, Inner Mongolia, China. *International Journal of Remote Sensing*, 27, 4039–4055.
- Geneletti, D., & Gorte, B. G. H. (2003). A method for object-oriented land cover classification combining Landsat TM data and aerial photographs. *International Journal of Remote Sensing*, 24, 1273–1286.
- Gopal, S., Woodcock, C. E., & Strahler, A. (1999). Fuzzy neural classification of global land cover from a 1 degree AVHRR Data Set. *Remote Sensing of Environment*, 7, 230–243.
- Guerschman, J. P., Paruelo, J. M., Bella, C. D. I., Giallorenzi, M. C., & Pacin, F. (2003). Land cover classification in the Argentine Pampas using multi-temporal Landsat TM data. *International Journal of Remote Sensing*, 24(17), 3381–3402.
- Guerschman, J.P., Paruelo, J.M., Di Bella, C., Giallorenzi, M.C., Pacin, F., 2003. Land cover classification in the Argentine Pampas using multi-temporal Landsat TM data. *International Journal of Remote Sensing* 24 (17), 3381–3402.
- Hansen, M. C., Defries, R. S., Townshend, J. R. G., & Sohlberg, R. (2000). Global land cover classification at 1 km spatial resolution using a classification tree approach. *International Journal of Remote Sensing*, 21(6 & 7), 1331–1364.

- Lee, J. S., Grunes, M. R., & Pottier, E. (2001). Quantitative comparison of classification capability: Fully polarimetric versus dual and single-polarization SAR. *IEEE Transactions on Geoscience and Remote Sensing*, 39, 2343–2351.
- Li, H. T., Gu, H. Y., Han, Y. S., & Yang, J. H. (2008). Object-oriented classification of polarimetric SAR imagery based on statistical region merging and support vector machine. *Proceedings of the 2008 International Workshop on Earth Observation and Remote Sensing Applications* (pp. 147–152). Beijing, China.
- Li, X., Yeh, A. G. O., Qian, J. P., Ai, B., & Qi, Z. X. (2009). A matching algorithm for detecting land use changes using case-based reasoning. *Photogrammetric Engineering and Remote Sensing*, 75, 1319–1332.
- Lombardo, P., M. Sciotti, T.M. Pellizzeri, and M. Meloni. (2003). “Optimum Model-Based Segmentation Techniques for Multifrequency Polarimetric SAR Images of Urban Areas.” *IEEE Transactions on Geoscience and Remote Sensing* 41: 1959–75.
- McNairn, H., Champagne, C., Shang, J., Holmstrom, D.A., and Reichert, G. (2009). Integration of optical and Synthetic Aperture Radar (SAR) imagery for delivering operational annual crop inventories.” *ISPRS Journal of Photogrammetry and Remote Sensing*, 64(5), pp. 434-449. doi : 10.1016/j.isprsjprs.2008.07.006.
- Moran, M. S., Vidal, A., Troufleau, D., Qi, J., Clarke, T. R., Pinter, P. J., et al. (1997). Combining multifrequency microwave and optical data for crop management. *Remote Sensing of Environment*, 61, 96–109.
- Nicolas B., Nathalie B., Pierre T., Mahmoud E. Agnès B., (2009), Potential of SAR sensors TerraSAR-X, ASAR/ENVISAT and PALSAR/ALOS for monitoring sugarcane crops on Reunion Island, *Remote Sensing of Environment*, Volume 113, Issue 8, Pages 1724-1738, ISSN 0034-4257, 10.1016/j.rse.2009.04.005.
- Niu, X., and Y. Ban. (2010). “Multitemporal RADARSAT-2 Polarimetric SAR Data for Urban Land Cover Classification Using Support Vector Machine.” In 30th EARSeL Symposium, 581–8, Paris, 31 May–3 June 2010, edited by R. Reuter. Hannover: EARSeL.

- OMAFRA, 2011 Census of Agriculture and Strategic Policy Branch, 2012. Ontario, Canada. Middlesex County at a Glance.
- Pellizzeri, T. M. (2003). "Classification of Polarimetric SAR Images of Suburban Areas Using Joint Annealed Segmentation and 'H / A / α ' Polarimetric Decomposition." *ISPRS Journal of Photogrammetry and Remote Sensing* 58: 55–70.
- Pellizzeri, T. M., P. Gamba, P. Lombardo, and F. Dell'acqua. (2003). "Multitemporal / Multiband SAR Classification of Urban Areas Using Spatial Analysis: Statistical Versus Neural Kernel-Based Approach." *IEEE Transactions on Geoscience and Remote Sensing* 41: 2338–53.
- Pierce, L. E., Ulaby, F. T., Sarabandi, K., & Dobson, M. C. (1994). Knowledge-based classification of polarimetric SAR images. *IEEE Transactions on Geoscience and Remote Sensing*, 32, 1081–1086.
- Qi, Z., Yeh, A. G. O., Li, X., & Lin, Z. (2012). A novel algorithm for land use and land cover classification using RADARSAT-2 polarimetric SAR data. *Remote Sensing of Environment*, 118, 21–39
- Reese, H.M., Lillesand, T., Nagel, D.E., Stewart, J.S., Goldman, R.A., Simmons, T.E., Chipmand, J.W., Tessar, P.A., 2002. Statewide land cover derived from multiseasonal Landsat TM data-A retrospective of the ISCLAND project. *Remote Sensing of Environment* 82 (2), 224–237.
- Remote Sensing and Geospatial Analysis, Agriculture Division, Statistics Canada. 2012. Canada Change in number of farms reporting cattle between 2006 and 2011.
- Shao, Y., Fan, X., Liu, H., Xiao, J., Ross, S., Brisco, B., et al. (2001). Rice monitoring and production estimation using multitemporal RADARSAT. *Remote Sensing of Environment*, 76, 310–325.
- Statistics Canada. 2012. 2011 Census: Population and dwelling counts. Statistics Canada . Ottawa.
- Statistics Canada. 2012. Net Farm Income Agriculture Economic Statistics. Ottawa.

- Tucker, C. J., Townshend, J. R. G., & Goff, T. E. (1985). African land-cover classification using satellite data. *Science*, 227(4685), 369–375.
- Turker, M., Arıkan, M., 2005. Sequential masking classification of multi-temporal Landsat7 ETM+ images for field-based crop mapping in Karacabey, Turkey. *International Journal of Remote Sensing* 26 (17), 3813–3830.
- Ulaby, F. T., A. Tavakoli, and T. B. A. Senior (1987), Microwave propagation constant for a vegetation canopy with vertical stalks, *IEEE Trans. Geosci. Remote Sens.*, 25(6), 714–725.
- Watts, J. D., Lawrence, R. L., Miller, P. R., & Montagne, C. (2009). Monitoring of cropland practices for carbon sequestration purposes in north central Montana by Landsat remote sensing. *Remote Sensing of Environment*, 113, 1843–1852.
- Wolter, P. I., Mladenoff, D. S., & Crow, T. R. (1995). Improved forest classification in the northern lake states using multi-temporal Landsat imagery. *Photogrammetry Engineering & Remote Sensing*, 61(9), 1129–1143.
- Xin Niu & Yifang Ban (2013): Multi-temporal RADARSAT-2 polarimetric SAR data for urban land-cover classification using an object-based support vector machine and a rule-based approach, *International Journal of Remote Sensing*, 34:1, 1-26
- Yang, J., Yamaguchi, Y., Yamada, H., Sengoku, M., & Lin, S. M. (1998). Stable decomposition of Mueller matrix. *IEICE Transactions on Communications*, 1261–1268 E81b.
- Zhang, L., B. Zou, J. Zhang, and Y. Zhang. (2010). “Classification of Polarimetric SAR Image Based on Support Vector Machine Using Multiple-Component Scattering Model and Texture Features.” *EURASIP Journal on Advances in Signal Processing* 2010: 1–9.
- Zhu, Z., C. Woodcock, J. Rogan, and J. Kellndorfer. (2011). “Assessment of Spectral, Polarimetric, Temporal, and Spatial Dimensions for Urban and Peri-Urban Land Cover Classification Using Landsat and SAR Data.” *Remote Sensing of Environment* 117: 72–82.

Chapter 2


2 Assessment of Multi-temporal Polarimetric RADARSAT-2 data for Land Use and Land Cover classification in an Urban/Rural Fringe Area

2.1 Introduction

2.1.1 Background

LU/LC information is the basis for many studies, such as carbon modeling, land use change detection, forest management, and crop yield estimation (Jung et al., 2006; Lark & Stafford, 1997; Wolter et al., 1995; Woodcock et al., 2001). In the recent decades, LU/LC changes caused by rapid urban expansion have been occurring all over the world.

The emergence of **urban/rural fringe zone** caused by urban expansion has led to serious land use problems, such as loss of agricultural land, unauthorized urban sprawl, high land values (Qi et al., 2012). The fringe zone, which was neglected in either rural or urban studies, has become a topic of great importance (Zhu et al., 2011). The complete and timely land surface information of the fringe areas is highly required to deal with the land use problems.

Remote sensing has the characteristics of broad coverage and repetitive visit, and thus provides a practical and economical source for LU/LC information detection. High spatial resolution Remote Sensing data have been commonly used in urban areas, such as boundaries detection, impervious surface extraction. In rural areas, high temporal resolution Remote Sensing are useful for delivering crop type inventory, and crop condition monitoring (McNairn et al., 2009; Hen , 2012). However, few research has focused on the application of Remote Sensing in the rural/urban fringe areas. The dynamic land use and complex LU/LC classes in this fringe zones has created challenging for either urban sprawl detection, or crop inventory (Zhu et al., 2011).

2.1.2 Previous Studies

Remotely sensed data have been widely used in LU/LC classification. Most LU/LC types in the urban areas remain unchanged in a short period, and therefore multi-temporal datasets are not necessary in distinguishing urban LU/LC classes. For example, using two images acquired at very close dates, Qi successfully distinguished several LU/LC classes in urban/sub-urban areas at a high overall accuracy of 86.64 % (Qi, et al., 2012). However, in Qi's study, all the croplands were considered as one LU/LC type.

Multi-temporal images are essential to identify different crop types. During the growing seasons, crops evolve through a series of phenological growing stages. Meanwhile, the structure and water content of crops varies from type to type or even field to field. Capturing the differences in temporal changes of crops is a key to their identification. For example, in Southwestern Ontario, the growing season of most winter wheat is from April to July. However, most of the soybeans and corn are not planted until late May. Therefore, without multi-temporal datasets, satisfactory classification results are unlikely to be obtained. In the classification of crops, the selection of multi-temporal sequences of SAR images is critical to the classification results. McNairn and Skriver reported that higher accuracy in crop identification could be achieved by adding more multi-temporal SAR images (McNairn et al., 2009; Henning, 2012).

Multi-temporal optical images are ideal data sources for LU/LC classification in urban/rural fringe areas. Remotely sensed images obtained from various optical sensors have been widely used in LU/LC mapping (Saatchi et al., 1997; Roberts et al., 2003; Thenkabail et al., 2005). However, high-quality optical images are not always available due to the frequent cloudy and rainy weather during the growing season. Take London, Ontario as an example, during the whole growing season in 2012 (May to September), merely three scenes of cloud free RapidEye optical images were obtained. The applications of optical remote sensing data in wide areas LU/LC classification are limited by weather conditions.

Synthetic Aperture Radar (SAR) sensors play an increasingly important role in LU/LC classification because of their ability to obtain images day and night through cloud cover

and haze. SAR data are able to capture the dielectric properties and structure of the Earth's surface materials, and thus provide complementary information for optical data.

Early studies have used **multitemporal SAR** data to investigate LU/LC information, but mainly focused on single polarization (Desons et al., 199; Weber et al., 2003; Li et al., 2007). In the past few decades, most of the orbital radar systems, such as the ERS-1 and ERS-2, JERS-1, and RADARSAT-1, only provided single or duple polarization data. The information contained in the single or duple polarization data is limited and may create confusion in distinguishing some LU/LC types (Ulaby et al., 1986; Li & Yeh, 2004).

In order to reduce the deficiency of single polarization SAR data, many researchers have utilized polarimetric SAR data in LU/LC classification (McNairn et al., 2009; Niu and Ban, 2013; Qi et al., 2012). Recently, high spatial and temporal resolution polarimetric data have been available through radar systems, such as C-band RADARSAT-2, X-band TerraSAR-X, and Phased Array type L-band SAR (PALSAR) sensors. With access to those multitemporal sequences of high-resolution and polarimetric SAR data, a SAR-only solution for surveying rapid urban sprawl in the urban/rural fringe areas becomes increasingly viable (Palubinskas, et al. 2011).

Polarimetric SAR data provide the description of land features from the observations of various polarizations. Therefore, more information can be explored from the polarimetric SAR data than single or duple polarization images (Lee et al., 2009; McNairn et al., 2009; Niu and Ban, 2013; Qi et al., 2012). Some researchers proved that by integrating polarimetric data in the classification, not only were the accuracies of vegetation enhanced, but also the separability between vegetation and built-ups was increased (McNairn et al., 2009; Henning Skriver, 2012; Qi et al., 2012). Using polarimetric decomposition methods, a complex radar signal can be decomposed as a combination of scattering responses from simpler objects with easier physical interpretation. Decomposed parameters provide information about corresponding target types in the image, and thus are able to facilitate the classification of various LU/LC classes.

2.1.3 Objectives

The objective of this study is to assess the potential of polarimetric RADARSAT-2 data for LU/LC classification in urban/rural fringe areas. More specific objectives are: (1) to exam the effectiveness of various polarimetric decomposition parameters in LU/LC classification; (2) to find the best combination of multi-date data for accurate and economic LU/LC classification; (3) to provide a suitable procedure for LU/LC classification.

2.2 Study Area and Data Description

2.2.1 Study Area

Study area is in the northwest of the urban and rural fringe areas of London, which is a city in the Southwestern Ontario, Canada. The whole area is generally flat, and surrounded by productive agricultural areas. In recent decades, the city London has been experiencing rapid urban expansion. Therefore, the study of LC/LU in this area is critical for urban sprawl detection as well as for monitoring the areas lost to urban development. There are a wide range of LU/LC classes, such as commercial areas, industrial areas, residential areas, construction sites, forests, grass and agricultural areas. The main crop types in this area including corn, soybeans, wheat, and field peas. The complex nature of LU/LC types in the urban/rural fringe area is both a challenge and an opportunity to test the potential of multi-temporal RADARSAT-2 data in mapping.

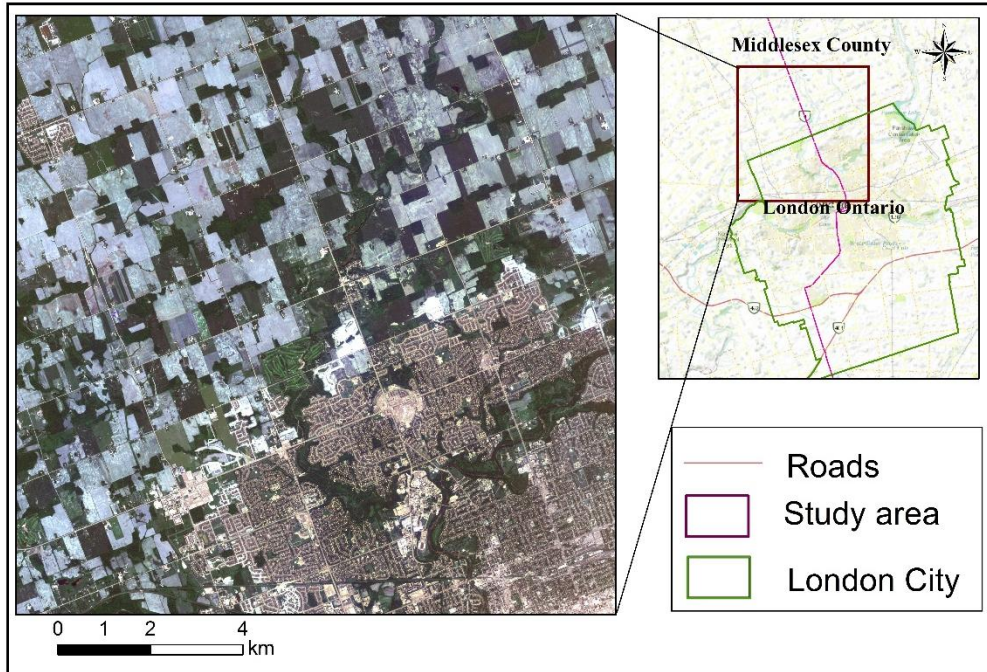


Figure 2.1 The location of London, Ontario, and the RapidEye image of the study area

2.2.2 The Optical Data

Five dates of RADARSAT-2 wide fine beam Quadpol images were acquired in ascending orbits over the study area from May 4th to Sept.1st. Polarimetric information is recorded in HH, VV, HV, VH bands, with a nominal pixel spacing of 4.7m and 4.7m in the range and azimuth directions. The incidence angles for the five images are very close, varying from 24.9° to 28.3° . The center frequency of the RADARSAT-2 data is C band 5.4 GHz at a wavelength of 5.6 cm.

The optical data used in the research is geometrically corrected RapidEye satellite imagery and air photos. The RapidEye images are multi-spectral optical data, which have five multispectral bands (from 440 nm to 850 nm) and 6.5m nadir resolution. The air photos used in the study were taken in April, 2011 at a 15cm spatial resolution (Provided by city of London). The optical data will be used as reference and auxiliary data for SAR data classification.

Table 2.1 RADARSAT-2 and RapidEye imagery

Satellite	Mode	Wave length	Dates	Resolution	Bands
RADARSAT-2	Wide FQ7	5.6cm	May 4, May 28, June 21, July 15, Sept.1, 2012	8-12m	HH, VV, HV, VH
RapidEye	Standard	440 - 850nm	June 7, July 16, July 24, Aug 25, 2012	6.5m	Blue, Green, Red, Red Edge, Near Infrared

2.2.3 Field Data Collection

The purpose of the field work was to investigate the crop growing conditions. Two general investigations of crop and other non-crop LU/LC types were completed in July and September. More frequent field work was conducted through the whole crop growing season, so as to guarantee that there was in situ data whenever RADARSAT-2 image was taken.

In the field, the accurate locations of various crop lands were recorded using GPS unites, the average crop height were measured and photos of typical crops were taken to observe the crops at different growing stages. Weather condition will influence the moisture of surface scatterers, such as soil and crops. The change of moisture leads to the change of dielectric constant, which might result in abnormal SAR backscattering values. In order to facilitate the interpretation of the SAR data, meteorological information was noted down on each date when a RADARSAT-2 image was taken.

2.3 Methodology

The methodology for this research consists of RADARSAT-2 image preprocessing; samples selections; multi-temporal RADARSAT-2 dataset classification; post classification processing, and accuracy assessment (Figure 2.2).

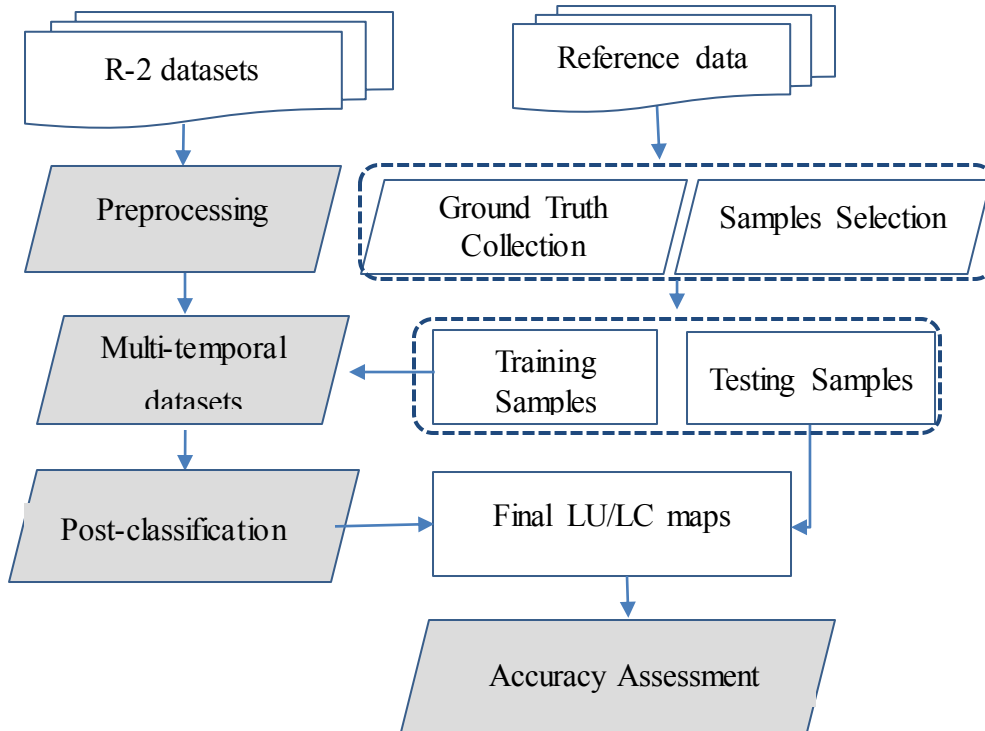


Figure 2.2 Flow chart of data processing methodology

2.3.1 RADARSAT-2 Data Pre-processing

The preprocessing of polarimetric SAR data is critical to achieving good classification results (Lee et al., 2009). In this research, three main pre-processing steps have been conducted in sequence, including polarimetric decomposition data extraction, speckle filtering, and geometric correction (Figure 2.2).

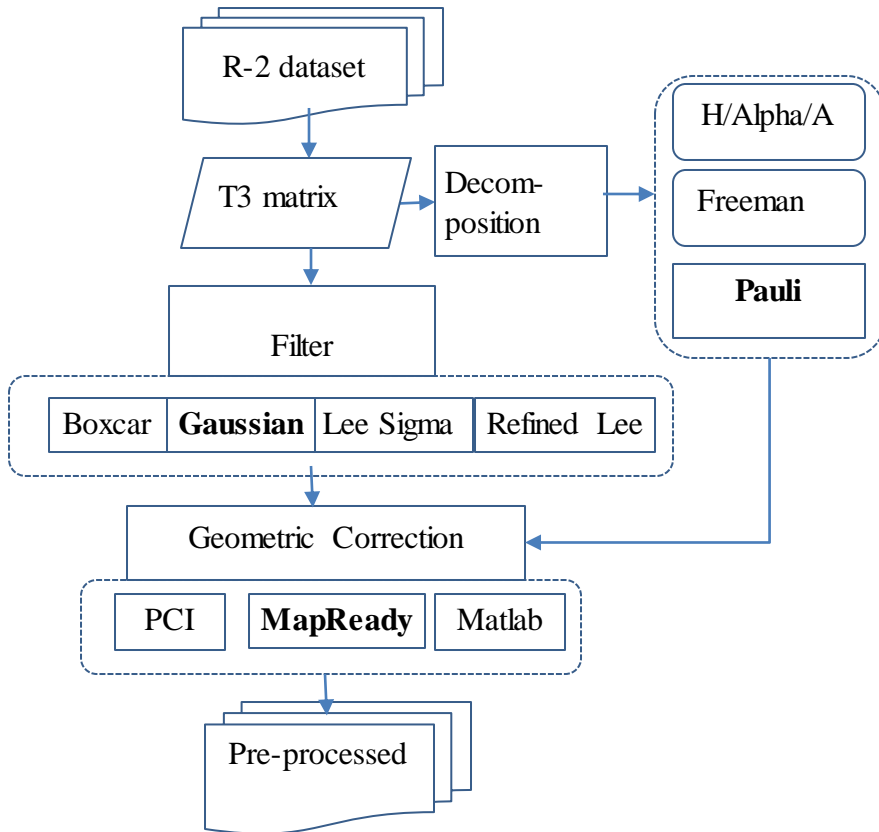


Figure 2.3 An overview of the preprocessing of RADARSAT-2 images

2.3.1.1 Coherency Matrix and Pauli Decomposition and

The raw polarimetric RADARSAT-2 data are contained in the four elements of the S matrix, see the function 2.1. First of all, the coherency matrix T_3 was extracted from the S matrix by using the PolSARpro software. The coherency matrix T_3 contained all the polarimetric information. Most of the decomposition parameters were then derived from coherency matrix T_3 , or covariance C_3 , which contains similar information, but in different form. The coherency matrix T_3 and covariance matrix C_3 can be expressed as:

$$S = \begin{bmatrix} S_{hh} & S_{hv} \\ S_{vh} & S_{vv} \end{bmatrix} \quad (2.1)$$

$$K = \frac{1}{\sqrt{2}} [S_{hh} + S_{vv} \quad S_{hh} - S_{vv} \quad S_{hv} + S_{vh}]^T \quad (2.2)$$

$$T_3 = \langle K \cdot K^{*T} \rangle \quad (2.3)$$

$$T_3 = \begin{bmatrix} T_{11} & T_{12} & T_{13} \\ T_{12}^* & T_{22} & T_{23} \\ T_{13}^* & T_{23}^* & T_{33} \end{bmatrix} \quad (2.4)$$

$$= \frac{1}{2} \begin{bmatrix} |S_{hh} + S_{vv}|^2 & (S_{hh} + S_{hv})(S_{hh} - S_{vv})^* & 2(S_{hh} + S_{vv})S_{hv}^* \\ (S_{hh} - S_{vv})(S_{hh} + S_{vv})^* & |S_{hh} - S_{vv}|^2 & 2(S_{hh} - S_{hv})S_{hv}^* \\ 2S_{hv}(S_{hh} + S_{vv})^* & 2S_{hv}(S_{hh} - S_{vv})^* & 4S_{hv} \end{bmatrix}$$

$$C_3 = \begin{bmatrix} C_{11} & C_{12} & C_{13} \\ C_{12}^* & C_{22} & C_{23} \\ C_{13}^* & C_{23}^* & C_{33} \end{bmatrix} \quad (2.5)$$

$$= \begin{bmatrix} |S_{hh}|^2 & \sqrt{2}S_{hh}S_{hv}^* & S_{hh}S_{vv}^* \\ \sqrt{2}S_{hv}S_{hh}^* & 2|S_{hv}|^2 & \sqrt{2}S_{hv}S_{vv}^* \\ S_{hv}S_{hh}^* & \sqrt{2}S_{vv}S_{hv}^* & |S_{vv}|^2 \end{bmatrix}$$

For the monocratic case, $S_{hv} = S_{vh}$, * denotes the conjugate and || denotes the module.

The Pauli decomposition parameters are composed of the three diagonal elements of the coherency matrix T_3 . The advantage of the Pauli decomposition is that each of the three elements corresponds to a basic scattering mechanism. $S_{HH} + S_{VV}$ represents single (odd) bounce scattering, $S_{HH} - S_{VV}$ indicates double bounce scattering, and $S_{HV} + S_{VH}$ is associated with volume. Typical LU/LC examples in the real field for those three scattering mechanisms are crop land, buildings and forests, respectively (Lee and Pottier, 2009).

2.3.1.2 Other Polarimetric Decomposition

(1) Freeman-Durden decomposition

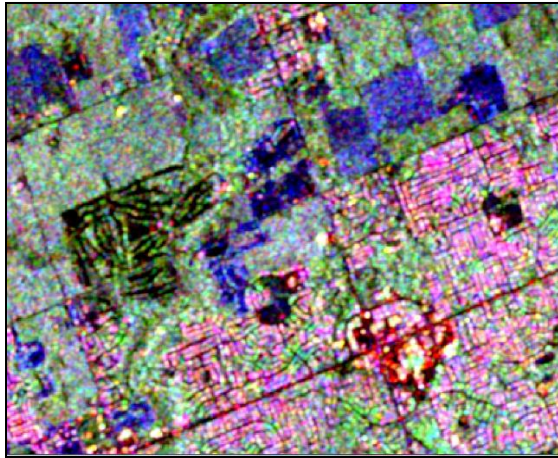
The Freeman-Durden decomposition is a method for fitting a physically based, three-component scattering mechanism model to the polarimetric SAR observations. The three-components scattering mechanism include surface, double-bounce and volume scattering mechanisms (Lee and Pottier, 2009). This approach can be used to determine the dominant scattering mechanisms and help to identify the current state of the surface cover. In

addition, the three-component scattering may provide features for distinguishing between different surface cover types. Although Freeman-Durden decomposition has been widely used in LU/LC classification, it has some limitations. Since Freeman-Durden method was intended to model the backscattering from terrain and forests, it might be invalid for other surface scattering.

(2) H/Alpha/A Decomposition

H/Alpha/A decomposition is an approach proposed by Cloude and Pottier for extracting average parameters from experimental data using a smoothing algorithm based on second-order statistics (Cloude and Pottier, 1996; Cloude and Pottier, 1997). Decomposition parameters are generated from an eigenvector analysis of the coherency matrix T_3 . The eigenvectors describe different scattering processes, and the eigenvalues indicate their relative magnitudes. Among all the parameters, the averaged Alpha angle (α) relates directly to underlying average physical scattering mechanisms. The value of Alpha ranges from 0° to 90° , which indicates the variance of dominant scattering from surface scattering mechanism moving into single scattering by a cloud of anisotropic particles, and finally reaching dihedral scatters. Entropy (H) describes the randomness of the scatter. The anisotropy (A) corresponds to the relative power of the second and third eigenvectors (Lee and Pottier, 2009).

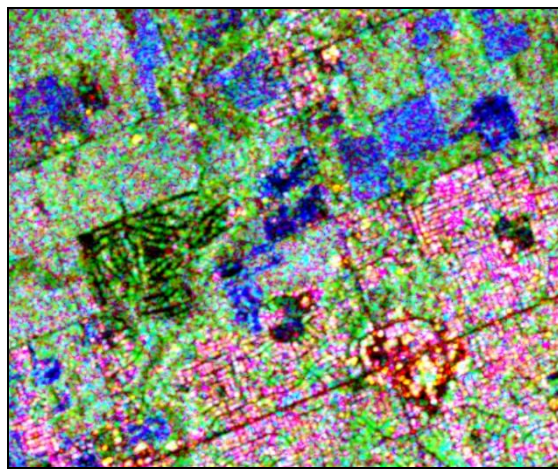
Both of the two polarimetric target decomposition methods were commonly used in the LU/LC classification (Qi et al., 2010; McNairn et al., 2009; Niu et al., 2013). In this study, in addition to Pauli decomposition, these two decomposition methods are also applied to every RADARSAT-2 image (Figure 2.3). The right window size is critical to the final classification results. After several tests, the window size of 3 for Freeman-Durden decomposition, and the window size of 7 for H/Alpha/A were applied, see the decomposition results in Figure 2.4.



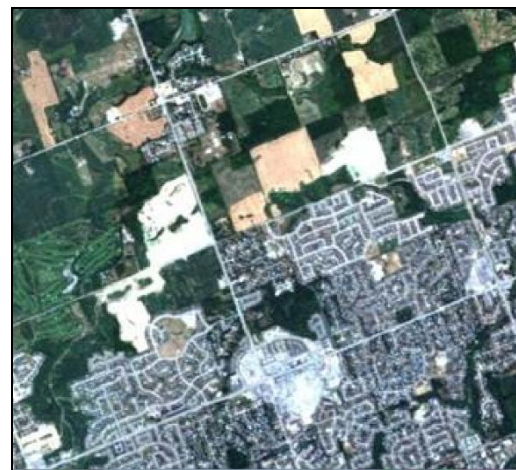
Pauli(a)



Freeman(b)



H/Alpha/A(c)



RapidEye(d)

Figure 2.4 RGB composition images presenting different polarimetric decomposition methods.

2.3.1.3 Speckle Filter

Speckle effects are inherent noises resulted from the coherent interference of the waves reflected from elementary scatters on SAR images (Lee and Pottier, 2009). In order to achieve the best speckle reducing effects, four different filters are tested and compared (Figure 2.5). Visually, Gaussian filter achieved the best result among all the filters. In the image after boxcar filter, boundaries of each LU/LC type were very blurring. On the Sigma Lee filtered images the separability among various classes were increased, but it kept some dark and bright points unfiltered. Refined Lee filter remained the sharp boundary of land

surface features, but introduced some false edges, even within homogenous crop fields, which looks like larger speckles.

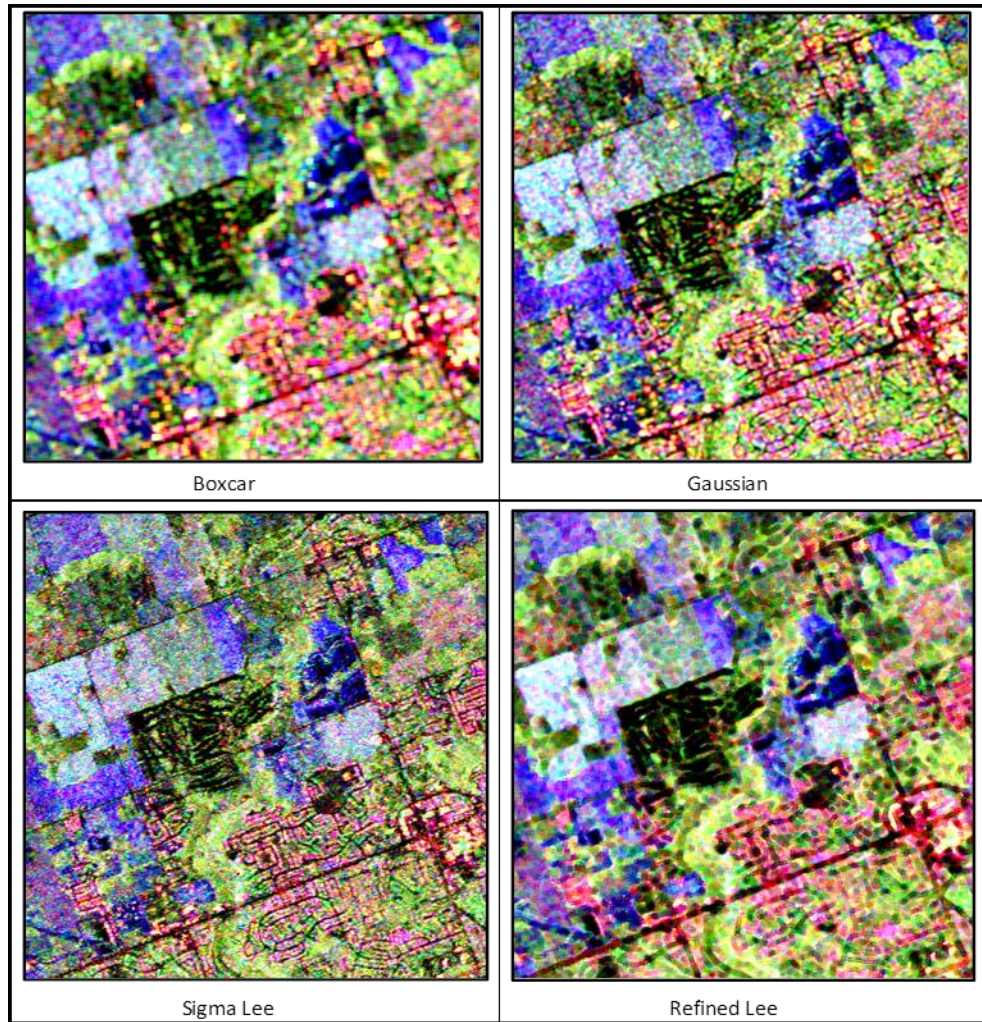


Figure 2.5 Filtered Pauli RGB images using different speckle filtering methods

The Gaussian function, which is also used to express the normal distribution, is applied to smooth an image by calculating the weighted averages in a filter box. In two dimensions image, the weight factors for a Gaussian distribution can be expressed as

$$G(x,y) = \frac{1}{2\pi\sigma^2} e^{-\frac{x^2+y^2}{2\sigma^2}} \quad (2.7)$$

Where x is the distance from the origin in the horizontal axis, y is the distance from the origin in the vertical axis. σ is the standard deviation of the Gaussian distribution (Cover,

2006). Gaussian filter is a low pass filter, and is able to reduce the image's high-frequency components. The Gaussian filter was applied to each of PolSAR image before further analysis.

2.3.1.4 Geometric Correction

Geometric correction is an essential step in SAR data preprocessing. Due to the unique SAR satellite imaging process, the image is formed in a slant range system. Distances were measured between the antenna and the target in the slant range system (Lee and Pottier, 2009). In areas with large elevation variation, serious geometric distortion can be easily observed in SAR images (Chen et al., 2008). Since this study area is generally flat, terrain effects, such as layover and shadowing, could be omitted. Effective geometric correction should be conducted to transfer the slant range system to ground range coordinate system. Subsequently, the five multitemporal SAR image would be georegistered together.

MapReady is a Remote Sensing Tool kit developed by Alaska Satellite Facility. This tool can be used to correct terrain effects, geocode polarimetric decomposition parameters and save to several common imagery formats. The MapReady tool kit used in this study is embedded in the PolSARpro software. Therefore, geometric correction can be applied directly on the datasets of T3, C3 matrix and other polarimetric parameters generated from the PolSARpro software. Firstly, the geometric imaging information of SAR images and the Digital Elevation Model (DEM) data of the study area are used to simulate an amplitude image. Then terrain effects are corrected through matching the real SAR image with the simulated SAR data.

Visually, after geometric correction, streets and boundaries of lakes and rivers in the geocorrected SAR images can match with the same features in the geometric corrected RapidEye images (Figure 2.5). The accurate geometric correction results provide a solid foundation for the subsequent image analysis and classification.

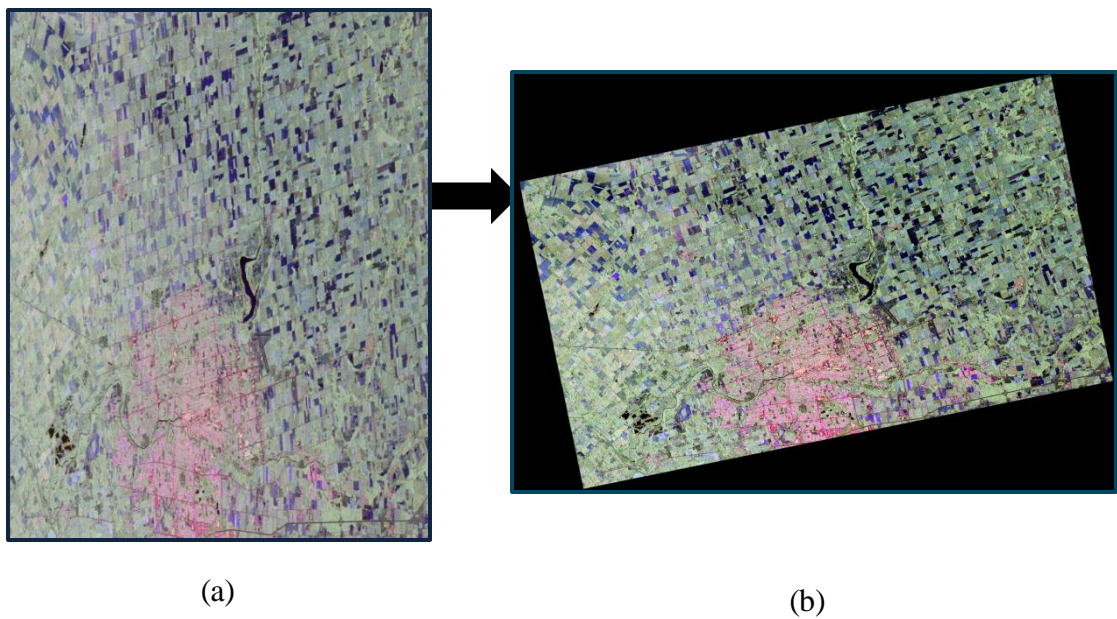


Figure 2.6 Pauli RGB image before(a) and after(b) geometric correction using MapReady

2.3.2 Classification Scheme and Training Samples

(1) Classification Scheme

A good classification scheme is important to achieve successful classification results. Theoretically, any classification scheme should be mutually exclusive and totally exhaustive (Russel C., & Kass G., 1999). In other words, any pixel should be classified into one and only one category or class, and also, every different LU/LC type should be considered in the classification. Ideally, a hierarchical classification scheme should be used to greatly distinguish each LU/LC class. Two or more detailed classes can be merged into a more general category, so as to meet the required accuracy standard.

In this study, LU/LC types can be first categorized into eleven classes, which include six crop types: alfalfa, grass, wheat, field peas, soybeans, corn; and four non-crop classes: forest, lawn, construction sites (CS), residential areas (RA), and commercial/industrial/institutional areas (CIIA). However, the primary objective of this research is to distinguish urban built-ups from vegetation, and identify several main crop types. Therefore, after classification the CS, RA, and CIIA classes are aggregated into built-up, and alfalfa and grass are combined into forage class.

(2) Training Sample Selection

In a supervised classification, a classification algorithm needs to be trained to distinguish those classes from each other. To achieve this purpose, representative samples, also known as prototypes, exemplars, or simply training samples for each class of interest with ground truth are required. The training samples of each category should be representative, homogeneous, and also include the range of variability of the category (Robert A., 2007). In this study, ground truth was acquired from the in-situ survey as well as by referencing to the RapidEye and aerial photo. All the training samples for each of the eleven LU/LC types evenly distributed and carefully selected to present each LU/LC type in the study area.

2.3.3 RADARSAT-2 Data Classification

Maximum Likelihood Classification (MLC) classifier is the most commonly used method adopted in supervised classification. MLC is based on the mean, variance or covariance statistics of class signal responses, and using a Bayesian Probability Function calculated from the training samples for each class. Each pixel is then classified to the class to which it most probably belong (Jensen, 2005). In this study, MLC based on two different probability functions, i.e. Gaussian and Wishart distributions are applied to find the better classification method.

(1) MLC Based on Gaussian distribution

MLC classification based on Gaussian (Normal) distribution (see Function 2.8) is widely used in optical image classification, because the distributions of each class spectral responses recorded in optical images are normally distributed (Jensen, 2005). However, due to the speckle effects, the radar responses in SAR image for each class can hardly follow the normal. However, some researchers have proved that when the number of look is large enough, the Gaussian probability density distribution is a valid approximation of multi-look SAR data (Skriver, 2012).

$$G(f; \mu, \sigma) = \frac{1}{\sigma\sqrt{2\pi}} e^{-\frac{(f-\mu)^2}{2\sigma^2}} \quad 2.8$$

In this study we found that the distributions of logarithm of T11, T22 and T33 polarimetric SAR data are extremely similar to the normal distribution. As the histogram of T11 (0.5|HH+VV|), T22 (0.5|HH-VV|) and T33 (2|HV|) shown in Figure 2.8, the majority of the original pixels value concentrated in the low zone. After the logarithmic operation, the histogram at T11, T22 and T33 became bell shape. Moreover, the curves of histograms of T11, T22, and T33 were well-matched with the corresponding normal distribution ones. The same shapes can be observed from the histograms of other classes. The amazing similarity between the curves mentioned above, further guaranteed that the Gaussian distribution can be a valid if not optimal approximation of logarithm T11, T22, T33 data.

Consequently, MLC for multivariate Gaussian statistics was adopted in the classification of multi-temporal PolSAR data derived from different decomposition parameters.

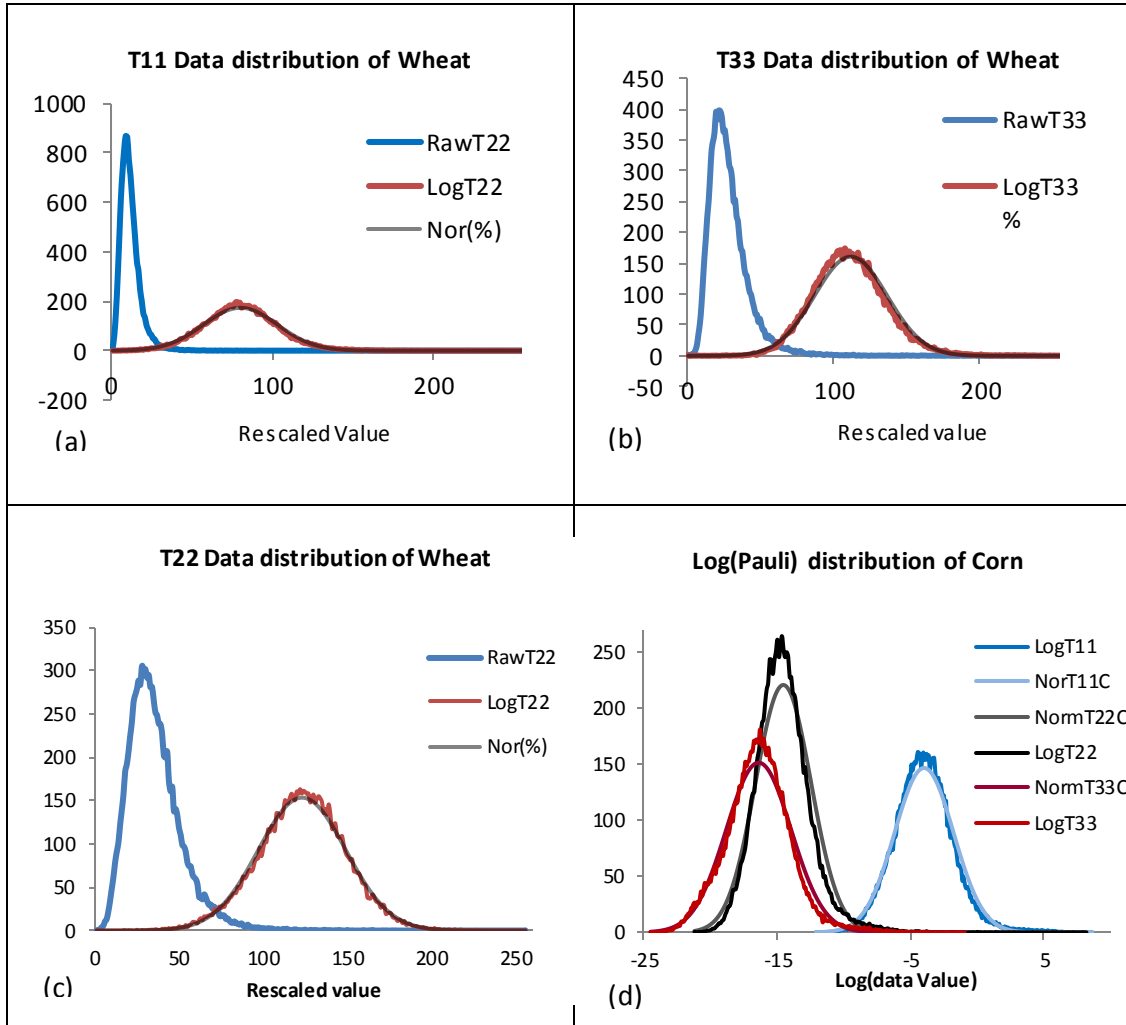


Figure 2.7 Data distributions of wheat from the raw Pauli parameters (blue), logarithm Pauli parameters (red), and simulated normal curve (black) at T11 (a), T22 (b) and T33 (c). (d) Comparison of fitted normal curves and logarithm Pauli parameters histogram curve

(2) MLC Based on Complex Wishart distribution

Complex Wishart distribution MLC is an algorithm proposed by Lee to deal with LU/LC classification using polarimetric SAR data (Lee, et al., 1994). Similar to MLC based on Gaussian distribution, Bayesian probability function is also adopted to determine to classification boundaries. Whereas the likelihood is derived from the probability density

functions of the coherency T3 (or covariance C3) matrix of polarimetric SAR data, named complex Wishart density function. The Wishart distance measure from a pixel to a class m can be simplified as:

$$d(Z, w_m) = n\text{Tr}(C_m^{-1}Z) + n\ln|C_m| - \ln[P(w_m)] \quad (9)$$

Where Z is the covariance matrix of the pixel to be classified, C_m is the average covariance matrix of the m class, n is the number of look. $P(w_m)$ is the priori probability of the class m.

MLC based on complex Wishart distribution has been used in the classification of single polarimetric SAR image. Some researchers investigate its usefulness in multi-frequency polarimetric SAR data classification (Lee et al. 1994). However, few studies have applied the Wishart supervised classifier in multi-temporal polarimetric SAR data classification (Skriver, 2012). Based on the assumption that multi-temporal data are uncorrelated, the joint probability density function will be the product of the probabilities for each image. Therefore the Wishart distance measure for multi-temporal polarimetric SAR classification becomes:

$$D(Z, w_m) = \sum_{j=1}^J n_j [\text{Tr}(C_m^{-1}(j)Z(j)) + \ln|C_m(j)|] - \ln[P(w_m)] \quad (10)$$

Where J is the total number of images. $C_m(j)$ is the average covariance matrix of the m class in the jth image. Z(j) is the pixel's covariance matrix from the jth image.

The comparison between the results generated from MLC based on Complex Wishart distribution and Gaussian distribution will be explained in the Results Analysis and Discussions section.

2.3.4 Post-classification Processing

Due to the serious speckle effects in SAR images, the preliminary classification results are not always satisfactory, no matter which filters are used to the images in the preprocessing stage. Visually, a small number of isolated, generally poorly classified pixels are often located at the boundaries between two clearly assigned areas or within a large classified

area. In order to produce better LU/LC maps, post-classification process is required to reduce those isolated misclassified pixels. Two commonly used post-classification methods are adopted in this study.

(1) Sieve Filter

Sieve filter merges image value polygons smaller than a user specified threshold with the largest neighboring polygon. Because the misclassification introduced by speckles in SAR images were mostly single pixels or small polygons, sieve filter is particularly useful in enhancing SAR image classification results.

(2) Segmentation

The segmentation post-classification method is process to group the pixels in the preliminary classification results into homogenous objects. Firstly, the original SAR images were used to generate homogenous object units using segmentation algorithms. Then the class type for each of the object units in the preliminary classification maps is assigned by the mode class within that object unit.

2.3.5 Classification Accuracy Assessment

(1) Testing Sample Selection

Testing samples are the portions of map that will be selected for accuracy assessment (Russel C., & Kass G., 1999). To generate a statistically valid and appropriate assessment for classification results, two vital factors should be taken into consideration. One is the sample size and the other is the method of testing sample selection. Firstly, adequate number of samples per class should be gathered so that the assessment is statistically valid. Secondly, the distribution and proportion of each class should also be fully considered while choosing sampling methods.

Usually, in urban areas where the classification maps less homogeneous than rural areas, the single pixel unit or clusters of pixel units are chosen as testing samples. In order to

obtain enough number of randomly distributed testing samples, which is a basic requirement for most assessments (Jenson, 2005), a compromising method is to select a homogeneous cluster of pixels around each of the randomly distributed points.

In rural areas where are mainly dominant by homogenous crop fields, polygons are the most common sample units. The testing samples and training samples should be exclusive, even if they are derived from the same ground truth data.

(2) Error Matrix

The error matrix is the most widely accepted measure for LU/LC mapping (Russel C., & Kass G., 1999). As defined by Russel, “An error matrix is a square array of numbers set out in rows and columns that expresses the number of sample units assigned to a particular category in one classification relative to the number of sample units assigned to a particular category in reference data”. It is a very effective way to present errors of omission and commission for individual classes. In addition, the error matrix can be used to calculate other accuracy measures, such as such as overall accuracy, Kappa accuracy, producer’s accuracy, and user’s accuracy.

Overall accuracy (OA) is simply the sum of the correctly classified sample units divided by the total number of sample units in the entire error matrix. Producer’s accuracy (PA) describe the accuracy of individual class from map producers’ perspective. PA for each category is performed through dividing the number of correct sample units by the total number the reference data in that class. “User’s accuracy” (UA) is defined from the map users’ perspective. It is computed by dividing the number of correct sample of one class by the total number of samples classified to that class in the map. Kappa can be used to determine if the values contained in an error matrix represent a result significantly better than random (Jensen 2005). Usually, while the OA is the same for two classification result, the one with higher the Kappa has better the classification accuracy.

2.4 Results Analysis and Discussions

This study was conducted following the processing introduced in the Methodology section.

(1) Preprocessing

The preprocessing of multi-temporal RADARSAT-2 datasets were conducted in PolSARpro software. Pauli, Freeman-Durden, and H/Alpha/A polarimetric decomposition parameters were generated from coherency T3 matrix and covariance C3 matrix. Gaussian filter at the window size of 5 was then applied to each of the decomposition parameters. The filtered decomposition parameters from each image was finally geometrically corrected and resampled into 10 meter resolution datasets, using a DEM data though MapReady tool kit.

(2) Training Samples Selection

In order to provide enough sample units for classifier training, over 200 polygons were manually selected, which include 7000 pixels, from the reference and ground truth data (see table 2.2).

Table 2.2 Number of the plots and pixels selected for each LU/LC class in the training groups.

	alfalfa	wheat	hay	peas	soybeans	corn	forest	lawn	CS	RA	CIIA
Plots	3	53	3	6	40	49	10	6	4	26	14
Pixels	45	762	40	71	1849	2397	695	155	158	553	524

CS: construction sites, RA: residential areas, CIIA: commercial/industrial/institutional areas.

(3) Multi-temporal dataset classification

To assess the potential of multi-temporal polarimetric RADARSAT-2 data in urban/rural fringe area mapping, a series of classifications were conducted using different RADARSAT-2 datasets (Figure 2.8). As the Figure shown, the different classification were conducted and compared in terms of different classifiers, polarimetric parameters, time selections and combinations of image dates, as well as different post-classification processing methods.

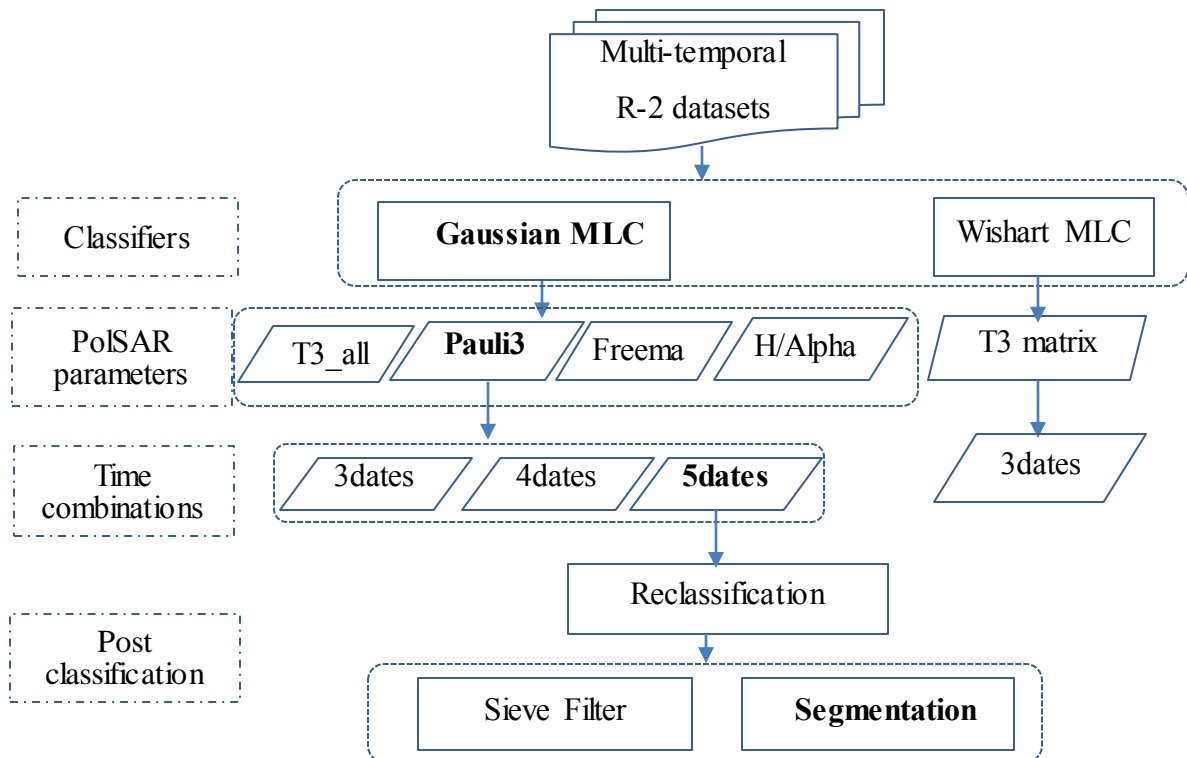


Figure 2.8 An overview of the comparisons among various classification strategies

(4) Testing Samples selection

Nine LU/LC classes, which include five crop types (i.e. forage, wheat, field peas, soybeans, corn) and four non-crop classes (i.e. forest, lawn, construction sites (CS), and built-up areas), were aggregated from the originally eleven detailed classes. To fully assess the classification for each LU/LC class in the fringe areas, two sets of testing samples were selected. For all the classes, 700 random points were generated using the PCI software, and over 500 clusters of more than 7000 pixels were selected around those points as the testing samples (table 2.3). In addition, to test classification results of the five crop types, all the field inventory data except for those selected as training samples were used for testing (table 2.4).

Table 2.3 Number of the plots and pixels selected for five crop types in the testing samples.

class	forage	wheat	peas	soybeans	corn
fields surveyed	23	44	3	63	57
pixels per class	6175	42200	6037	69311	76583
% of total	3%	21%	3%	35%	38%

Table 2.4 Number and percentage of pixels selected for the testing samples of all LU/LC classes

	forage	wheat	peas	soybean	corn	Bups	CS	forest	lawn
Pixels #	79	765	72	1859	2395	1079	159	698	161
Class%	1%	11%	1%	26%	33%	15%	2%	10%	2%

CS: construction sites, Bups: Built-ups

(4) Accuracy Assessment

Finally, error matrix for each of the classification results was generated to assess the classification accuracy. The advantages and disadvantages of each classification method are analyzed and discussed based on the error matrix and LU/LC maps in the following sections.

2.4.1 Training Data Analysis

To briefly analysis the separability of different classes, the responses of polarimetric parameters to different land surface at different images are analyzed. Based on the training sample units, the mean values and standard deviations of the polarimetric parameters in each image for every LU/LC class have been extracted.

(1)Pauli Decomposition Parameters

The temporal profiles of Pauli decomposition parameters (T11, T22, and T33) of RADARSAT-2 data for the six crop types were shown in Figure 2.6. Generally, T11 represents the surface scattering, and T33 indicates the volume scattering. In T11 parameter, the separability of various crops is higher in May 4th and June 21st than that in the other dates. However, in both T22 and T33 parameters, the May 28th, July 15th, and Sept. 1st dates' data provide higher separability among various crops.

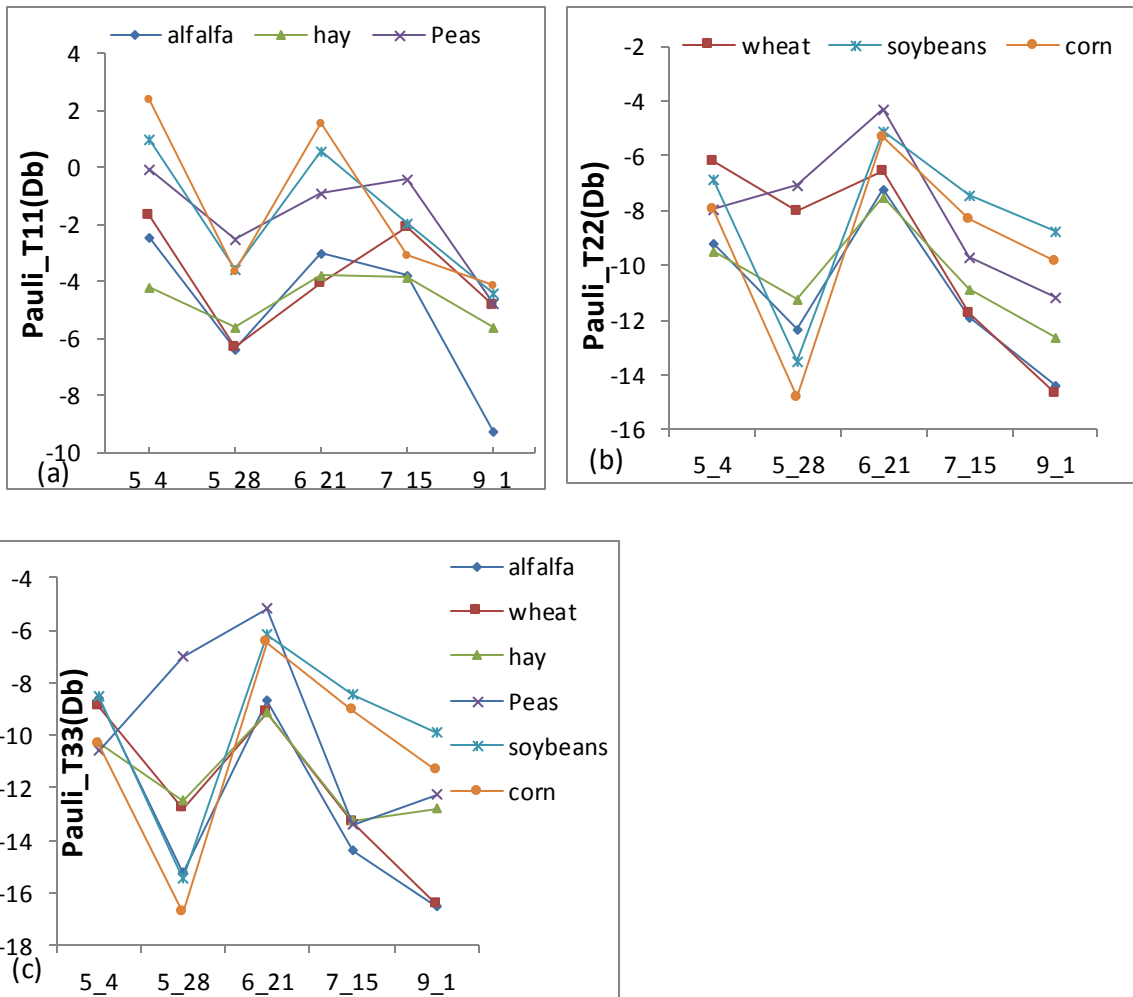


Figure 2.9 Temporal profiles of Pauli decomposition parameters value for various crop types in Pauli T11 single bounce (a), Pauli T22 double bounce (b), and Pauli T33 volume scattering(c).

For each crop type, the separability varies from parameter to parameter and image to image. For example, peas can be easily separated from other crops using T33 on the May 28th date image alone. The mean T33 value of peas is at least 6 dB higher than those of the other crops. The curves of the wheat, hay, and alfalfa at T11 are very close to each other, but greater difference is observed between the wheat and hay at T22 on May 28th and also between the hay and alfalfa at T33 on Sept. 1st. The curves of corn and soybeans are particularly different from those of other crops. The sharp increase of double bounce (T22)

and volume (T33) scattering from May 28th to June 21st is corresponding to the rapid growth of soybeans and crop. Before May 28th, the SAR backscattering from the fields of soybeans (height<15cm) and crop (height<20cm) was dominated by the soil. However, since June 21st, the fields were fully covered by soybeans plants (height >25cm) and corn plants (height>70cm).The marginal difference is observed between the soybeans and crop at T22 and T33, which might lead to the misclassification of them.

(2)Freeman-Durden and H/Alpha/A Decomposition Parameters

The values of Freeman-Durden decomposition parameters indicate the contributions of different scattering mechanisms, such as double-bounce, volume, and odd-bounce scattering mechanisms. In Figure 2.10(b), the mean values of Freeman volume scattering are close to each other for most classes, but at double and odd bounced scatterings, the differences between the mean values among different classes are more significant. Figure 2.10 (a) shows that the separability of H/Alpha/A parameters between crop and non-crop types is much larger than that among crops.

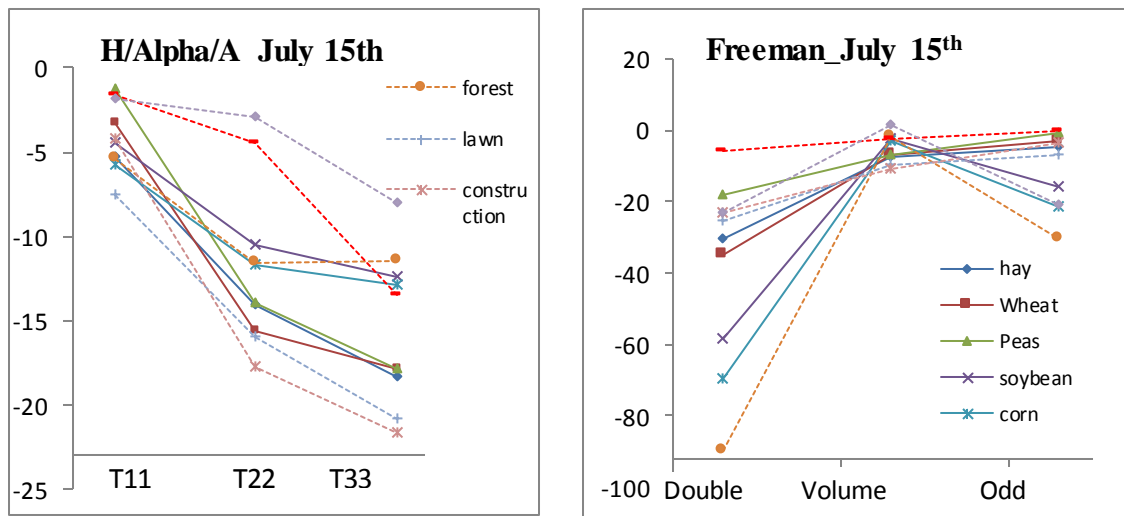


Figure 2.10 H/Alpha/A (a, T11, T22, T33 scattering value in dB) and Freeman decomposition parameters (b, Double Volume and Odd scattering value in Db.) from ten LU/LC classes.

2.4.2 Classification Results Using Gaussian and Wishart

The classification results using Gaussian distribution (Gaussian) are better than those using complex Wishart distribution (Wishart). Gaussian method generates a better classification results mainly in non-crop classes. For example, considering the nine LU/LC classes, the results given by Gaussian are 86.3% (OA) and 0.83(Kappa), but those given by Wishart are 78.4% (OA) and 0.73 (Kappa).

However, in terms of crop classification accuracy, Gaussian is slightly superior to Wishart. Using the five main crop type testing samples, the assessment results show that Gaussian is merely 1%(OA) and 0.01(Kappa) better than Wishart.

The results revealed that the Gaussian is more suitable than complex Wishart for LU/LC classification in urban/rural fringe areas with various crop and non-crop LU/LC classes.

2.4.3 Classification Results Using Different Polarimetric SAR Parameters

To fairly compare the classification accuracy using different polarimetric parameters, the same Gaussian MLC classifier was adopted. Classification results using four sets of decomposition parameters (i.e. coherency matrix, Pauli, H/Alpha/A, and Freeman) were compared respectively.

(1) Coherency Matrix and Pauli Decomposition Parameters

Pauli decomposition parameters (Pauli3) are consisted of the diagonal elements of coherency matrix (T3all). Classification results show that Pauli3 outperforms T3all, although T3all contains more polarimetric information than Pauli3.

The classification accuracies using Pauli3 (in red) and T3all (in blue) parameters from the same four-date datasets. Overall, the results given by Pauli3 is 89 %(OA) at 0.87 (Kappa), while those by T3all is only 84.8 %(OA) at 0.81 (Kappa). Specifically, for most crops (hay, wheat, and peas) and other vegetation types, such as forest, the Pauli3 gives higher accuracy than T3all in either producer's or user's accuracy.

The comparison reveals that diagonal parameters in the Pauli decomposition parameters contain the most useful polarimetric information in T3 matrix. The other off-diagonal elements in the T3 matrix introduced more noise rather than useful information to the classification.

(2) Freeman-Durden and H/Alpha/A Decomposition Parameters

The classification results using H/Alpha/A decomposition parameters are better than those yielded by Freeman decomposition, but were much worse than those using the Pauli decomposition parameters. The OA given by H/Alpha/A was 84.1% at 0.79 (Kappa), while those accuracies achieved by Freeman were merely 76.9 % (OA) at 0.71(Kappa).

(3) Separability Analysis of Different Parameters

Among the three polarimetric parameter datasets, the Pauli3 gives the best results, while the Freeman gives the lowest accuracy. The inferior performance of Freeman can be explained by the poor separability among different classes in the decomposed images. According to the concept of feature separation (Cumming and Van Zyl 1989, Shi et al. 1994), features can be separated well if the distance between the class mean values is larger than the standard deviations. Richards (Richards 1987) proposed a criteria, named Bhattacharya distance, to quantitatively measure the separability between two classes, such as in class i and j :

$$S_{i,j} = \frac{|u_i - u_j|}{S_i + S_j} \quad (11)$$

Where u and s are mean value and standard deviation of the classes. The higher the $S_{i,j}$ is, the more useful the feature is in distinguishing class i and j .

Taking the separability between corn and soybeans as an example. In the same image taken on July 15th, the $S_{i,j}$ of Freeman T22, H/Alpha/A T22, and Pauli T22 parameter is 0.09, 0.22, and 0.36 respectively. The classification results also indicates that polarimetric parameters with higher $S_{i,j}$ value, such as Pauli2, generated better results.

2.4.4 Classification Results Using Different Time Combinations

Dataset with high temporal resolution are preferable for LU/LC classification, particularly for crop type's identification. However, due to the limitation of budget, the quality of data, and the image processing ability, selection and combination of multi-temporal data has become especially valuable. In this study, in order to find the optical multi-temporal data combination, images with one to five dates were tested under the same classification procedure.

(1) Overall Trends

Generally, the classification accuracy increases as more dates of images are included in the classification (Table 2.5). The highest accuracy was achieved by using all the **five-date** dataset at 91% (OA) and 0.888 (Kappa). The best classification results generated by **four-date** dataset, 90.1% (OA) and 0.877 (Kappa), was very close to that of five-date one. The classification results given by **three-date** and **two-date** datasets are less satisfactory, with the highest OA of 87.8% and 83.3% respectively. The best result generated by **one-date** data is as low as 62.4% (OA).

The greatest enhancement of classification accuracy (over 20%) is observed from **one-date** datasets to **two-date** ones. Less than 1% increase in OA is observed from the highest **four-date** datasets to **five-date** one, which indicates that a well-selected **four-date** datasets is preferable than **five-date** one.

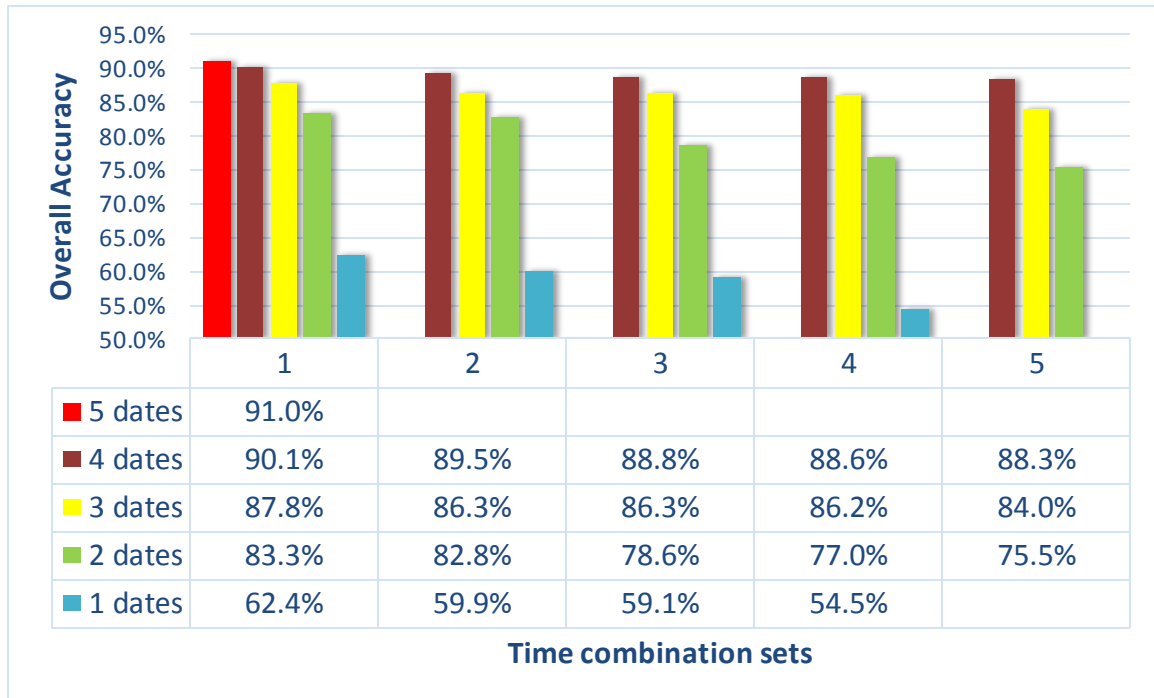


Figure 2.11 the classification result using different time combination ranking by classification OA from highest to lowest.

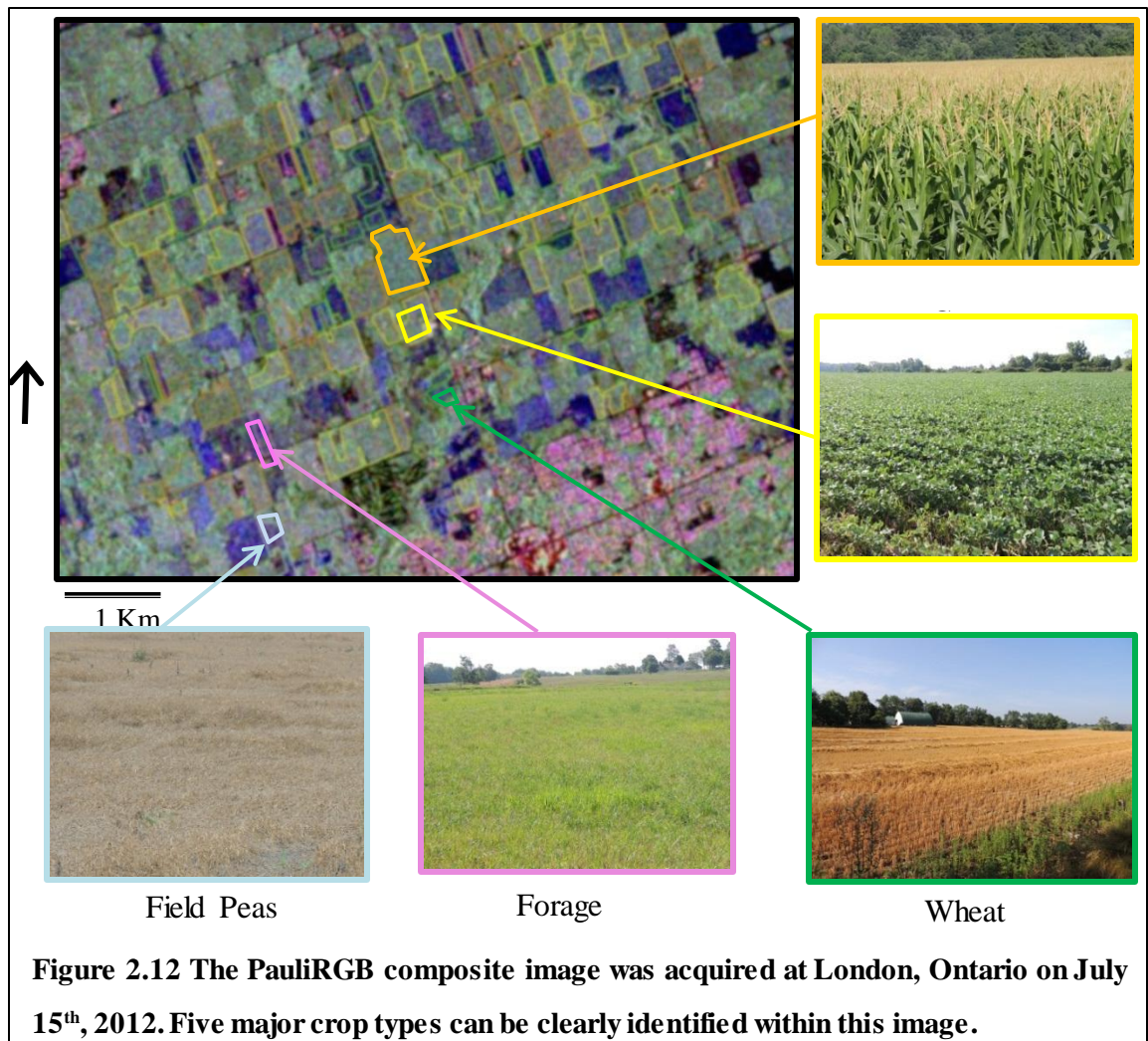
(2) Four-date Dataset

The overall accuracy of four-date dataset varies from 88.3% to 90.1%. Among these four-date combinations, datasets without May 28th (528) or July 15th (715) date image give the lowest overall accuracy. In other words, the May 28th and July 15th images contained the most useful information in multi-temporal classification. By referencing to the ground truth, the greatest separability among various crops was also observed on those two periods, particularly in Mid-July, 2012.

Table 2.5 The classification results from four-date data by different combinations

	May 4	May 28	June 21	July 15	Sep.1	overall	kappa
4 dates						90.1%	0.877
						89.5%	0.869
						88.8%	0.86
						88.6%	0.858
						88.3%	0.855

As Figure 2.12 shows, in the Mid-July, 2012, crops in Southwestern Ontario were in different growing stages. Most wheat was harvested, while forage grew very well. Field peas were withered and dry. The soybeans plants could just cover the soil, and started flowering. Corn had begun tasseling, but some of them were already as tall as 200cm.



(3) Three-date Datasets

The overall accuracy of three-date dataset varies from 87.8% to 84.0%. As the [table\(\)](#) shows, the classification results given by images obtained in early and middle growing seasons (May to July) are relatively better than that of the late seasons. For example, the OA given by the 504_528_715 dataset is 3.8% higher than that given by 621_715_901. In the early growing seasons, as most crops have not been planted yet, non-crop vegetation and other built-ups classes can be identified more easily. In the late crop growing season,

some harvested and unrealed crop fields might still be confused, due to various kinds of residues.

Table 2.6 The classification results from three-date data by different combinations

	May 4	May 28	June 21	July 15	Sep.1	overall	kappa
3 dates						87.8%	0.849
						86.3%	0.83
						86.3%	0.83
						86.2%	0.83
						84.0%	0.801

In sum, a wise selection and combination of multi-temporal data sets, instead of using more dates of images, is an economic and effective method to increase the classification accuracy. As the study show, satisfactory classification OA (over 87%) can be achieved using images from four-date or even three-date datasets, as long as the images at the key seasons were included.

2.4.5 Classification Results Using Different Post-classification Processing Methods

In general, both sieve filter and segmentation methods are effective in enhancing classification accuracy after classification. For example, the overall accuracy of five-date MLC results was 87% before any post-classification processing. The OA increased to 91% and 92% after using sieve filter (Figure 2.15) and segmentation method respectively.

A detailed analysis of each class types reveals that both methods are effective for most classes, but also induced some omission errors in the classification of LU/LC classes with small and fragmentized patches. The forage class is a good example. Because some field areas of forage were so small that were reassigned to their neighboring classes in the segmentation, its producer's accuracy decreased by 40%.

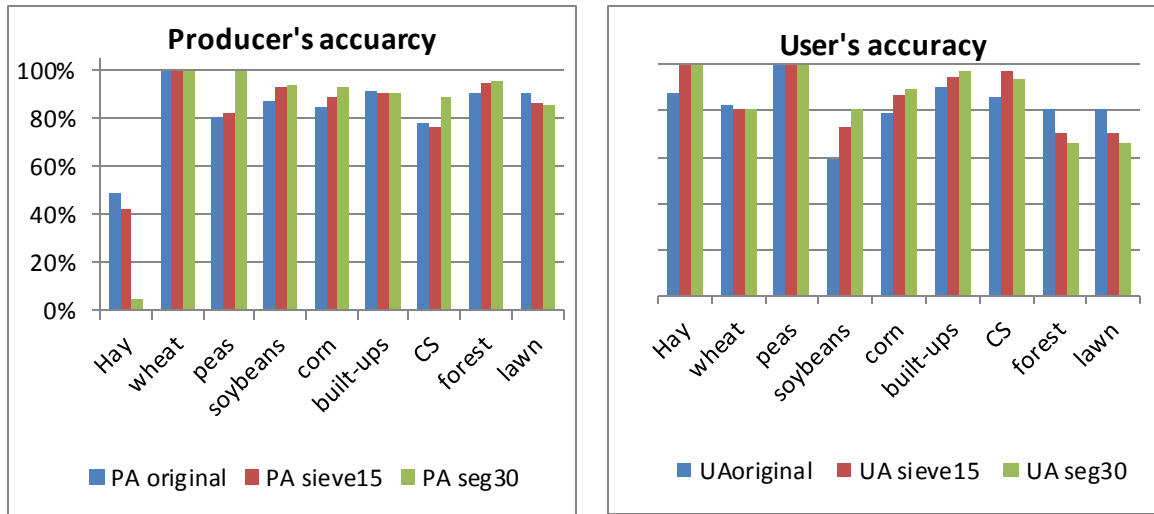


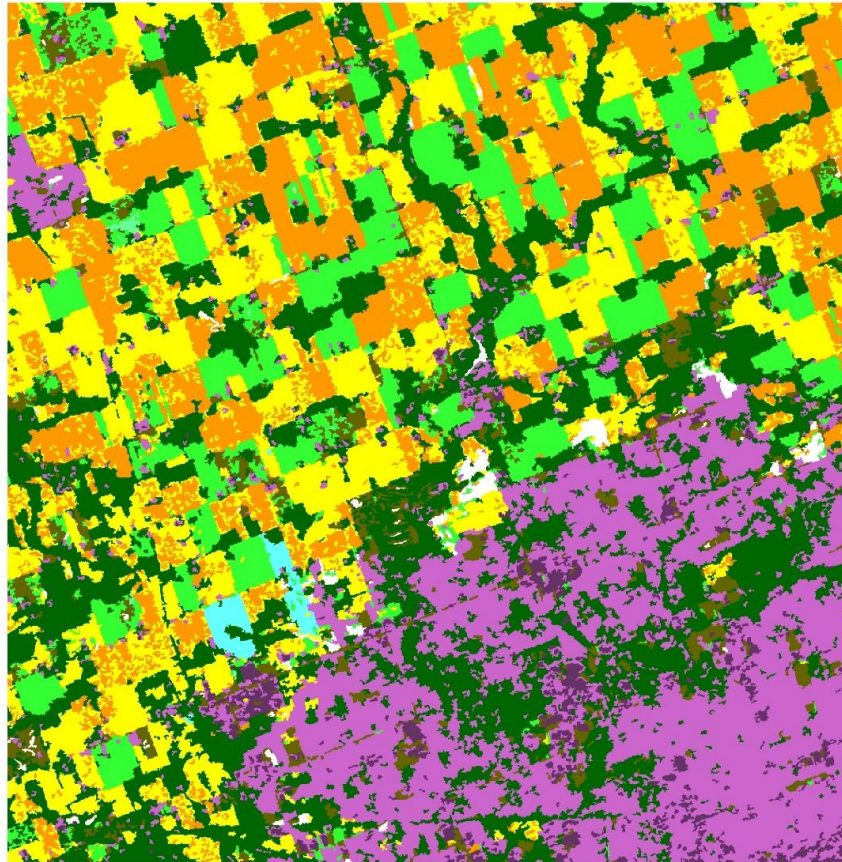
Figure 2.12 Accuracy statistics using different post-classification processing methods

2.5 Conclusions

In sum, the capabilities of multi-temporal polarimetric RADARSAT-2 data for LU/LC classification in urban/rural fringe areas have been well proved and assessed by using the basic MLC supervised classification method in this study.

Generally, LU/LC classes in urban/rural fringe areas can be successfully identified using multi-temporal polarimetric RADARSAT-2 datasets. An accurate LU/LC map of study area has been generated (Figure 2.13). Most non-crop classes and crop types in the rural areas have been well-separated. Within crop-fields, some confusion can still be observed, such as misclassifications between corn and soybeans, wheat and forage. Some construction sites have been successfully detected in the north boundaries of London city, which indicates the happening of urban expansion.

504_528_621_715_901 Pauli3 LU/LC Sieve Map



0 1.5 3 6 9 12 Km

alfalfa	hay	soybeans	residential	high_building	lawn
wheat	peas	corn	construction site		forest

Figure 2.13 LU/LC map of the study area generated by five-date image after sieve filtering

To assess the potential of multi-temporal polarimetric RADARSAT-2 data, four aspects of classification have been evaluated: classifiers, decomposition parameters used for classification, time combinations of images, and post-classification processing methods. The major findings of this study are as follows.

(1) Gaussian is more suitable than complex Wishart based MLC for LU/LC classification in urban/rural fringe areas with various crop and non-crop LU/LC classes.

(2) An appropriate decomposition method is essential for polarimetric RADARSAT-2 classification. Using Pauli decomposition parameters, the overall accuracy increased by 12% than that using Freeman-Durden decomposition parameters.

(3) Using the same classification method, the accuracy can still be significantly improved through carefully selecting and combining multi-date images. Although more dates can obtain slightly higher accuracy, satisfactory classification accuracies (over 87%) have been achieved using images from three dates, as long as the images at the key seasons were included.

(4) A right post-classification processing method is also useful in improving the classification results. In this study, the overall accuracies of classification results have been improved by 5% and 4% by using segmentation and filter post-classification processing method, respectively.

The classification procedure provided in this study might have significant applications in annual crop inventory, or LU/LC change detection in urban/rural fringe areas.

2.6 Reference

- Chen, Z., Wang, J., 2008. A new method for minimizing topographic effects on RADARSAT-1 images: an application in mapping human settlements in the mountainous Three Gorges Area, China. *Canadian Journal of Remote Sensing*, Vol. 34, No. 1, pp. 13-25.
- Cloude, S. R. and E. Pottier (1996). "A review of target decomposition theorems in radar polarimetry." *Geoscience and Remote Sensing, IEEE Transactions on* 34(2): 498-518.
- Cloude, S. R. and Pottier, E., 1997. An entropy based classification scheme for land applications of polarimetric SAR. *IEEE Transactions on Geoscience and Remote Sensing*, 35(1).
- Cover, Thomas M.; Thomas, Joy A. (2006). *Elements of Information Theory*. John Wiley and Sons. p. 254.
- Cumming, I.G. and Van Zyl, J.J., 1989, Feature utility in polarimetric radar image classification. In *Proceedings of IGARSS'89, Vancouver, Canada* pp. 1841–1846.
- Dan Wang, Hui Lin, Jinsong Chen, Yuanzhi Zhang & Qiwei Zeng (2010): Application of multi-temporal ENVISAT ASAR data to agricultural area mapping in the Pearl River Delta, *International Journal of Remote Sensing*, 31:6, 1555-1572, *IEEE Journal of Selected Topics in Applied Earth Observations and Remote*.
- Desnos Y.-L., Laur H., Lim P., Meisl P., and Gach T., "The ENVISAT-1 advanced synthetic aperture radar processor and data product," in *Proc. IGARSS'99, Hamburg, Germany, July 1999*.
- Esch, T., Thiel, M., Schenk, A., Roth, A., Muller, A., & Dech, S. (2010). Delineation of urban footprints from TerraSAR-X Data by analyzing speckle characteristics and intensity information. *IEEE Transactions on Geoscience and Remote Sensing*, 48, 905–916.
- Freeman, A. and Durden, S. L., 1998. A three-component scattering model for polarimetric SAR data. *IEEE Transactions on Geoscience and Remote Sensing*, 36(3), pp. 963-973.

- Hu, H., and Y. Ban. 2008a. "Urban Land Use / Land-Cover Mapping with High-Resolution SAR Imagery by Integrating Support Vector Machines into Object-Based Analysis." In SPIE Conference on Remote Sensing for Environmental Monitoring, GIS Applications, and Geology VIII, vol. 7110, 71100K1-8, Cardiff, September 15–18, edited by U. Michel, D. L. Civco, M. Ehlers and H. J. Kaufmann. Bellingham, WA: SPIE.
- J. W. Goodman, "Some fundamental properties of speckle," *J. Opt. Soc. Amer.*, vol. 66, no. 11, pp. 1145–1150, Nov. 1976.
- Jensen, J. R. (2005). *Introductory digital image processing: a remote sensing perspective*. (3rd ed.). Upper Saddle River, NJ: Pearson Education Inc.
- land cover (LULC) and irrigated area mapping using continuous streams of MODIS data. *Remote Sensing of Environment*, 95, 317–341.
- Lee, J. S. (1981). "Speckle analysis and smoothing of synthetic aperture radar images." *Computer graphics and image processing* 17(1): 24-32.
- Lee, J. S., M. R. Grunes, et al. (1994). "Classification of multi-look polarimetric SAR imagery based on complex Wishart distribution." *International Journal of Remote Sensing* 15(11): 2299-2311.
- Lee, J.S., and Pottier, E. 2009. *Polarimetric radar imaging: from basics to applications*. Taylor & Francis Group, New York.
- Leinenkugel, P., T. Esch, et al. (2011). "Settlement detection and impervious surface estimation in the Mekong Delta using optical and SAR remote sensing data." *Remote Sensing of Environment* 115(12): 3007-3019.
- Li, J., Chen, W., Touzi, R. Optimum RADARSAT-1 configurations for wetlands discrimination: A case study of the Mer Bleue peat bog (2007) *Canadian Journal of Remote Sensing*, 33 (SUPPL. 1), pp. S46-S55.
- Li, X., & Yeh, A. G. (2004). Multitemporal SAR images for monitoring cultivation systems using case-based reasoning. *Remote Sensing of Environment*, 90, 524–534.

- López-Martínez, C., Ferro-Famil, L., and Pottier, E., 2005. PolSARpro v4.0 Polarimetry Tutorial.
- McNairn, H., C. Champagne, et al. (2009). "Integration of optical and Synthetic Aperture Radar (SAR) imagery for delivering operational annual crop inventories." *Isprs Journal of Photogrammetry and Remote Sensing* 64(5): 434-449.
- Niu X., & Ban Y.F., (2013): Multi-temporal RADARSAT-2 polarimetric SAR data
- Palubinskas, G., A. Makarau, et al. (2011). Multi-sensor remote sensing information fusion for urban area classification and change detection. *Multisensor, Multisource Information Fusion: Architectures, Algorithms, and Applications* 2011. Bellingham, Spie-Int Soc Optical Engineering. 8064. pp. 68-78.
- Panigrahy, S., Jain, V., Patnaik, C., Parihar, J.S. Identification of Aman Rice Crop in Bangladesh Using Temporal C-Band SAR - A Feasibility Study (2012) *Journal of the Indian Society of Remote Sensing*, 40 (4), pp. 599-606.
- Qi, Z.; Yeh, A.G.; Li, X.; Lin, Z. Land Use and Land Cover Classification Using RADARSAT-2 Polarimetric SAR Image. In *Proceedings of the ISPRS Technical Commission VII Symposium: 100 Years ISPRS Advancing Remote Sensing Science*, Vienna, Austria, 5–7 July 2010; In *International Archives of Photogrammetry, Remote Sensing and Spatial Information Sciences*, Volume XXXVIII, Part 7A, pp. 198-203.
- Richards, J.A., Woodgate, P.W. and Skidmore, A.K., 1987, An explanation of enhanced radar backscattering from flooded forests. *International Journal of Remote Sensing*, 8, pp. 1093–1100.
- Robert A. Schowengerdt, Chapter 9 - Thematic classification, *Remote Sensing* (Third edition), Academic Press, Burlington, 2007, Pages 387-456, XXVII-XXXIII, ISBN 9780123694072, 10.1016/B978-012369407-2/50012-7.
- Roberts, D. A., Keller, M., & Soares, J. V. (2003). Studies of land-cover, land-use, and biophysical properties of vegetation in the large scale biosphere atmosphere experiment in Amazonia. *Remote Sensing of Environment*, 87, 377–388.

- Rogan, J., and D. Chen (2004). "Remote sensing technology for land cover and land use mapping and monitoring." *Progress in Planning*, 61(4):301-325. *Sensing (J-STARS)*, 4 (2), 423- 431.
- Russel C., and Kass G.(1999). *Assessing the accuracy of remotely sensed data: principles and practices*. CRC Press,
- Saatchi, S. S., Soares, J. V., & Alves, D. S. (1997). *Mapping deforestation and land use in*
- Shang, J., Champagne, C., and McNairn,H.(2006).Agriculture land use using multi-sensor and multi-temporal Earth Observation data. *Proceedings of the MAPPs/ASPRS 2006 Fall Specialty conference*, San Antonio, Texas, USA.
- Shang, J., McNairn,H., Champagne, C., and Jiao X.F. (2009)Contribution of multi-frequency, multi-sensor, and multi-temporal radar data to operational annual crop mapping. *International Geoscience and Remote Sensing Symposium*, Boston,7-11 July 2008,4 pp. Invited paper.
- Shi, J., Dozier, J. and Rott, H., 1994, Snow mapping in Alpine regions with Synthetic Aperture Radar. *IEEE Transactions on Geoscience and Remote Sensing*, 32, pp. 152–158.
- Skriver, H. (2012). "Crop Classification by Multitemporal C-and L-Band Single-and Dual-Polarization and Fully Polarimetric SAR." *Geoscience and Remote Sensing, IEEE Transactions on* 50(6): 2138-2149.
- Thenkabail, P. S., Schull, M., & Turrall, H. (2005). *Ganges and Indus river basin land use/*
- Ulaby, F. T., Kouyate, F., Brisco, B., & Williams, T. H. L. (1986). Textural information in SAR images. *IEEE Transactions on Geoscience and Remote Sensing*, 24, 235–245.
- Weber, F., Nixon, D., Hurley, J.Semi-automated classification of river ice types on the Peace River using RADARSAT-1 synthetic aperture radar (SAR) imagery (2003) *Canadian Journal of Civil Engineering*, 30 (1), pp. 11-27.

Zhu, Z., C. E. Woodcock, et al. (2012). "Assessment of spectral, polarimetric, temporal, and spatial dimensions for urban and peri-urban land cover classification using Landsat and SAR data." *Remote Sensing of Environment* 117: 72-82.

Chapter 3

3 Sensitivity of RADARSAT-2 Polarimetric SAR Data to Normalized Difference Vegetation Index and Crops Height

3.1 Introduction

3.1.1 Background

Agriculture plays a critical role in Canada's economy, and accounts for more than 8% of Canada's Gross Domestic Product (Longtin, 2006). The timely information on agricultural land use and land management, the estimation and prediction of crops yields are essential for the agriculture and economic suitability.

Remote Sensing technology has the capability of providing timely and wide coverage of land surface information at a range of spatial and temporal scales. Thus, space borne or airborne Remote Sensing images have been widely used in agricultural applications, such as crop type inventory, crop health, soil analysis, crop condition monitoring and even yield prediction.

Traditionally, agricultural survey and crop condition monitoring is mainly depended on in situ measurement, and thus used to be time and labor consuming. Currently, with the development of Remote Sensing techniques, the plant biological parameters observed in the field, can also be derived from remotely sensed data, and extend to a wide area ().

Optical Remote Sensing data have been primarily used to extract vegetation index, such as Normalized Difference Vegetation Index (NDVI), Perpendicular Vegetation Index (PVI), Soil Adjusted Vegetation Index (SAVI), and Transformed Soil Adjusted Vegetation Index (TSAVI) (). These indices are provided to be sensitive to canopy characteristics such as Leaf Area Index (LAI) or plant biochemical constituents (), and thus are useful in crop condition monitoring, and biomass estimation, or even yield prediction.

Vegetation indices (VI), such as Normalized Difference Vegetation Index (NDVI), Perpendicular Vegetation Index (PVI), Soil Adjusted Vegetation Index (SAVI), and Transformed Soil Adjusted Vegetation Index (TSAVI), are important biophysical parameters for monitoring vegetation growth. These indices are provided to be sensitive to canopy characteristics such as Leaf Area Index (LAI) or plant biochemical constituents. Tracking VI change through the growing season is critical for crop growth modeling and yield forecast. Conventionally, optical data have been widely used to calculate VI (Liu et al, 2012). However, due to unfavorable weather conditions, optical sensors cannot meet the time requirement when information on key growth stages is needed.

3.1.2 Previous Studies

Synthetic Aperture Radar (SAR) sensors are able to transmit microwaves through the haze and clouds, and therefore offer an alternative data source. Different from traditional optical data, SAR signals respond to the crop structure (size, shape, and orientation of leaves, stalks, and fruits), the dielectric properties of the canopy, as well as the roughness and moisture of the underlying soil (McNairn et al. 2009a, Steffen et al., 2012). Meanwhile, the crop structure and water content are indicative of each crop type in various growth stages and crop conditions. The existence of the connection between the SAR signals and crops parameters has been proved by previous researches (McNairn et al. 2004). However, how robust the connections are has not yet been fully explored.

SAR data acquired at different frequency bands have different transmission abilities, and thus are sensitive to different plants' properties at different components' scales (Lopez-Sanchez et al.2009). The selection of SAR sensors for agricultural applications is highly dependent on the crop types and objectivities. Indeed, many successes have resulted from using multi-frequency SAR data in a wide range of agricultural applications, such as crop-type mapping (McNairn et al. 2009b, Shang et al.2009), crop condition monitoring (Ferrazzoli et al. 1997, Paloscia S 1998), and soil moisture retrieval (Lievens et al. 2011). Baghdadi et al. investigated the potential of TerraSAR-X, ASAR/ENVISAT and PALSAR/ALOS for monitoring sugarcane crops, and results show that cross polarizations at long radar wavelengths are mostly sensitive to the changes in sugarcane crops' height and NDVI early in the growing stages (Baghdadi et al. 2009). The C band SAR data was

proved to be appropriate for biomass estimation of crops such as colza, wheat, alfalfa, and soybeans (Ferrazzoli et al. 1997). Compared to L and P band SAR data, C band has a relatively short wave, and thus is less able to penetrate into crop plants with large biomass. Therefore, the sensitivity of C band SAR data to crop biomass is also restricted by the presence of signal saturation effects of other crops, such as the corn and sugarcane (McNairn et al. 2000).

Multipolarization SAR data provide more information about crop growing conditions than the single polarization data set. The potential of single polarization SAR data in crop monitoring was well explored in the previous studies. For example, strong correlations have been reported between HH polarization backscattering values from multitemporal RADARSAT data and plant height, age, and biomass of rice (Shao et al. 2001, Li et al. 2003, Chakraborty et al. 2005). However, the sensitivity of the wave polarization to the orientation, shape and dielectric properties of the plants is less studied. Recently, as more Quadpol polarization data are provided by satellites such as C band RADARSAT-2, PAISAR L band ALOS, and X band TerraSAR sensors, increasing number of studies have focused on the application of multi-polarization data in crop conditions monitoring. For instance, studies show that for both corn and soybeans, significant correlation has been reported between volume scattering indicative RADARSAT-2 Quadpol parameters and the LAI (Jiao et al. 2011). In addition, Steffen et al compared TerraSAR-X Quadpol backscattering with RapidEye multispectral vegetation indices over rice fields, and the results showed that significant correlations are found between VV and cross-polarized images and the modified chlorophyll absorption ratio index/second modified triangular vegetation index(MCARI/MTVI2) on an object basis (Steffen et al.,2012).

The temporal and spatial dimensions of remotely sensed data are also critical to certain agricultural applications, such as crop phenological stages monitoring, and plant pathology detection (Lopez-Sanchez et al.2009). Most of the crops in North America change rapidly in the summer season, when weather conditions are optimal. Also, the variation of crops in the same field is sometimes significant. As the results in a campaign in 2007 showed, variations of 20% in LAI, 20% in vegetation height and 40% in biomass were measured within the same corn fields (Gerighausen et al., 2007). Therefore, high temporal and spatial

resolution of remotely sensed data is necessary for accurate farming and time critical agricultural applications. Several newly launched SAR sensors, such as RADARSAT-2 and TerraSAR, have short revisit intervals and fine spatial resolution, and thus are able to provide great opportunity for these applications.

3.1.3 Objectives

The objectives of this study are to investigate the potential of RADARSAT-2 polarimetric SAR data in monitoring crops growth conditions of wheat, peas, soybeans and corn in Southwestern Ontario.

3.2 Study Areas and Data Description

3.2.1 Study Area

The study site is in Middlesex County, Ontario, Canada (43 ° 02 N, 81 ° 19 W), one of the most agriculturally productive areas in Ontario, Canada. The terrain is generally flat. The soils are mainly Huron Lobe Glacial till with loamy and clayey texture, and some stratified sand, and gravel along the rivers. The climate is ideal for farming, with plenty of sunshine and precipitation. Metrology data show that, during most of the crop growing season from May to September in 2012, the average monthly temperature ranged from 13 °C to 20 °C, and the monthly precipitation was 82 to 87 cm. In that same time, the mean relative humidity at 3pm was 55%-60%, and monthly total hours of bright sunshine was 221 – 262 hours. The main crops in this area include corn, soybeans, wheat, forage, and field peas.

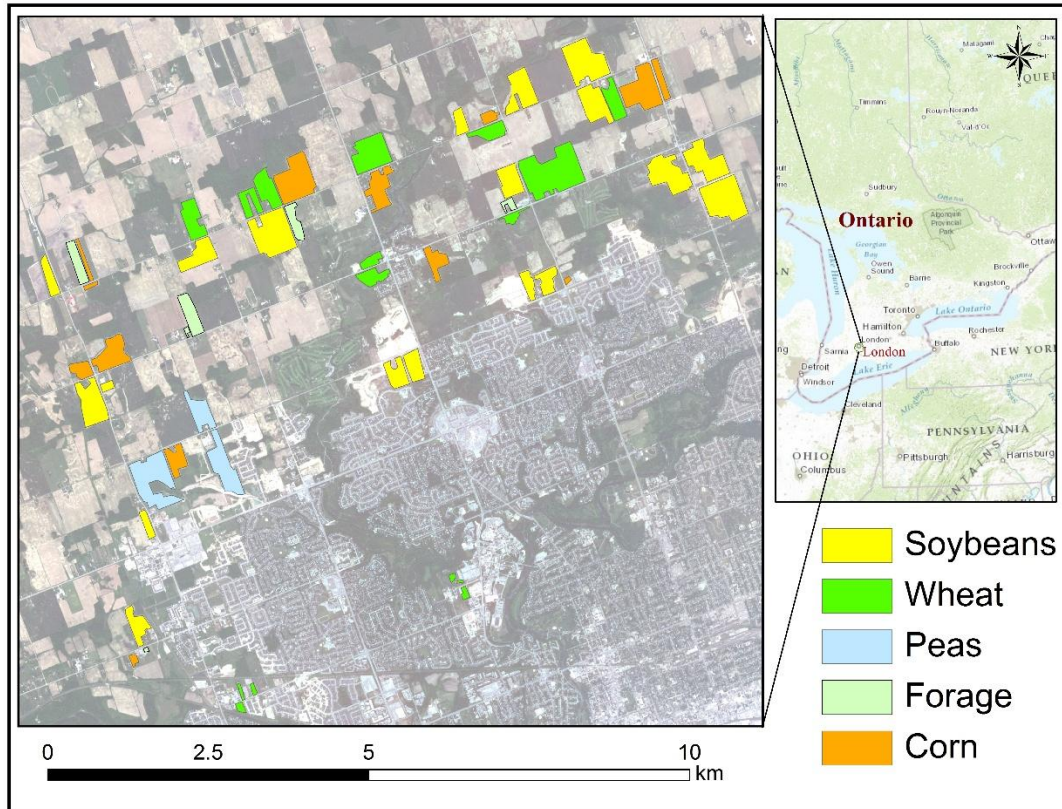


Figure 3.1 Study fields presented on the true color combined RapidEye image

3.2.2 Satellite Data

Two sets of multi-temporal RADARSAT-2 Wide Swath Quad-pol data, FQ7 and FQ21, were acquired over the 2012 growing season. The FQ7 has a steeper incidence angles (25.7° - 27.6°), while those for FQ 21 ranges are much shallower (40.2° - 41.6°). The nominal pixel spacing for the Quad-pol image is 4.7m in range \times 5.1m in azimuth (Table 3.1).

During the same crop growing season, four scenes of RapidEye images were obtained (June 7th, July 20th, August.5th and August 25th). The multispectral RapidEye sensors are particularly useful in vegetation applications because they observe the Earth in a wide spatial range and five spectral bands ranging from 400 to 850nm at 6.5m resolution at nadir.

Table 3.1 Summarizing of Satellite images and acquiring dates

Satellites	RapidEye	R-2 FQ7	R-2 FQ21
Dates		5-04-2012	5-07-2012
d-mm-yyyy	6-07-2012	5-28-2012	5-31-2012
	7-16&24-2012	7-15-2012	7-18-2012
	8-05-2012		8-11-2012
	8-25-2012	9-01-2012	9-04-2012
			9-28-2012

3.2.3 Field Work

The in situ measurements were taken **coincident** with the satellites overpasses. Measurement were conducted on a field-based. The croplands selected in the fields are representative of the main crops in the Southwestern Ontario. As corn, soybeans, wheat are the most common field crop types in this areas, 13 corn, 19 soybeans, and 16 wheat croplands as well as 6 forage and 3 peas' fields were selected, respectively. The polygons for each field were manually drawn from the RapidEye images.

Information investigated from the fields including the field management information, crop phenological stages, height, and general soil conditions. **Height information** is one of the most important characters in describing the plant growing conditions. The plants' heights are usually homogenous for the most of the fields, and thus are measurement by averaging three samples in one fields. As SAR signals might be responsive to the **soil moisture**, the soil wetness are also recorded in each field on every image acquiring date. Soil conditions are briefly measured by hand and recorded in five categories, i.e., dry, slightly moist, moist, wet, and extremely wet.

The meteorological information is very useful in analysis the SAR signal, which is sensitive to the moistures in the land surface. Detailed meteorological information was downloaded from local weather network online. Hourly weather information on the image acquiring date are recoded, such as participation, temperature, wind, and pressure.

3.3 Methodology

The methodology of this study can be separated into three main steps (Figure 3.2): (1) RADARSAT-2 polarimetric data decomposition; (2) NDVI mapping and segmentation; (3) Correlation analysis between crop parameters (height and NDVI) and polarimetric parameters. The detailed concepts and methods are explained below.

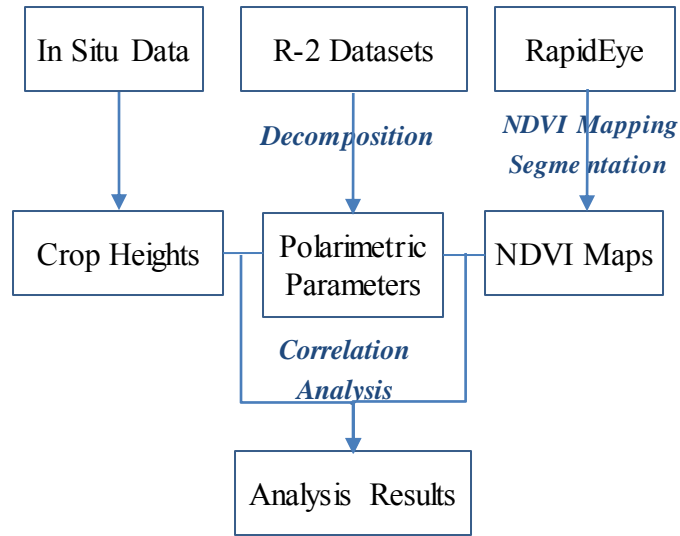


Figure 3.2 The methodology of the data processing and Analyzing

3.3.1 Polarimetric Data Processing

The polarimetric information contained in the RADARSAT-2 is related to the crop parameters, such as crop height, density, moisture, as well as the canopy structures. Using polarimetric decomposition methods, a variety of parameters can be extracted from the original RADARSAT-2 datasets. Different parameters contain different physical meaning, and thus each of them might have different sensitivities to each kind of crops. Among all the polarimetric parameters, the most commonly used one can be separated into two main categories: (1) the basic matrix and intensity ratios; (2) decomposition parameters.

(1) Basic Polarimetric Parameters

T3 coherency and C3 covariance matrix are fundamental matrices, basic on which other decomposition parameters can be derived (Lee and Pottier, 2009). Among all the parameters in T3, the diagonal parameters T11 ($|HH+VV|$), T22 ($|HH-VV|$), and T33 ($|HV|$) contained the most useful polarimetric information. The widely used Pauli Decomposition is based on the T3 matrix. Each of the parameters has clear physical meaning: T11 represents single (odd) bounce scattering, T22 indicates double bounce scattering, and T33 is associated with volume (Lee and Pottier, 2009).

From the C3 matrix, the intensity of different polarization bands can also be easily extracted from the diagonal parameters. C11 ($|HH|$) and C33 ($|VV|$) represent horizontal and vertical polarization band intensities, respectively. C22 ($|HV|$) is similar to T22, which indicates the intensity in volume scattering.

The intensity ratios are also sensitive to the canopy characteristics of different crops at various growing stages. Three main intensity ratios have been studied in this study, including HH/VV, HV/HH, and HV/VV.

(1) Polarimetric Decomposition Parameters

The Freeman-Durden decomposition is a method for fitting a physically based, three-component scattering mechanism model to the polarimetric SAR observations. The three-components scattering mechanism include surface, double-bounce and volume scattering mechanisms (Lee and Pottier, 2009). This approach can be used to determine the dominant scattering mechanisms in the land surface. The crop land, as the plants development, the dominant scattering mechanisms would be change accordingly. Therefore, the decomposition results from Freeman-Durden might related to the crop growing stage and conditions.

(2) H/Alpha/A Decomposition

H/Alpha/A decomposition is an approach proposed by Cloude and Pottier for extracting average parameters from experimental data using a smoothing algorithm based on second-order statistics (Cloude and Pottier, 1996; Cloude and Pottier, 1997). Decomposition parameters are generated from an eigenvector analysis of the coherency matrix T_3 . The eigenvectors describe different scattering processes, and the eigenvalues indicate their relative magnitudes. Among all the parameters, the averaged Alpha angle (α) relates directly to underlying average physical scattering mechanisms. The value of Alpha ranges from 0° to 90° , which indicates the variance of dominant scattering from surface scattering mechanism moving into single scattering by a cloud of anisotropic particles, and finally reaching dihedral scatters. Entropy (H) describes the randomness of the scatter. The anisotropy (A) corresponds to the relative power of the second and third eigenvectors (Lee and Pottier, 2009).

Among the three H, Alpha, A parameters, H has been reported to be most sensitive to the density and randomness of some plants canopy (Lee and Pottier, 2009, McNairn et. al, 2009). The sensitivity of H to crop parameters, such as height and NDVI, has not been fully investigated yet, and thus deserve more studies.

(3) Pedestal Height and Span

Pedestal height is another way of measuring randomness in the scattering. Pedestal height is equivalent to measuring the ratio of the minimum eigenvalue to the maximum eigenvalue. It is an indicator of the presence of an unpolarized scattering component in the received signal, and thus is related to the degree of polarization of a scattered wave (Lee and Pottier, 2009). Span is a measurement of total power by adding all the intensities from different polarization bands.

As the Figure 3.3 show, in this study, all the parameters were extracted from the multi-temporal Radarsat-2 Quadpol data after filtering. After all the decomposition parameters extraction, all parameters images are orthorectified and registered together. All the polarimetric data processing are conducted in the PCI Geomatica 10.3 software and the additional Polarimetric SAR Work Station.

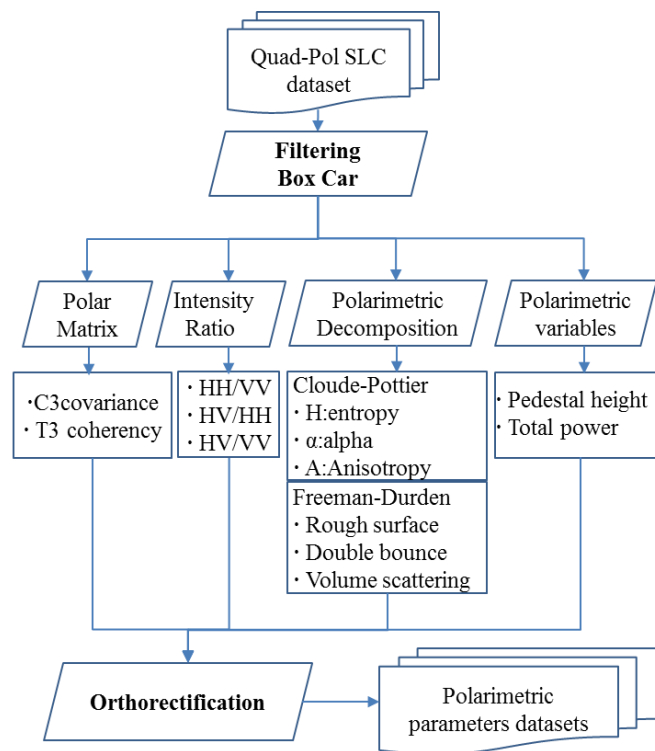


Figure 3.3 Flowchart showing the polarimetric RADARSAT-2 datasets processing

3.3.2 NDVI Calculation

NDVI is one of the most commonly used vegetation indices derived from optical Remote Sensing data. It is calculated from the visible and near-infrared (NIR) light reflected by vegetation (). NDVI is able to reflect the health conditions of vegetation because healthy vegetation absorbs most of the visible light that hits it, and reflects a large portion of the near-infrared light. However, unhealthy or sparse vegetation (right) reflects more visible light and less near-infrared light. The normalized difference between NIR and Red reflectance (Function 3.1) is able to characterize the healthiness of vegetation.

The RapidEye images have a wide coverage of NIR and visible spectral wavelength, and thus has great potential in vegetation indices derivation. However, due to the different atmospheric condition of each image taken at different time, the merely using Digital Number is not accurate enough to derive high quality NDVI maps. Atmospheric Correction is necessary to be conducted on each images, particularly in vegetation monitoring applications, which usually require multi-temporal images over the whole growing seasons. In this study, the atmospheric correction module ATCOR, which is an embedded in PCI software, has been used to do the correction.

Pixel based analysis of the sensitivities between polarimetric parameters and vegetation indices is usually unstable, due to the serious speckle effects in the SAR images.

Therefore, the object unites have been adopted in this study to investigate the relationship between polarimetric SAR parameters and NDVI.

In this study, NDVI maps were segmented into homogenous zones using the multi-resolution algorithm in ECognition software. In addition, as the crop growing conditions various a lot from date to date even within the same crop land, each NDVI map from different images should be segmented independently. The mean values of the NDVI and polarimetric parameters within each of the homogenous zones were extracted for the correlation analysis.

$$NDVI = \frac{\rho_{NIR} - \rho_{Red}}{\rho_{NIR} + \rho_{Red}} \quad (3.1)$$

Where ρ_{NIR} , and ρ_{Red} are the reflectance in NIR, and Red bands.

3.3.3 Correlation Analysis

The most widely used Pearson product-moment correlation coefficient (Pearson's r) is utilized in this study for correlation analysis (Wilcox, 2005). Pearson's r is a measure of the linear correlation (dependence) between two variables X and Y , giving a value between +1 and -1 inclusive.

In this study, take as NDVI example, the Pearson's r between NDVI and SAR parameter is defined as the covariance of the two variables divided by the product of their standard deviations. The absolute value of Pearson's r s are less than or equal to 1. The higher the absolute value of Pearson's r , the stronger correlations between two variables are.

3.4 Results and Discussion

This study was conducted from three aspects as mentioned in methodology section.

(1) The crop height information was measured from each of the cropland at every image acquiring date. The crop phenological information was observed in the field. The vegetation characteristics changes are tracking and analysis based on the field measurements results.

(2) The NDVI maps were first generated from RapidEye maps, and then segmented. Over 1000 objects with mean NDVI values have been extracted for the sensitivity analysis.

(3) A high dimension of polarimetric dataset were derived from the multi-temporal RADARSAT-2 data. Their responses to the vegetation parameters (both height and NDVI) at different image incidence angles (FQ7 and FQ21) were analysis respectively.

Detailed analysis of study results are discussed below.

3.4.1 Field Data Collection

Over 20 times of field work were conducted from early May to the end of September. One of the most important crop information- height, has been carefully recorded (See Appendix 2.4).

(1) Corn and Soybeans

Six stages of corn growing were captured, from the end of May to the end of September: stalk initiation, stalk development, tasseling and flowing, ear development, kernel development, and maturation (Figure 3.4). The height of corn start increasing dramatically in the end of May with corn stalk initiation (20cm) and the growth rate slowed down with corn start initiation in the middle of July (200cm).

For the soybeans, five images taken at the different soybean growing stages are presented in Figure 3.4. The average soybean height varied from 20cm in late June to 70cm in early September. Most soybeans were planted in late May. On June 24th, the 2-trifoliolate was fully developed for the majority of the soybeans. The height of soybeans increased stably through the stages of flowering, bean filling, and reached its climax when leaves began shedding in early September, and decreased by 5cm when the soybeans matured.

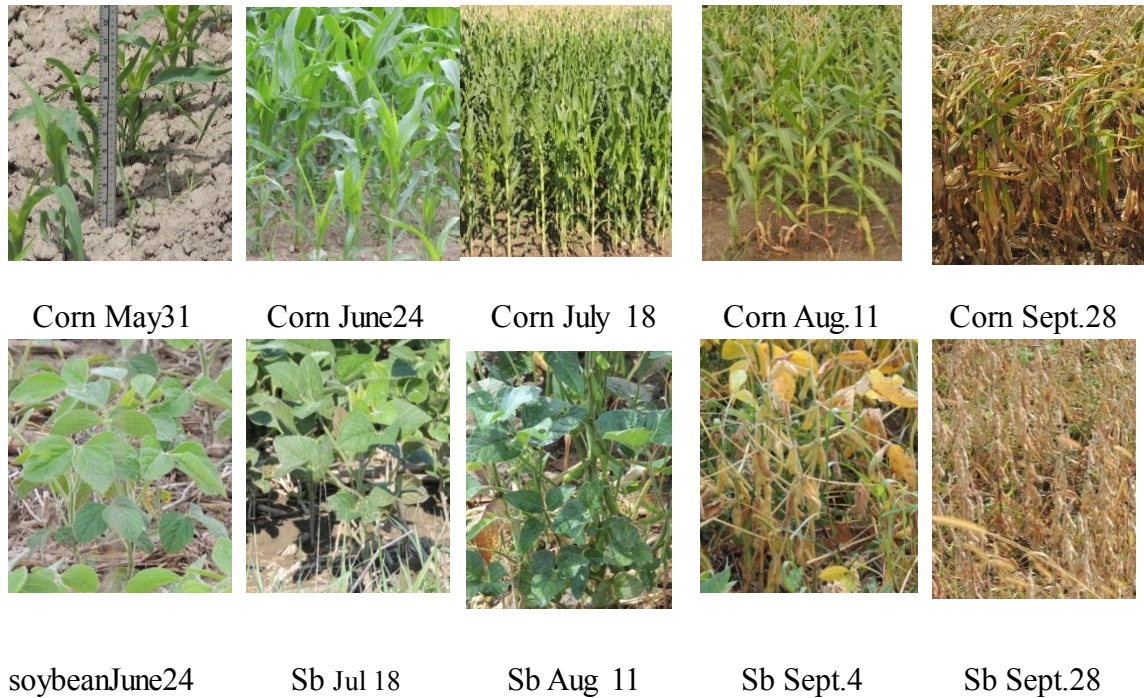


Figure 3.4 Key crop growing stages for corn and soybeans during the growing season

(2) Wheat and Field peas

For wheat, four main growing stages were captured by the RADARSAT-2 images taken from early May to the middle of July, 2012 (Figure 3.5). The height of wheat increased rapidly from tillers forming in early May at 30cm, and reached the climax at heading and flowering stages by the end of May at 75cm. Most wheat began ripening at the end of June, and were harvest at the middle of July.

For field peas, the development stages in 2012 were similar to those of wheat. The majority of pea plants emerged in early May, and bloomed in early June. The pea pods were fully developed at the end of June, and were finally harvested in the middle of July (Figure 3.4). The height of pea plants varied from 10cm to 55cm (Figure 3.5).

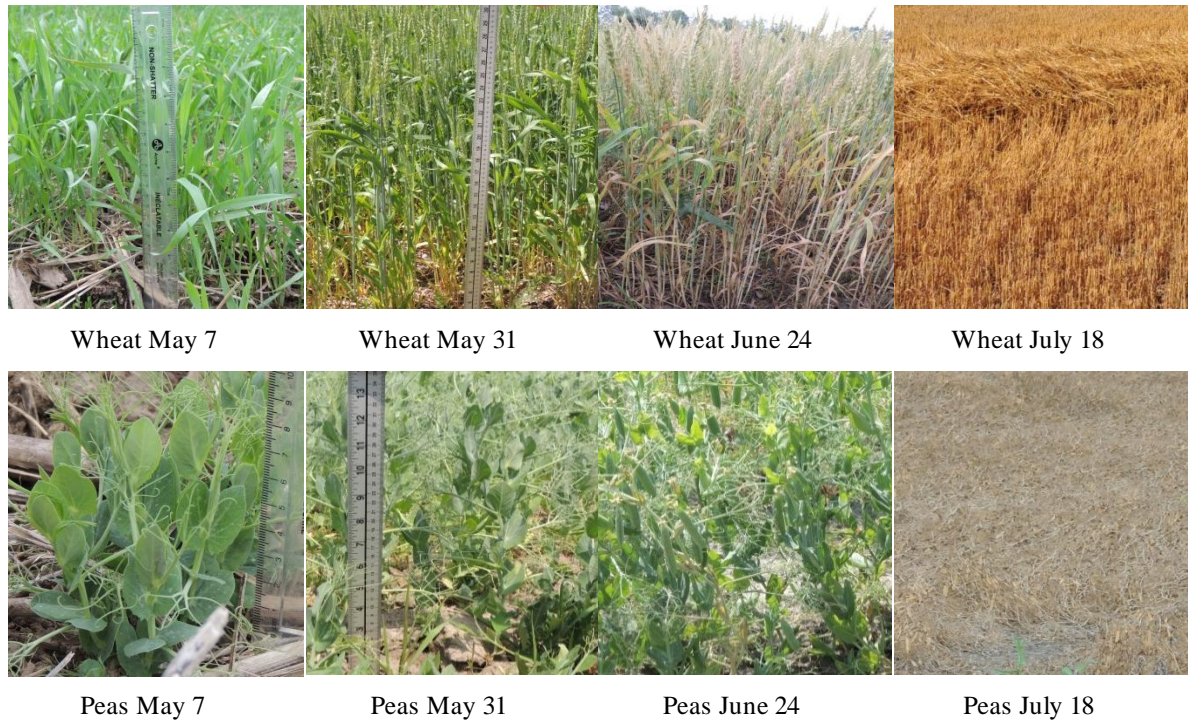


Figure 3.5 Key crop growing stages for wheat and field Peas during the growing season

3.4.2 Correlation Analysis between RADARSAT-2 Polarimetric SAR Data and Crop Height

The correlation between crop height and RADARSAT-2 polarimetric parameters are summarized in Table 2. The average heights of each crop field were observed in the field at each date when the satellite passed by. The mean values for each SAR parameter at corresponding field points were extracted from the polarimetric parameters datasets.

(1) Overall Trend

Relative high correlations(r) were observed in corn and peas. That highest r varied from 0.7 to 0.8. For soybeans and wheat, the correlations were relatively low, with the highest r around 0.55. To further investigate the relationship between crop height and SAR parameters, one typical field for each crop was selected for detailed analysis.

Table 3.2 The correlation between crop height and SAR parameters

	Corn	Soybean	Wheat	Peas
Linear Backscatter coefficient(dB)				
C11(HH)	0.57	0.41	-0.49	0.26
C22(HV)	0.68	0.52	-0.57	0.82
C33(VV)	0.47	0.35	-0.20	0.54
T11(HH+VV)	0.36	0.23	-0.40	0.54
T22(HH-VV)	0.70	0.56	-0.36	0.31
Intensity ratio				
HH/VV	0.51	0.16	-0.22	-0.46
HV/HH	0.43	0.45	-0.15	0.82
HV/VV	0.67	0.49	-0.56	0.51
Freeman-Durden decomposition parameters				
Single	-0.61	-0.38	0.15	-0.26
Double	-0.49	0.24	0.17	-0.72
Volume	0.68	0.52	-0.57	0.82
Cloude-Pottier decomposition parameters				
Entropy	0.79	0.42	-0.05	0.18
Alpha (deg.)	0.79	0.47	-0.11	0.01
Anisotropy	0.04	-0.23	0.51	-0.75
Polarimetric variables				
PH	0.71	0.54	-0.40	0.62
Total power	0.59	0.44	-0.45	0.59

(2) Corn

The volume scattering indicative parameters, such as HV and Fre_V, are sensitive to the corn height. The volume scattering values increase as the growth of corn height. Large amount of rainfall accumulated around June 24 might also contribute to the high volume scattering value.

The Entropy and Alpha parameters were more sensitive to the change in corn height ($r=0.79$) than the other parameters. The variation of the corn height was well characterized by the change of Entropy value, even at the late of corn growing season. A minor decrease of Entropy was observed at the corn maturation stage, which might be a result of the withering of most leaves.

The Alpha angle indicates the dominant scattering mechanism. In the early stage of the corn growing season (stalk initiation and development) the dominant mechanism was surface scattering since the plants could barely cover the ground. The Alpha increased from 40 to 50 degrees during the period from the tasseling to the maturity of most corn, which indicate that the main scattering mechanism was volume scattering. High densities of canopy corn were also observed in the in-situ investigation during that period. At the corn maturation stage, the Alpha was approaching to 50 degrees, which indicated that increasing double bounce scattering was also observed. As the canopies were less dense than before, more reflectance was backscattered from the semi-double-faced geometry between stalks and the surface.

In sum, both Entropy and Alpha angle from Cloud-Pottier decomposition parameters and HV scattering are good indicators of corn height.

(3) Soybeans

The values of both Pedestal Height (Ph) and HH-VV (T22) correlated well with the height of soybeans. Ph is an indicator of the presence of an unpolarized scattering component, and the randomness of scattering. A high Ph value indicates targets that are dominated by volume scattering or multiple-surface scattering. Researchers reported that (Evans, et al. 1988) pedestal height was directly proportional to vegetation density.

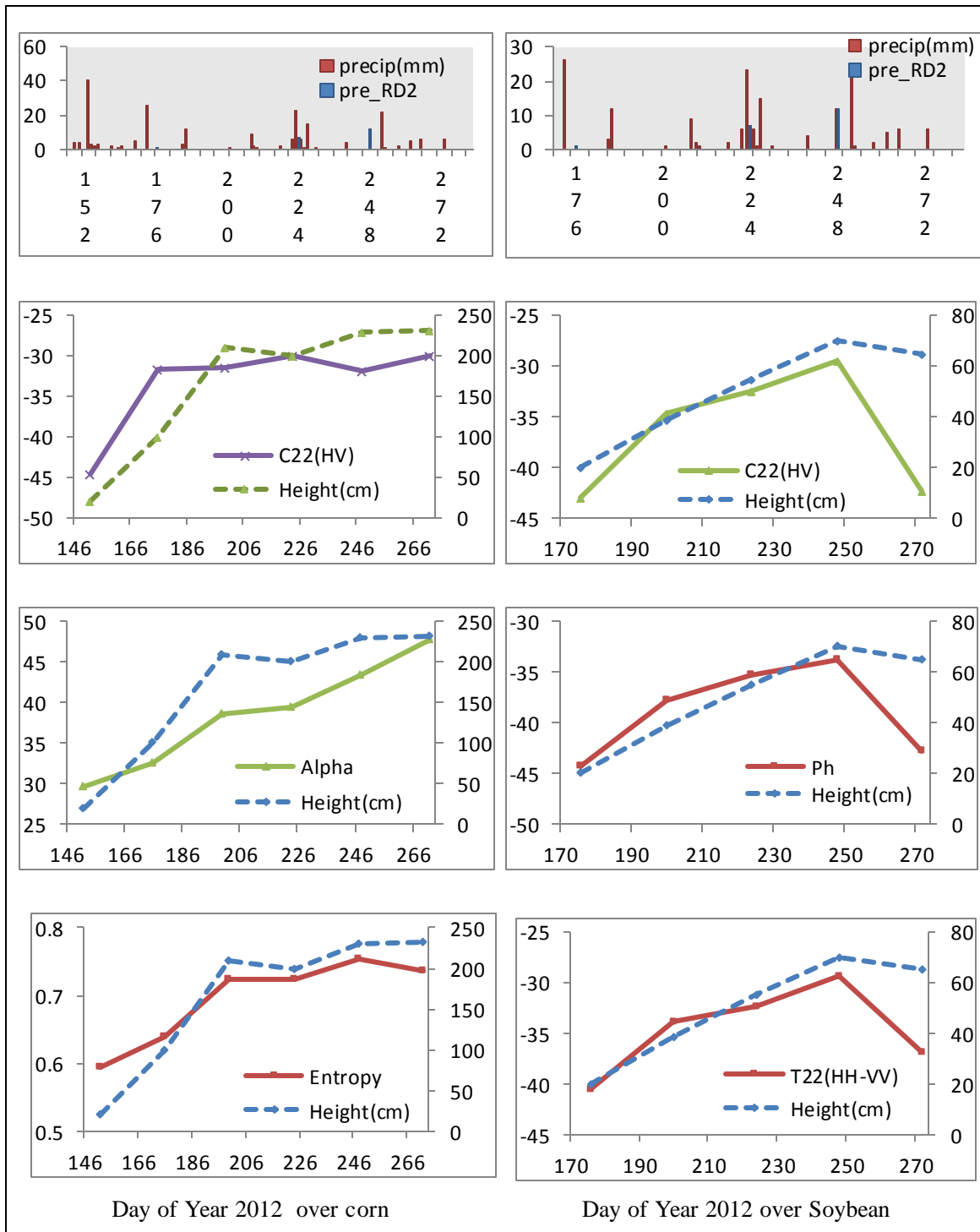


Figure 3.6 Temporal evolution of the SAR responses over corn and soybean. SAR parameters are presented together with crop height and precipitation amounts.

The sensitivity of Ph to soybean height was also observed in this study. However, the decrease in Ph value was much greater than the drop of height after the maturation of soybeans. The plants of soybeans became sparse as most leaves had been defoliated at the maturation stages, which resulted in the decrease of crop density, and consequently the decrease in Ph value. Similar results were also observed in the HV and HH-VV parameters, which are the indicators of volume and double scattering, respectively.

(4) Wheat and Field Peas

Fig.5 shows that the backscattering in the HH polarization channel of RADARSAT-2 is negatively correlated with the wheat height. HH is an indicator of surface scattering. The value of HH decreased as the wheat leaves and stems developed, and reached its minimum when the biomass was at its highest. The temporal change in HH indicated that, as wheat grew, the signals scattering from the bare soil were less intensive. The value in the Anisotropy of Cloude-Pottier decomposition is positively correlated with the wheat height. Anisotropy represents the relative power of the second and third eigenvectors of the covariance matrix.

The value of HV and the HV/HH positively corresponded to the growth of the peas. The rise in the value of HV/HH and HV indicated that the volume scattering, instead of surface scattering, became the dominant components as the pea's biomass increased.

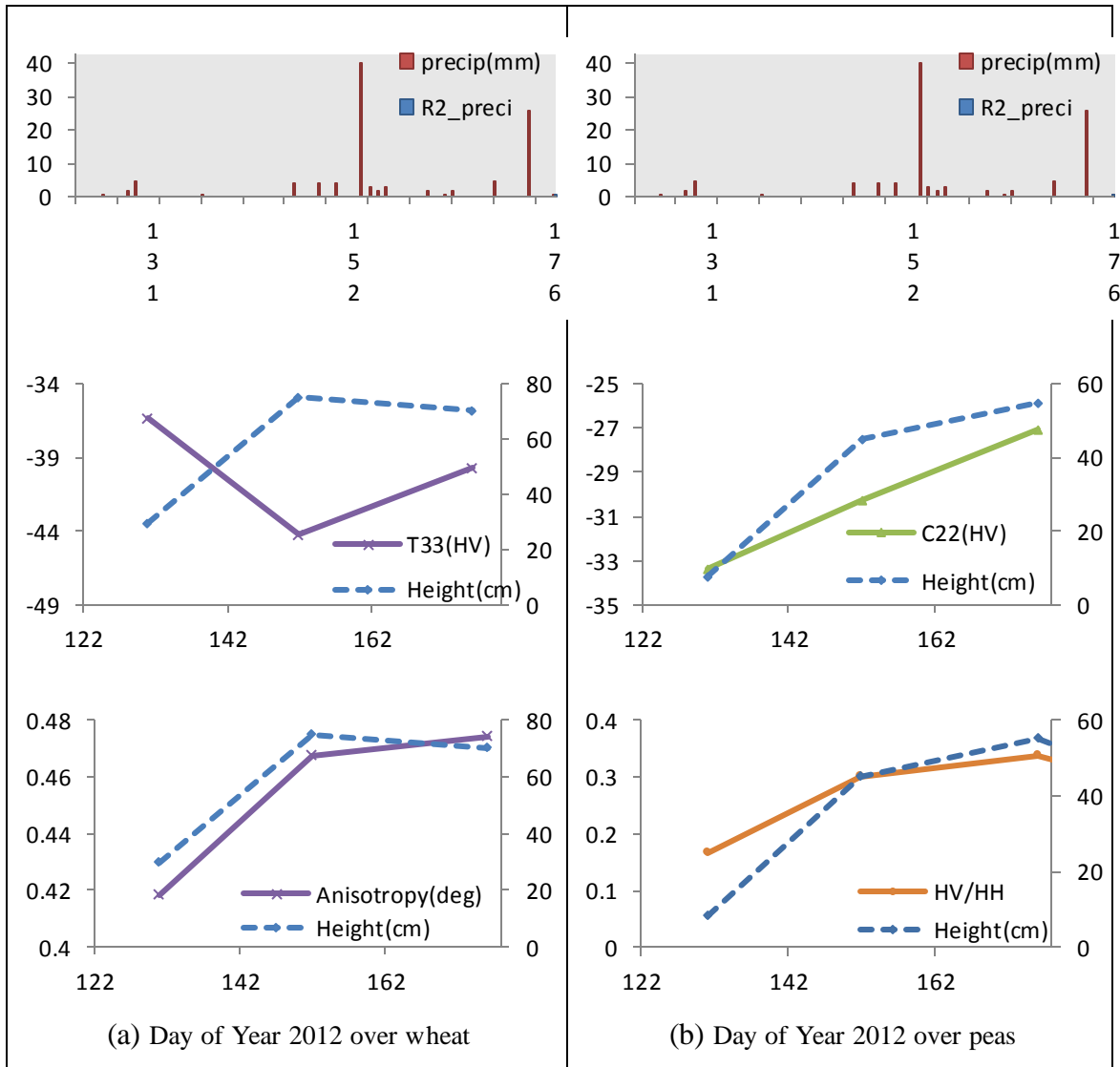


Figure 3.7 Temporal evolution of the SAR response over wheat (a) and peas (b). SAR parameters presented together with crop height and precipitation amount

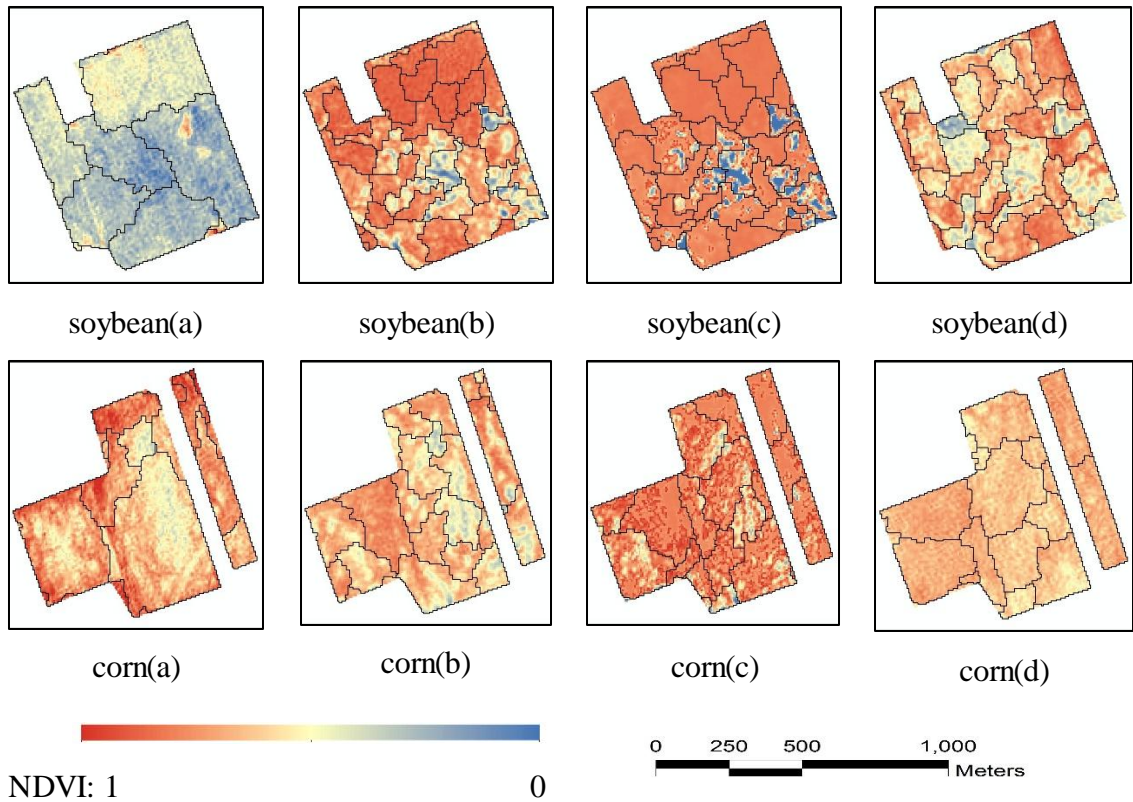
3.4.3 Correlation Analysis between RADARSAT-2 Polarimetric SAR Data and Crop NDVI

The NDVI maps of both soybeans and corn were generated from multi-temporal RapidEye images. The segmentation results give the basic units for the correlation analysis. In the following part, the segmentation results, the correlation between NDVI and basic polarimetric parameters, the correlation between NDVI and polarimetric decomposition parameters were analyzed from two incidence angles respectively.

(1) NDVI Segmentation

The statistics between NDVI and RADARSAT-2 polarimetric parameters were conducted on the object level. Four NDVI maps were generated on the dates of June 7th, July 16th and 24th, August 5th, and August 25th, 2012. Each NDVI map was segmented into homogeneous objects at the scale of 15 (Table 3.3). Objects covered by clouds or other non-crops land cover classes were extracted from the maps. The number of objects included for statistics is 212 for June 7th, 365 for July 16&24th, 382 for August 5th, and 295 for August 25th. The correlation analyses were conducted for the fields of corn and soybeans using the images taken on the FQ7 or FQ21 angle independently.

Table 3.3 Sampling segmentation results for soybean and corn fields superimposed on the June 7th (a), July 16th and 24th (b), August 5th (c), and August 25th (d) 2012, NDVI maps.



3.4.3.1 Basic Polarimetric Parameters

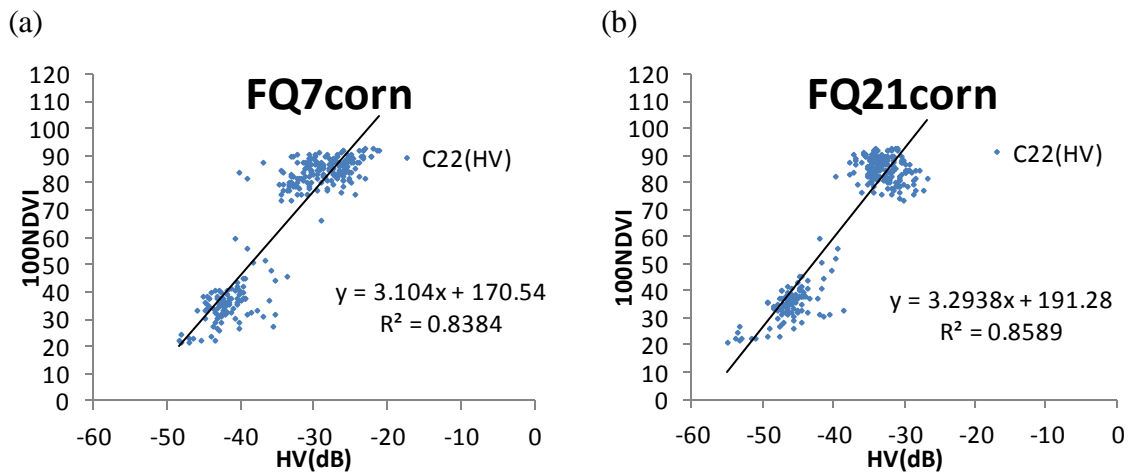
For both corn and soybeans, **significant correlations** between linear cross-polarization HV and NDVI were observed at FQ7 and FQ21. Also, strong correlations were observed between the T22 (HH-VV) and the NDVI at FQ7 ($r= 0.89$ for corn, 0.9 for soybeans). At FQ21, however, T22 (HH-VV) was slightly lower compared to NDVI for both corn($r=0.83$) and soybeans($r=0.83$). In Figure 6, the HV and HH-VV parameters are plotted against derived NDVI for both corn and soybean crops. HV is associated with volume and HH-VV represents double or even-bounce scattering from within the target. The significant correlation between HV, HH-VV and NDVI reflects that both HV and HH-VV are sensitive to physical structure of crops. Early in the crop growing season, most scattering originated directly from the soil surface. Therefore, the volume and multiple scatterings

were low during that period. With the growth of leaves and stems of plants, more scattering was reflected from the canopies of plants, as well as from the geometry between the stalks and soil surface. Consequently, the volume and multiple scattering increased rapidly.

Table 3.4 The correlation between soybean and corn NDVI to basic polarimetric parameters in FQ7 and FQ21

	R(FQ7, NDVI)		R(FQ21,NDVI)	
	Soybean	Corn	Soybean	Corn
Linear Backscatter coefficient(dB)				
C11(HH)	0.42	0.56	0.80	0.79
C22(HV)	0.93	0.92	0.89	0.93
C33(VV)	0.43	0.43	0.79	0.75
T11(HH+VV)	0.25	0.38	0.73	0.75
T22(HH-VV)	0.89	0.90	0.83	0.83
Intensity Ratio				
HH/VV	-0.90	-0.80	-0.07	0.48
HV/HH	0.63	0.74	0.67	0.65
HV/VV	0.76	0.78	0.63	0.73

The **saturation** of HH-VV to NDVI was observed once the NDVI reached 0.8 at the FQ21 angle for both soybean and corn crops. In the samples of corn crops with an NDVI higher than 0.75, see the (f) in Figure 3.6, half of the samples have HH-VV values, which are positively relative to NDVI, while the HH-VV values of the other samples are in negative relation to the NDVI value. This difference might be because after the maturation of most corn, the NDVI decreased due to the drop in chlorophyll in the plant. In the meantime, the double bounce increased when most leaves were dry. Stronger signals were reflected from the double bounced scatter between corn stalks and soil surface. For the soybeans, the sensitivity of HH-VV to NDVI matured when the NDVI values were higher than 0.8, particularly in FQ21 images. Compared with the FQ7 image, the shallower angle at FQ21 provides less penetration into the canopy, thus, it is less sensitive to NDVI.



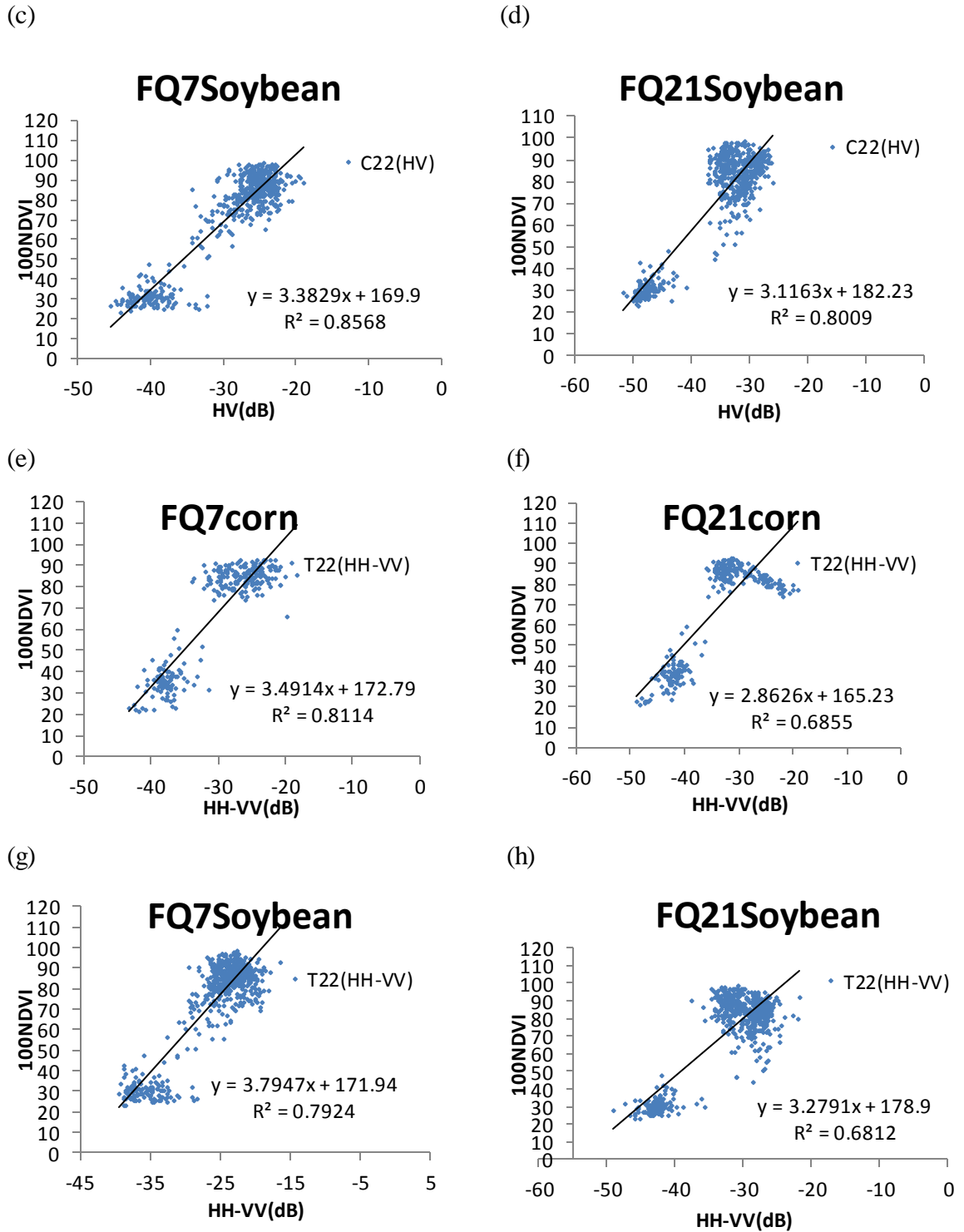


Figure 3.8 Correlation between the HV, HH-VV for the RADARSAT-2 FQ7 and FQ21 acquisitions and NDVI for corn and soybean

3.4.3.2 Decomposition Polarimetric parameters

(1) Freeman-Durden and Pedestal Height

The volume scattering of Freeman-Durden decomposition parameters was significantly correlated with NDVI for both soybeans and corn. In addition, pedestal height was highly correlated with NDVI for both crops. Pedestal height describes the degree of polarization of a scattered wave. Studies demonstrate that pedestal height is directly proportional to vegetation density [8]. In this study, it is also positively correlated with the NDVI. Also, the saturation of Pedestal Height to NDVI was observed when the NDVI of crop samples was higher than 0.75, particularly in the FQ21 images.

(2) Entropy

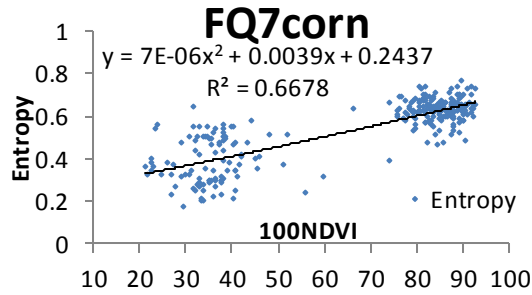
A slightly weak correlation was reported between Entropy and crop NDVI. Entropy characterizes the randomness of scattering occurring within a target. As crops develop, the randomness increases because scattering from the soil, the vegetation, as well as the soil-vegetation interaction all contribute to the total scattering. As Figure 3.7 shows, the correlation between Entropy and crop NDVI is slightly higher for soybeans than that for corn. It might be interpreted from the figure that the Entropy is more sensitive to the low biomass plants, such as soybeans, than those with high biomass.

(3) Overall

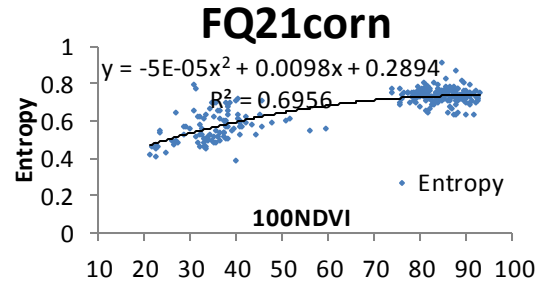
In summary, the sensitivity of crop NDVI to polarimetric parameters varied from parameter to parameter. The correlation between the same parameter to the crop NDVI also depends on the crop types, and incidence angles of images. In general, parameters that are indicative of volume and multi-scattering, such as HV, HH-VV, and volume scattering from Freeman-Durden decomposition, are relatively highly related to the value of crop NDVI. Also, parameters related to the density and randomness of plants, like the pedestal height and entropy in the Cloude-Pottier decomposition, are correlated with the crop NDVI. However, due to the lack of high quality optical images in mid-June, the NDVI values of

most samples were clustered in the high and low zones. The statistical results might be more convincing if NDVI maps from various dates were available.

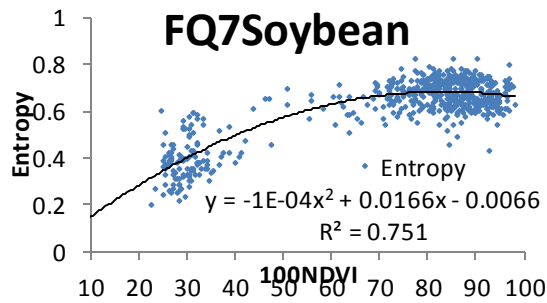
(a)



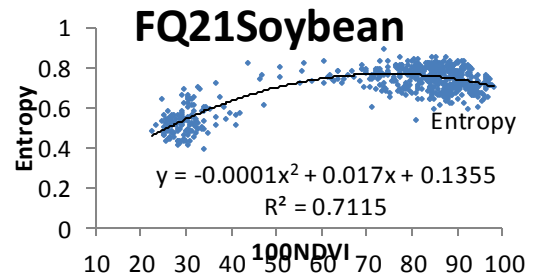
(b)



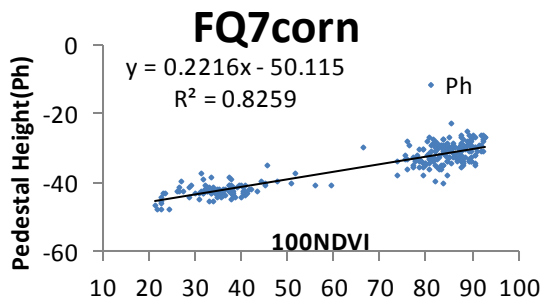
(c)



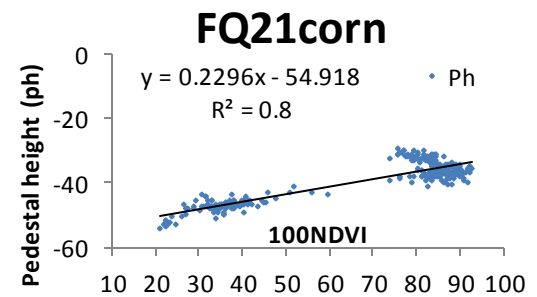
(d)



(e)



(f)



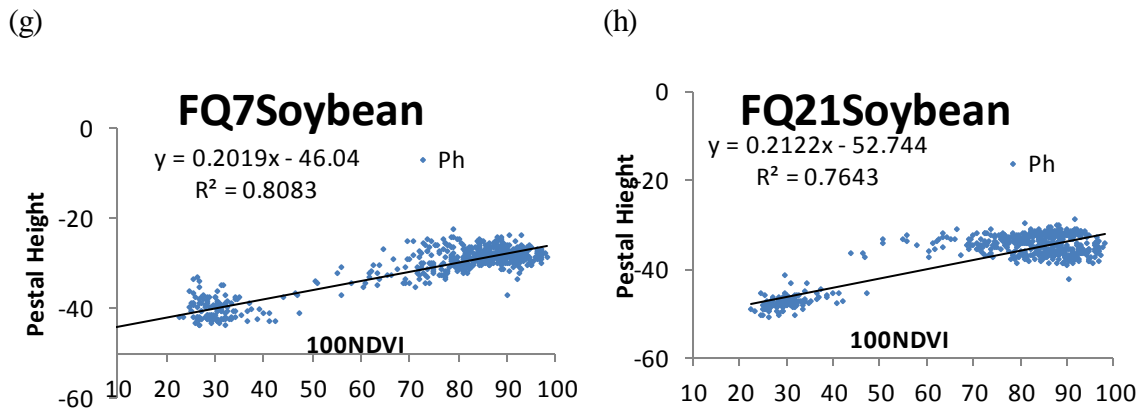


Figure 3.7 Scatter plots between the Entropy, Pedestal and NDVI for corn and soybeans at FQ7 (a, c, e, g), and FQ21 (b, d, f, h) image.

3.4.3.3 Comparison of all Polarimetric Parameters

By comparing the correlation between NDVI and polarimetric parameters, the rankings of the coefficients for soybean and corn have been generated.

(1) Soybeans

For **soybeans**, the volume scattering derived from HV intensity and Freeman-Durden decomposition parameters are most correlated to the value of NDVI, with a Pearson's r of 0.93. The Pedestal Height and HH/VV are very sensitive to the NDVI values of soybeans, as well, with the same Pearson's r of 0.9. The correlation between T22 (|HH-VV|) and NDVI is the third place, with a Pearson's r of 0.89.

As discussed in the above sections, serious saturations were observed while using FQ21 image, due to the less penetration of canopy. Parameters derived from FQ7 images, at a steeper incidence angle, higher correlation were generated than other from FQ21.

Table 3.5 the ranking of correlation coefficients between polarimetric parameters and NDVI for soybeans

Ranking	Recommended parameters	Better Mode	r
1	C22 (HV)	FQ7	0.93
1	Freeman(Vol)	FQ7	0.93
2	PH	FQ7	0.9
2	HH/VV	FQ7	-0.9
3	T22(HH-VV)	FQ7	0.89

(1) Corns

The volume scatterings from HV intensity and Freeman-Durden decomposition are strongest correlated to corn NDVI, with the Pearson's r as high as 0.93. Pedestal Height and T22 are second and third sensitive to NDVI values.

The better mode for volume scatterings is FQ21, and that for PH and T22 is FQ7. However, the difference between FQ7 and FQ21 is not significant, which is less than 0.02. Therefore, no absolute better angle mode was found in this study.

Table 3.6 The ranking of correlation coefficients between polarimetric parameters and NDVI for corn.

Ranking	Recommended parameters	Better Mode	R
1	C22(HV)	FQ21	0.93
1	Freeman(Vol)	FQ21	0.93
2	PH	FQ7	0.91
3	T22(HH-VV)	FQ7	0.9

3.5 Conclusion

This study investigates the sensitivity of RADARSAT-2 polarimetric SAR signals to structural changes of wheat, field peas, soybeans, and corn during the growing season in 2012, Southwestern Ontario. Several conclusions have been drawn from this study:

(1) Polarimetric SAR are able to provide complement information for optical data in time critical agricultural applications, such as crop condition monitoring, when high quality optical data are not available under unfavorable weather conditions.

(2) The potential of polarimetric SAR parameters in characterizing the temporal change of crop height have been proved in this study. The high correlation coefficients of 0.82 and 0.79 were observed in peas and corn. And the recommended parameters for field pea height estimation are Freeman-Durden volume scattering and HV/VV, and those for con height estimation are Entropy, Alpha.

(3) Strong correlation coefficients have been observed between polarimetric parameters and NDVI values for both corn and soybeans. The highest correlation coefficient is 0.93, between HV, Freeman-Durden Volume and NDVI for both corn and soybeans. Pedestal Height is also sensitive to crop NDVI, and the correlation coefficients are 0.9 and 0.91 for soybeans and corn.

(4) Marginal differences were observed between the images taken at FQ21 and FQ7 incidence angles. FQ7 is slightly better than FQ21 in estimation soybeans NDVI from some polarimetric SAR parameters, such as HH-VV, HH/VV, Pedestal Height, and volume scattering.

The potential of deriving NDVI from C band polarimetric SAR data has been demonstrated in this study. More researches should focus on investigating the relationship between the SAR parameters and other plant parameters, such as LAI and biomass, so as to facilitate the estimates of crop yields.

3.5 References

- Baghdadi, N., et al. (2009). "Potential of SAR sensors TerraSAR-X, ASAR/ENVISAT and PALSAR/ALOS for monitoring sugarcane crops on Reunion Island." *Remote Sensing of Environment*, Vol.113, pp.1724-1738.
- Bugden, J.L., Pattey, E., et McNairn, H. (2009). «Classification of crop and soil homogenous 6 zones using Multipolarization C-Band SAR. » *Canadian Journal of Remote Sensing* , 35(2), p. 130-140. doi : 10.5589/m09-001
- Chakraborty , M., M ANJUNATH , K.R., P ANIGRAHY , S., K UNDU , N. and P ARIHAR , J.S. (2005),Rice crop parameter retrieval using multi-temporal, multi-incidence angle Radarsat SAR data. *ISPRS Journal of Photogrammetry and Remote Sensing*, 59, pp. 310–322.
- Ferrazzoli, P., S. Paloscia, et al. (1997). "The potential of multifrequency polarimetric SAR in assessing agricultural and arboreous biomass." *Geoscience and Remote Sensing, IEEE Transactions on* 35(1): 5-17.
- Gerighausen, H., et al. (2007), DEMMIN—A test site for the validation of remote sensing data products: General description and application during AgriSAR 2006, in *Proceedings of the AGRISAR and EAGLE Campaigns Final Workshop*,Eur. Space Res. and Technol. Cent., Noorwijk, Netherlands.
- Jiao, X., et al. The sensitivity of RADARSAT-2 polarimetric SAR data to corn and soybean leaf area index (2011). *Canadian Journal of Remote Sensing*, Vol. **37**, pp. 69-81.
- Li , Y., L IAO , Q., L I , X., L IAO , S., C H I , G. and P E N G , S. (2003). Towards an operational system for regional-scale rice yield estimation using a time-series of

- Radarsat ScanSAR images. *International Journal of Remote Sensing*, 24, pp. 4207–4220.
- Lievens, H., Verhoest, N., De Keyser, E., Vernieuwe, H., Matgen, P., Alvarez-Mozos, J., & De Baets, B. (2011). Effective roughness modelling as a tool for soil moisture retrieval from C-and L-band SAR. *Hydrology and Earth System Sciences*, 15(1), 151-162.
- Liu, J., E. Pattey, et al. (2012). Assessment of vegetation indices for regional crop green LAI estimation from Landsat images over multiple growing seasons. *Remote Sensing of Environment* 123(0): 347-358.
- Lopez - Sanchez, J. M., & Ballester - Berman, J. D. (2009). Potentials of polarimetric SAR interferometry for agriculture monitoring. *Radio Science*, 44(2).
- McNairn, H., and B. Brisco (2004), The application of C-band polarimetric SAR for agriculture: A review, *Can. J. Remote Sensing*, 30(3).
- McNairn, H., Champagne, C., Shang, J., Holmstrom, D.A., et Reichert, G.(2009a). Integration of optical and Synthetic Aperture Radar (SAR) imagery for delivering operational annual crop inventories. *ISPRS Journal of Photogrammetry and Remote Sensing*, 64, pp. 434–449.
- McNairn, H., J. van der Sanden, R. Brown, and J. Ellis (2000) The potential of RADARSAT-2 for crop mapping and assessing crop condition, in *Proceedings of the 2nd International Conference on Geospatial Information in Agriculture and Forestry*, vol. 2, pp. 81 – 88, Veridian ERIM Int. Conf.,Ann Arbor, Mich.
- McNairn, H., Shang, J., Jiao, X., et Champagne, C. (2009b). The Contribution of ALOS PALSAR Multi-polarization and Polarimetric Data to Crop Classification. *IEEE Transactions on Geoscience and Remote Sensing*, 47(12, Article No. 5233805), p. 3981-3992. doi : 10.1109/TGRS.2009.2026052
- Paloscia,S. (1998). "An empirical approach to estimating leaf area index from multifrequency SAR data." *International Journal of Remote Sensing* 19(2): 359-364.

- Shang, J., McNairn, H., Champagne, C., et Jiao, X. (2009). «Contribution of multi-frequency, multi-sensor, and multi-temporal radar data to operational annual crop mapping. » IEEE Geoscience and Remote Sensing Letters, 3(1), p. III378-III381. doi : 10.1109/IGARSS.2008.4779362
- Shao , Y., F AN , X., L IU , H., X IAO , J., R OSS , S., B RISCO , B., B ROWN , R. and S TAPLES , G. (2001) Rice monitoring and production estimation using multitemporal RADARSAT. Remote Sensing of Environment, 76, pp. 310–325.
- Steffen Gebhardt , Juliane Huth , Lam Dao Nguyen , Achim Roth & Claudia Kuenzer (2012): A comparison of TerraSAR-X Quadpol backscattering with RapidEye multispectral vegetation indices over rice fields in the Mekong Delta, Vietnam, International Journal of Remote Sensing, 33:24, 7644-7661

Chapter 4

4 Conclusion

4.1 Summary

The successful management of LU/LC planning and agricultural applications relies on continuous monitoring of LU/LC changes and crop growing conditions. This is even more critical in Southwestern Ontario, Canada, where rapid urban expansion has a great influence on agricultural production and the economy. Frequent monitoring permits complete and accurate assessments of the impacts of urban development on the local and regional agriculture. Remote Sensing provides an efficient and effective tool for this purpose.

Traditional optical Remote Sensing data are not reliable for crop type identification and conditions monitoring during the growing seasons due to the frequent cloudy and rainy weather. SAR images are a good complementary data source for optical images. Newly available Quadpol SAR data contain full polarization information, and have great potential in extracting more LU/LC mapping and vegetation change monitoring.

Chapter 2 presented a classification procedure for the LU/LC mapping of urban/rural fringe areas using multi-temporal Quadpol RADARSAT-2 images. Nine classes were identified with a high accuracy of over 90% in OA. The classification results were compared and analyzed in four aspects: decomposition parameters, classifiers, multi-date images combination, and post-classification processing methods.

Chapter 3 described the sensitivities of RADARSAT-2 polarimetric parameters to vegetation parameters over the crop growing season from two aspects: (1) the responses of polarimetric parameters to the change of crop heights in different phenological stages. (2) The statistical relationship between polarimetric parameters and crop NDVI.

4.2 Conclusions

The research presented in this thesis has given answers to the questions listed in the introduction:

1. How accurately can LU/LC be classified in this urban/rural fringe areas from the fine beam multi-temporal RADARSAT-2 satellite images?

An accurate LU/LC map of the urban and rural fringe area of the city London, Ontario has been generated with a high accuracy of 91.0% (OA) at 0.888 (Kappa). The results are satisfactory considering the complex natural of the boundary areas and various kinds of crop types growing in the rural areas.

2. What is the suitable classification procedure for LU/LC classification in urban/rural fringe areas using RADARSAT-2 satellite images?

We find that the classification procedure using Pauli decomposition parameters and Gaussian distribution MLC yielded better classification results than other parameters or the Wishart based MLC methods.

3. What is the appropriate multi-date combination of RADARSAT-2 images in crop types' classification?

Although slightly higher accuracy can be obtained from more than four-date images, satisfactory classification accuracies (over 87%) have been achieved using images from three dates, as long as the images at the key seasons were included. The images taken in the early and middle of growing seasons give better classification results than those from the other seasons.

4. What is the potential of RADARSAT-2 Quadpol in monitoring crop growing changes?

The temporal and spatial variation of crop height over the crop growing season are well characterized by the polarimetric SAR parameters. The curves of entropy, HH-

VV, and Anisotropy, as well as HV/VV were shown to be most close to the temporal profile of height in corn, soybeans, wheat, and peas respectively.

5. How sensitive is the RADARSAT-2 polarimetric parameters to the crop vegetation index and parameters in terms of NDVI and crops height?

Strong correlations were observed between the NDVI values and HV, volume scattering in Freeman-Durden decomposition, and Pedestal Height for soybean and corn. Insignificant differences were observed between the images taken at FQ21 and FQ7 incidence angles. However, polarimetric SAR parameters, such as HH-VV, HH/VV, PH, in FQ7 were slightly more sensitive to plant parameters than those in FQ21.

4.3 Contributions of This Research

4.3.1 Technical Contribution

In Chapter 2 the capabilities of Gaussian based Maximum Likelihood Classifier (MLC) in polarimetric SAR image classification have been proved in this study. The classification results indicates that Gaussian distribution is an effective method of characterizing logarithm Pauli parameters probability distribution function.

4.3.2 4. 3. 2 Application Contribution

The main contributions of the study in Chapter 2 are demonstrated in two aspects:

(1) An operational procedure has been provided for LU/LC classification in the urban/rural fringe areas using polarimetric RADARSAT-2 data. Using this procedure, detailed LU/LC classes, including the crop types and urban land use classes, can be classified with a high accuracy.

(2) An accurate and economic combination strategy of multi-date data for LU/LC classification has been recommended by comparison. This strategy can be used for annual crop inventory in Southwestern Ontario, particularly in the urban/rural fringe areas.

The main contributions in Chapter 3 is that it explored the potential of polarimetric RADARSAT-2 data for crop conditions monitoring in Southwestern Ontario, Canada.

(1) Some polarimetric parameters are proved to be responsive to the variation of crop plants in Southwestern Ontario, and thus might be used for vegetation change monitoring.

(2) The capabilities of deriving NDVI from polarimetric RADARSAT-2 data for corn and soybeans in Southwestern Ontario have been demonstrated through statistical correlation analysis. Several polarimetric parameters with high correlation coefficients were recommended for NDVI estimation.

4.4 Possible Future Research

4.4.1 Texture Analysis and Object Classification

The advantages of the object-based method are not obvious while merely applied in post-classification processing. More researches would be worthwhile in studying the benefits of applying object-based method to the multi-temporal Quadpol RADARSAT-2 data classification. In the meanwhile, the texture information from the SAR images, such as the gray-level co-occurrence matrices (GLCM), within each object might be useful in improving classification accuracy. Future research could focus on using the texture features extracted from the polarimetric SAR data on an object-based analysis classification.

4.4.2 Correlation Analysis with Other Agricultural Parameters

Crop height and NDVI are two of the most important parameters that can describe crop growing conditions. However, in order to accurately estimate the biomass of crops as well as give early predictions of field yields, more information is necessary. The correlation between the polarimetric SAR parameters and other crop parameters, such as Leaf Area Index, enhanced vegetation index, and soil moisture, deserve more study.

Appendices

A Polarimetric Decomposition Theorem and Results

A1 H/Alpha/A Decomposition and Pedestal Height

H/Alpha/A Decomposition method was proposed by Cloude and Pottier in 1997. This method is based on an eigenvector analysis of 3X3 coherency T3 matrix.

The Entropy (H) indicates the randomness of scattering surface. It is given by Eq.(A1)

$$H = \sum_{i=1}^3 -P_i \log_3 P_i \quad \text{Where} \quad P_i = \frac{\lambda_i}{\sum_{j=1}^3 \lambda_j}$$

λ_i is the coherency matrix eigenvalues. (A1)

The alpha angle identified scattering types. It is defined by Eq. (A2)

$$\vec{e}_i = \exp(i\phi_i) \begin{bmatrix} \cos \alpha_i \\ \sin \alpha_i \cos \beta_i \exp(i\delta_i) \\ \sin \alpha_i \sin \beta_i \exp(i\gamma_i) \end{bmatrix}$$

where \vec{e}_i is the coherency matrix eigenvalues.

δ is the phase difference between $S_{HH} + S_{VV}$ and $S_{HH} - S_{VV}$.

γ is the phase difference between $S_{HH} + S_{VV}$ and S_{HV} .

ϕ is the decomposition phase $S_{HH} + S_{VV}$.

The mean alpha angle is defined by: $\bar{\alpha} = P_1 \alpha_1 + P_2 \alpha_2 + P_3 \alpha_3$.

The α_i is the alpha angle corresponding to the \vec{e}_i eigenvector. (A2)

The anisotropy is defined by Eq. (A3)

$$A = \frac{\lambda_2 - \lambda_3}{\lambda_2 + \lambda_3}; \lambda_i \text{ is the coherency matrix eigenvalues, } \lambda_1 > \lambda_2 > \lambda_3 \quad (A3)$$

The Pedestal Height is defined by Eq. (A4)

$$PH = \frac{\lambda_3}{\lambda_1} \quad (A4)$$

A 2 Freeman Decomposition

The Freeman-Durden decomposition is a method for converting the polarimetric SAR observations into a physically based, three-component scattering model, without any ground truth measurements (Freeman & Durden, 1998). The scattering model is composed of surface, double- or even- bounce and volume scatter.

$$R_H = \frac{\cos\theta - \sqrt{\varepsilon_r - \sin^2\theta}}{\cos\theta + \sqrt{\varepsilon_r - \sin^2\theta}}, \quad R_V = \frac{(\varepsilon_r - 1)\{\sin^2\theta - \varepsilon_r(1 + \sin^2\theta)\}}{(\varepsilon_r \cos\theta + \sqrt{\varepsilon_r - \sin^2\theta})^2},$$

$$S = \begin{bmatrix} R_H & 0 \\ 0 & R_V \end{bmatrix}, \quad F_S = |R_V|^2,$$

$$S = \begin{bmatrix} e^{2j\gamma_H} R_{TH} R_{GH} & 0 \\ 0 & e^{2j\gamma_V} R_{TV} R_{GV} \end{bmatrix}, \quad F_D = |R_{TV} R_{GV}|^2, \quad F_V = \frac{3}{2} \langle R_{VH} R_{HV}^* \rangle.$$

where θ is the local incidence angle, ε_r is the relative dielectric constant of the surface. $R_{TV} R_{TH}$ are the reflection coefficients from vertical trunk surface for vertical and horizontal polarizations, respectively. $R_{GV} R_{GH}$ are the reflection coefficients from Fresnel reflection coefficients for vertical and horizontal polarizations, respectively. γ_V and γ_H represent any propagation attenuation and phase change effects in vertical and horizontal polarizations, respectively.

B Reference Data and Samples

The reference data used in this study including air photo, RapidEye images, as well as pictures and height measurements taken in the field.

B1 Optical Images

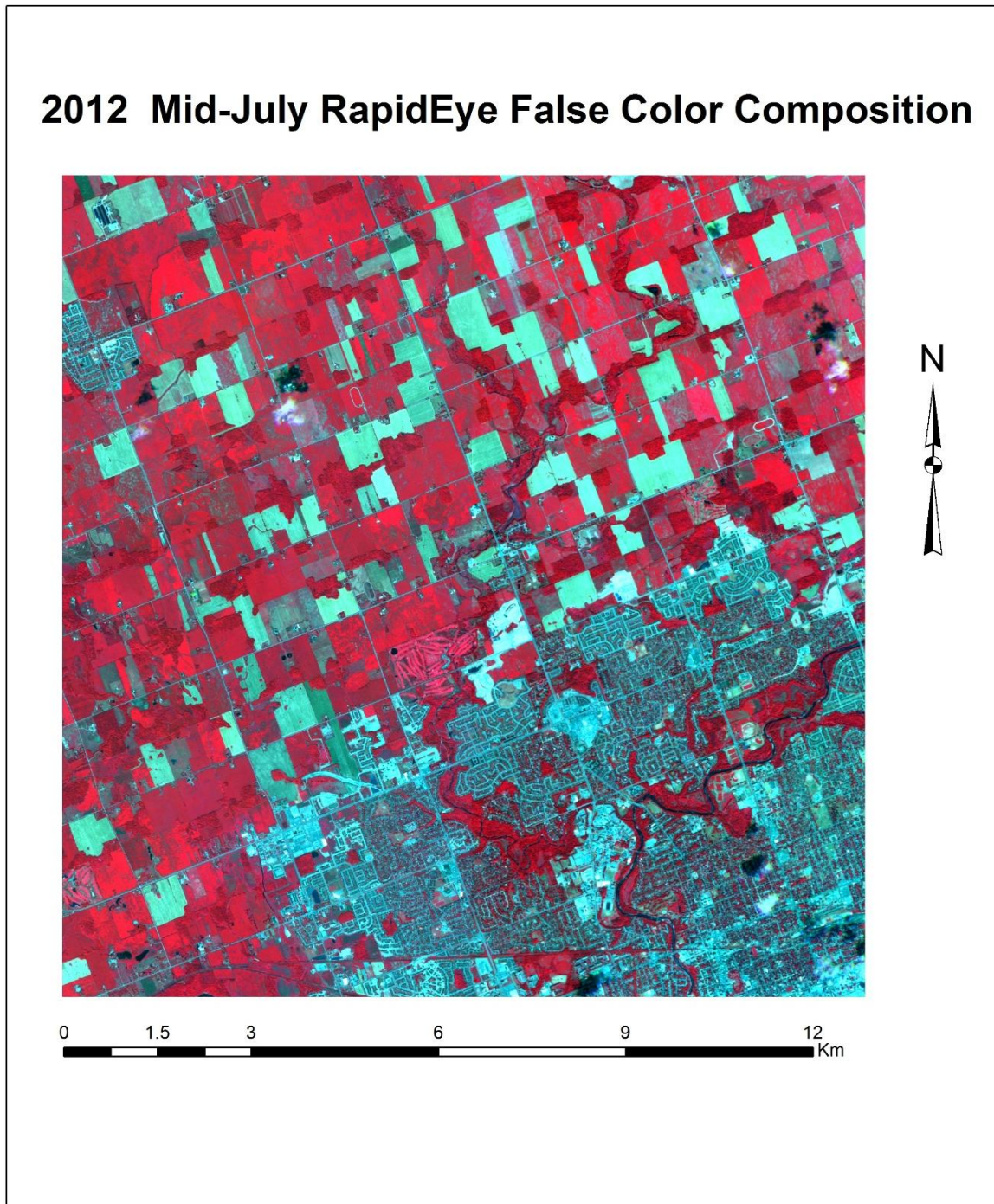


Figure B.1 The RapidEye image by false color composition taken in July, 2012



Figure B.2 The air photo of London, Ontario taken in 2009

B2 Training Samples and Testing Samples

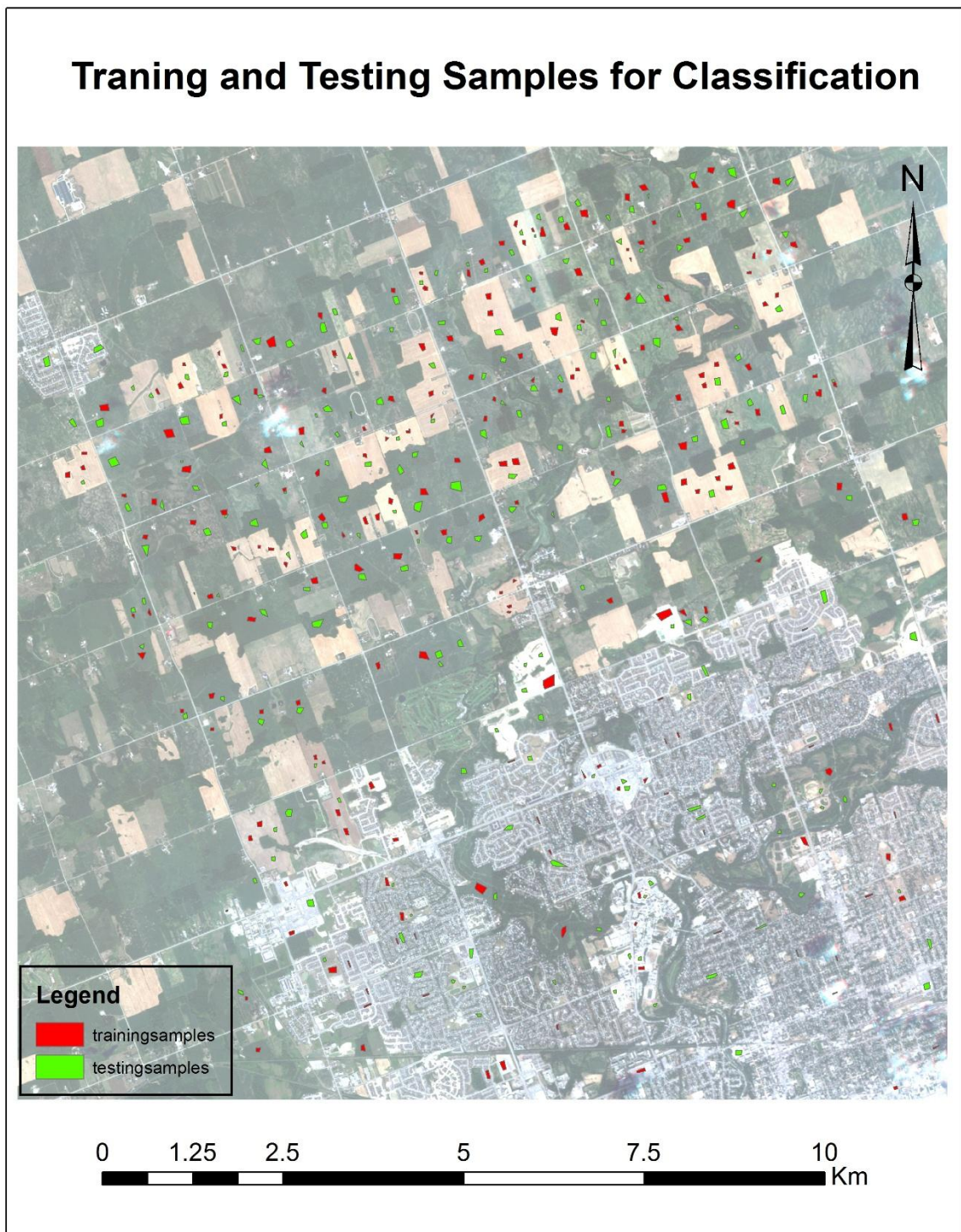


Figure B.3 Training and testing samples shown in a RapidEye image

Crop Samples Collected from the Field Work

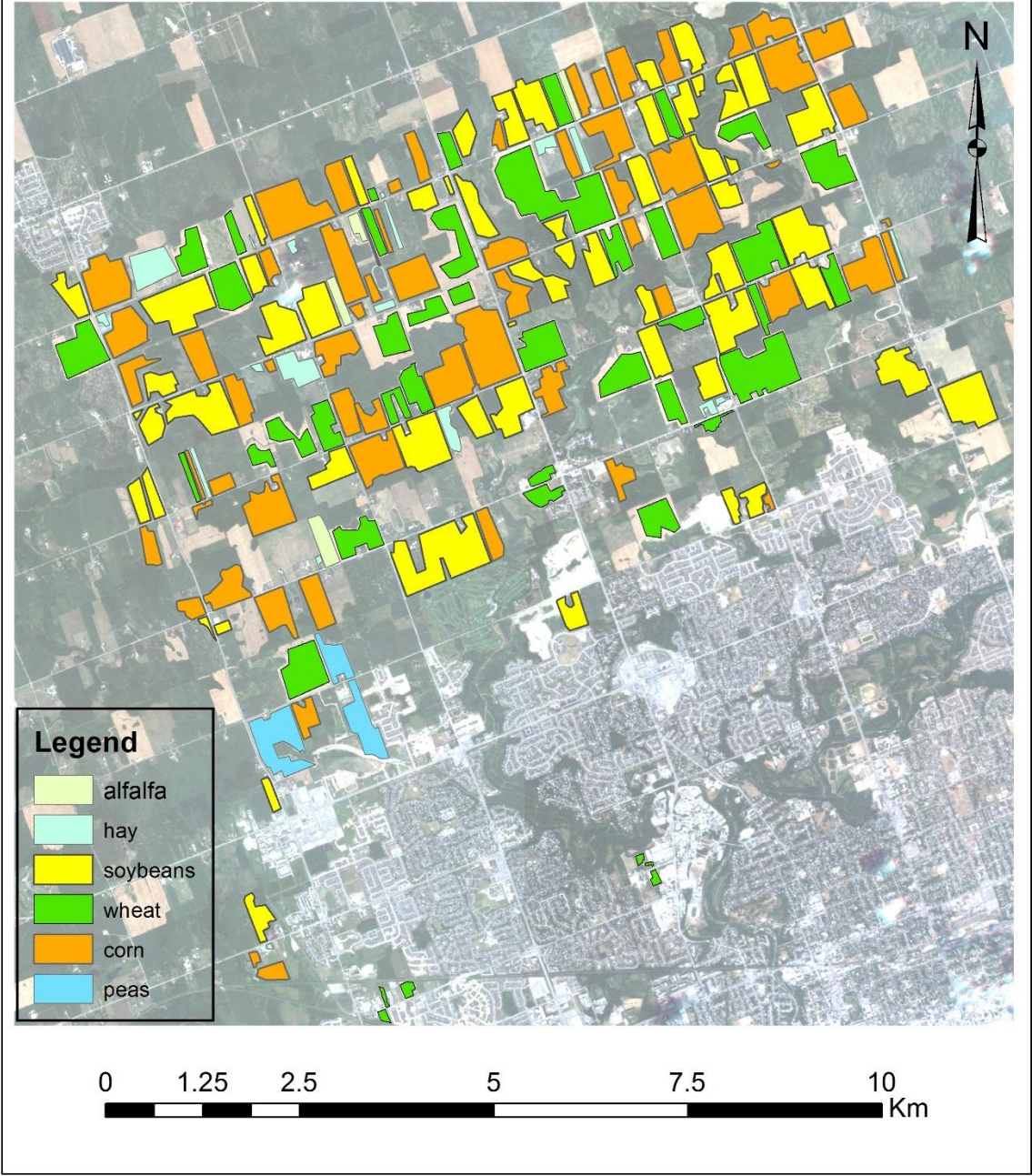


Figure B.4 Crop samples collected from the fields shown in a RapidEye image

B3 LU/LC Classes and Field Work Pictures



Figure B6 LU/LC classes pictures, (a) commercial area, (b) construction site, (c) industrial areas

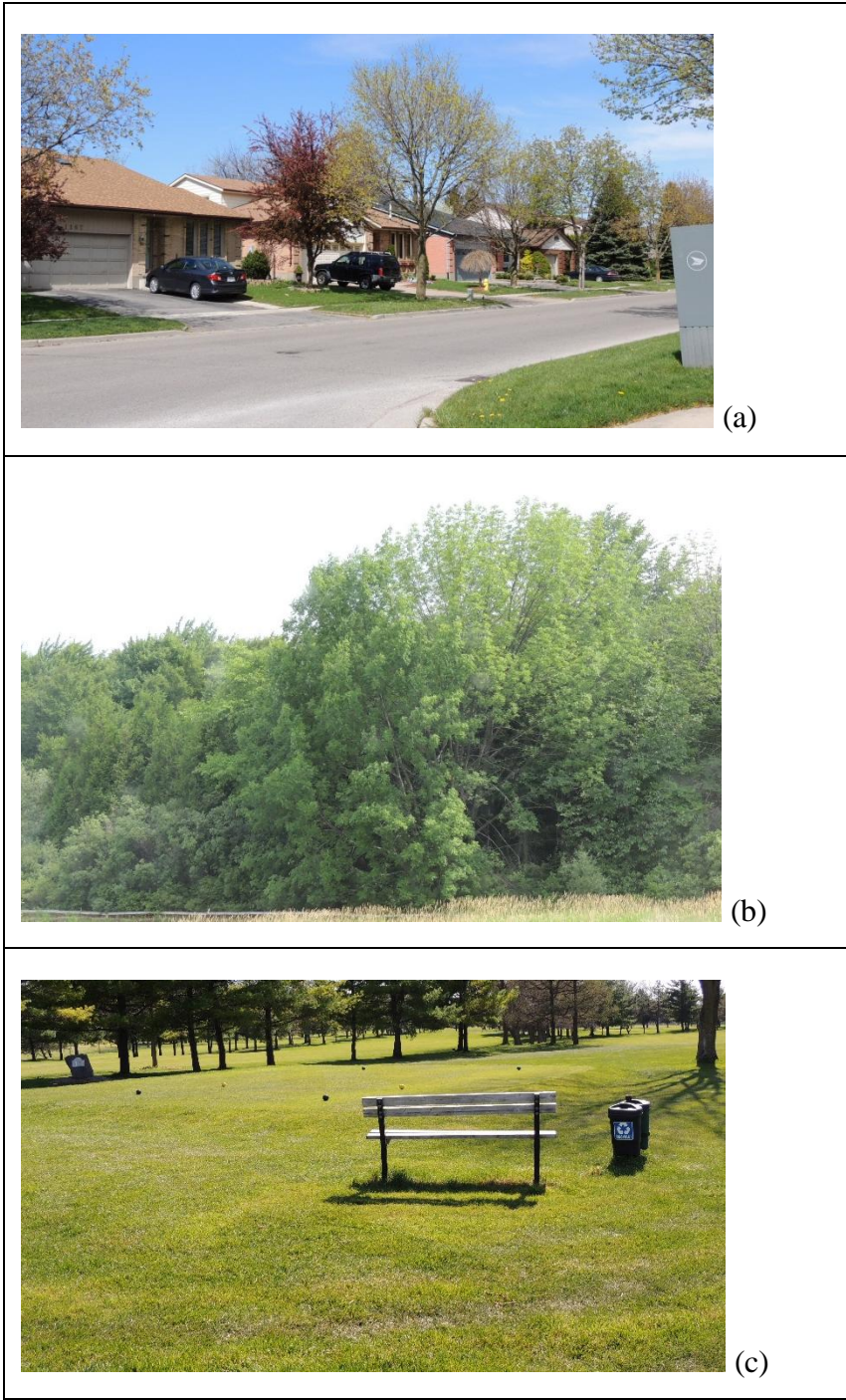


Figure B7 LU/LC classes pictures, (a) residential area, (b) forest, (c) lawn

B 4 Crop Height Measurements

Table B.1 the height measurement results from the field work. **H:** Height (cm), **Wt:** Wheat, **Sb:** Soybeans, **Soil:** bare soil, **NSb:** new soybeans, **Gr:** Grass,

field name		May_4/7	May_28/31	June_21/24	July_16/18	Aug_8/11	Sep_2/5	Sep_25/28
1	Type	Wt	Wt	Wt	Wt Cut	Wt Cut	Wt Cut	Wt Cut
	H	30	75	70		<30		<20
2	Type	Wt	Wt	Wt	Wt Cut	Wt Cut		Wt Cut
	H	30	75	70		<30		<20
3	Type			Sb	Sb	Sb	Sb	Sb
	H			20	39	55	70	65
4	Type		Sb	Sb	Sb	Sb	Sb	Sb
	H			20	37	70	80	65-75
5	Type	Soil	corn	corn	corn	corn	corn	corn
	H		20	76	180	190	230	215
6	Type	Soil	corn	corn	corn	corn	corn	corn
	H		20	80-120	210	200	230	232
7	Type	Soil	Sb	Sb	Sb	Sb	Sb	Sb
	H			25	43	63	70	60
8	Type	Soil	corn	corn	corn	corn	corn	corn
	H		35	80-120	210	215	230	Cut
9	Type			Wt Cut	Gr	Gr	Gr	Gr

	H			<15	35	<15	50	
10	Type	Cut corn		Sb	Sb	Sb	Sb	Sb
	H			20-25	40	65	50	50
11	Type	Wt	Wt	Wt	Wt Cut	NSb	NSb	N Sb
	H	25	70	50-60	<10	<15	33	45
12	Type	Cut corn		Sb	Sb	Sb	Sb& Gr	Sb& Gr
	H			33-40	50	60	70	Cut
13	Type	Wt	Wt	Wt	Wt Cut			
	H	28	53	70				
14	Type		Wt			NSb	NSb	NSb
	H		55				43	55
15	Type		corn	corn	corn	corn	corn	corn
	H		30	100	225	235	250	175
16	Type	Gr	Gr	Gr cut	Gr	Gr	Gr	Gr
	H		60	<15			<15	25
17	Type	Soil	corn	corn	corn	corn	corn	corn
	H		25	100-120	210	230	275	220
18	Type	Wt	Wt	Wt	Wt Cut			
	H	30	70	66				
19	Type	Wt	Wt	Wt	Wt Cut			
	H	30	70	69				
20	Type		Sb	Sb	Sb	Sb	Sb& G	Sb& G

	H			27	57	60	155	100
21	Type			Sb	Sb	Sb	Sb	Sb Cut
	H			26	45	63	60	
22	Type		Sb	Sb	Sb	Sb	Sb	Sb Cut
	H			30	55	65	65	
23	Type	Soil	Sb	Sb				Sb
	H			30	55	65	65	100
24	Type	Wt	Wt	Wt	Wt Cut			
	H	24	73	90				
25	Type	Soil	corn	corn	corn	corn	corn	corn
	H		25	150	200	220	Cut	Cut
26	Type	Soil	corn	corn	corn	corn	corn	corn
	H		25	120-130	200	220	240	Cut
27	Type			Soil	corn	corn	corn	corn
	H				<15	60	160	Cut
28	Type			Sb	Sb	Sb	Sb	Sb
	H			24	53	57	45	Cut
29	Type	Wt	Wt	Wt	Wt Cut			
	H		72	70				
30	Type	Gr	Gr	Gr	Gr	Gr	Gr	Gr
	H		72	<15	15	35	<10	25
31	Type	Wt	Wt	Wt	Wt Cut			

	H	24	60	60				
32	Type	Soil	corn	corn	corn	corn	corn	corn
	H		25	120	190	200	210	210
33	Type	Wt	Wt	Wt	Wt Cut	Wt Cut	Gr	
	H	45	75	77			40	
34	Type	Wt	Wt	Wt	Wt Cut	Wt Cut	Gr	
	H	50	74	74			60	
35	Type	Wt	Wt & Gr	Wt & Gr	Wt Cut	Wt Cut	Gr	
	H	50	90	80			80	
36	Type	Wt	Wt	Wt Cut				
	H	23	50					
37	Type	Wt	Wt	Wt Cut				
	H	33	60					
38	Type	Wt	Wt	Wt	Wt Cut			
	H	31	68	40				
39	Type			Sb	Sb	Sb	Sb	Sb
	H			22	63	75	80	Cut
40	Type	Gr	Gr	Gr	Gr	Gr	Gr	Gr
	H			70	160	160	160	160
41	Type		corn	corn	corn	corn	corn	corn
	H		20	120	210	275	310	300
42	Type		Sb	Sb	Sb	Sb	Sb	Sb

	H			20-22	48	66	67	55
43	Type	peas	peas	peas	NSb	NSb	NSb	NSb
	H	8	45	55	<10	30	63	75
44	Type		corn	corn	corn	corn	corn	corn
	H		20	64				
45	Type	peas	peas	peas	Cut peas		N Pea	Cut Pea
	H	8	35	34			20	
46	Type	peas	peas	peas	Cut peas			
	H	8	35	30				
47	Type			Sb	Sb	Sb	Sb	Sb
	H			20	47	53	50	Cut
48	Type			Sb	Sb	Sb	Sb	Sb
	H			18	47	53	50	Cut
49	Type	Sb		Sb	Sb	Sb	Sb	Sb
	H			30	63	65	63	Cut
50	Type	Sb		Sb	Sb	Sb	Sb	Sb
	H			35	55	60	63	Cut
51	Type			Sb	Sb	Sb	Sb	Sb
	H			25	50	47	Cut	Cut
52	Type			corn	corn	corn	corn	corn
	H			70	190	220	220	230
53	Type			corn	corn	corn	corn	corn

	H			80-100	210	220	250	220
--	---	--	--	--------	-----	-----	-----	-----

C Classification Results

The comparisons of classification results are compared in four aspects, Gaussian V.S. Wishart distribution, four sets of polarimetric parameters, different time combinations, and three different post-processing methods.

C.1 Gaussian MLC and Wishart MLC

Table C.1 Error matrix for Wishart MLC using 528, 715, and 901 images

Reference Data										
class	Hay	wheat	peas	soybeans	corn	built-ups	CS	forest	lawn	UA
Hay	56	0	0	0	0	0	4	7	63	43%
wheat	0	659	0	6	1	0	7	0	0	98%
peas	0	13	61	0	0	11	6	0	1	66%
soybeans	0	0	0	1072	325	1	14	16	3	75%
corn	1	0	0	591	1585	0	9	10	0	72%
built-ups	4	7	0	0	9	1197	8	5	15	96%
CS	0	0	0	0	5	0	106	0	5	91%
forest	0	0	0	0	8	358	1	793	5	68%
lawn	9	0	0	0	1	16	0	0	77	75%
PA	80%	97%	100%	64%	82%	76%	68%	95%	46%	

OA	0.78		KP	0.73						
-----------	------	--	-----------	------	--	--	--	--	--	--

Table C.2 Error matrix for Gaussian MLC using 528, 715, 901 images

Reference Data										
class	Hay	wheat	peas	soybeans	corn	built-ups	CS	forest	lawn	UA
Hay	43	0	0	0	0	0	0	2	7	83%
wheat	4	732	0	0	5	5	23	0	0	95%
peas	0	0	68	0	0	0	0	0	0	100%
soybeans	8	0	0	1553	396	0	17	27	15	77%
corn	0	0	0	219	1636	0	3	0	0	88%
built-ups	0	0	0	0	2	1479	4	7	3	99%
CS	5	0	0	0	1	0	121	0	0	95%
forest	0	2	0	0	11	226	3	855	6	78%
lawn	13	6	0	0	0	40	0	0	178	75%
PA	83%	95%	100%	77%	88%	99%	95%	78%	78%	
OA	0.86		KA	0.83						

C.2 PolSAR Parameters

Table C.7 Error matrix for Gaussian MLC using all T3 elements from 504, 528 , 621,715 images

Reference Data										
class	Hay	wheat	peas	soybeans	corn	built-ups	CS	forest	lawn	UA
Hay	4	23	0	0	0	0	0	0	1	14%
wheat	47	1368	0	0	2	15	7	4	5	94%
peas	1	25	85	0	7	0	0	0	0	72%
soybeans	9	12	2	1328	272	49	4	246	10	69%
corn	19	2	0	180	2013	15	0	4	0	90%
built-ups	0	0	0	10	0	1321	5	22	26	95%
CS	3	0	0	0	0	14	97	0	6	81%
forest	21	9	0	71	4	79	0	949	34	81%
lawn	8	4	0	0	0	45	4	0	256	81%
PA	4%	95%	98%	84%	88%	86%	83%	77%	76%	
OA	0.85		KP	0.81						

504_528_621_715 T3all MLC LU/LC Map

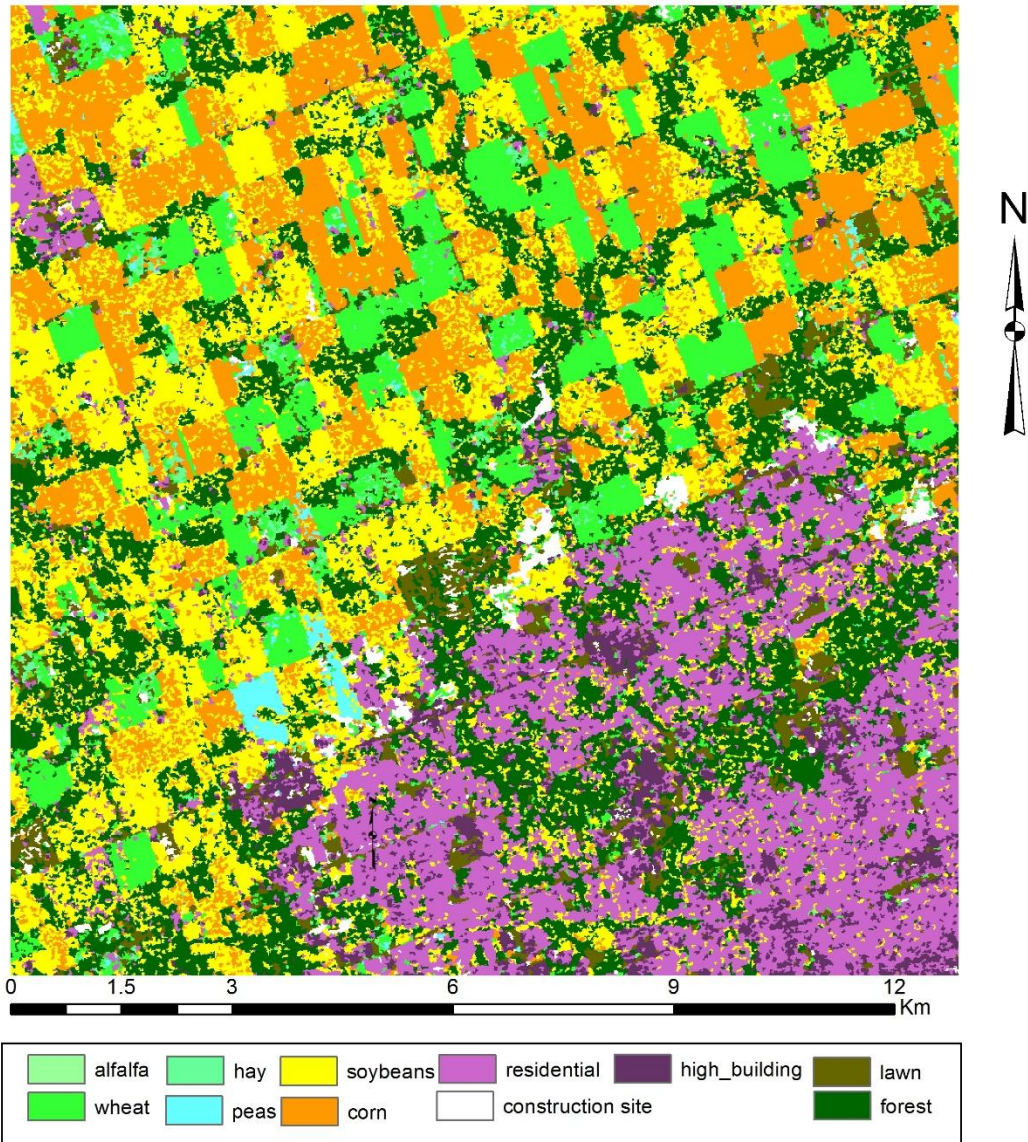


Figure C.1 classification map for Gaussian MLC using all T3 elements from 504, 528, 621,715 images

Table C.4 Error matrix for Gaussian MLC using Pauli3 elements from 504, 528, 621,715 images

Reference Data										
class	Hay	wheat	peas	soybeans	corn	built-ups	CS	forest	lawn	UA
Hay	4	23	0	0	0	0	0	0	1	66%
wheat	47	1368	0	0	2	15	7	4	5	97%
peas	1	25	85	0	7	0	0	0	0	100%
soybeans	9	12	2	1328	272	49	4	246	10	78%
corn	19	2	0	180	2013	15	0	4	0	94%
built-ups	0	0	0	10	0	1321	5	22	26	92%
CS	3	0	0	0	0	14	97	0	6	90%
forest	21	9	0	71	4	79	0	949	34	85%
lawn	8	4	0	0	0	45	4	0	256	80%
PA	19%	99%	100%	94%	85%	88%	70%	92%	74%	
OA	0.89		KP	0.87						

504_528_621_715 Pauli3 MLC LU/LC Map

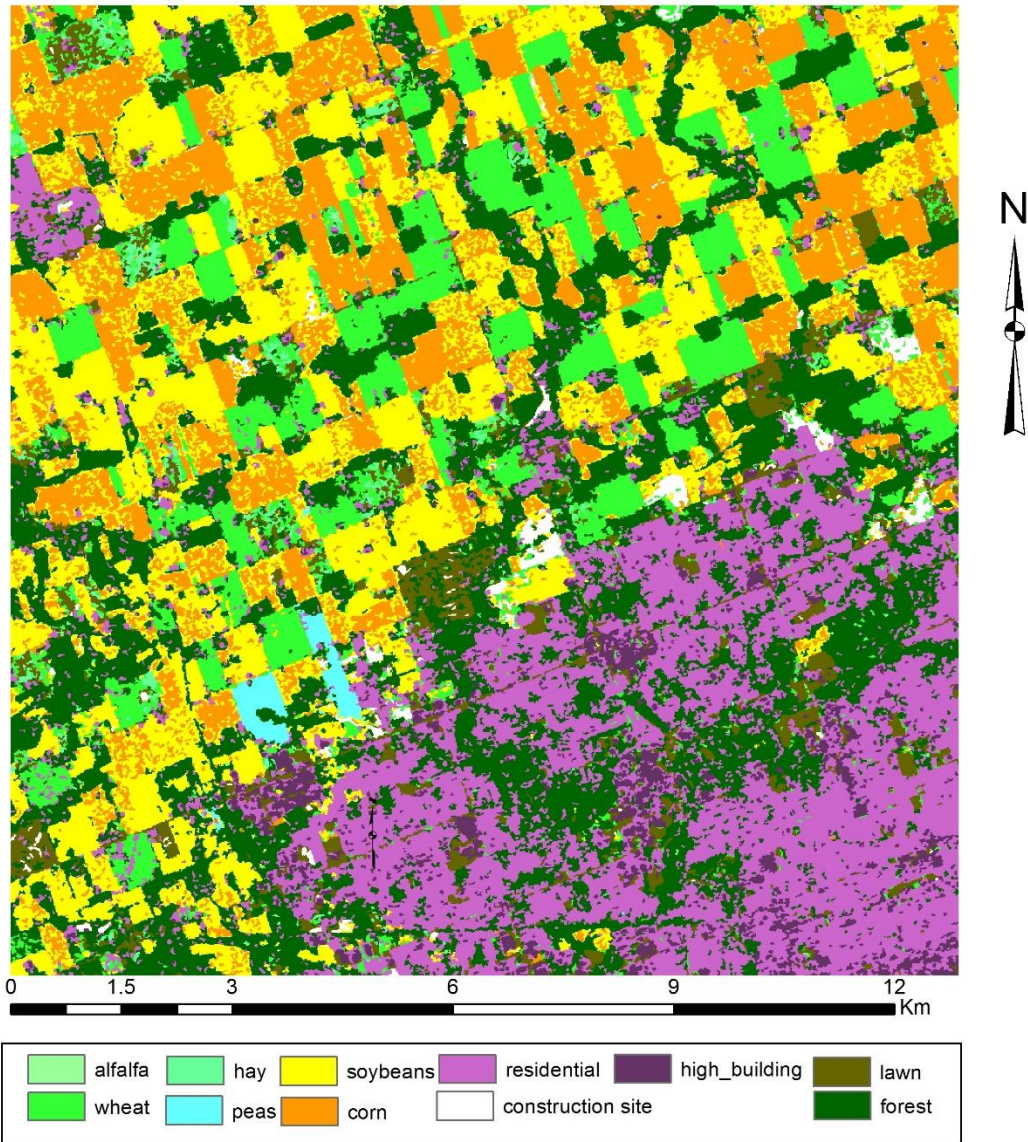
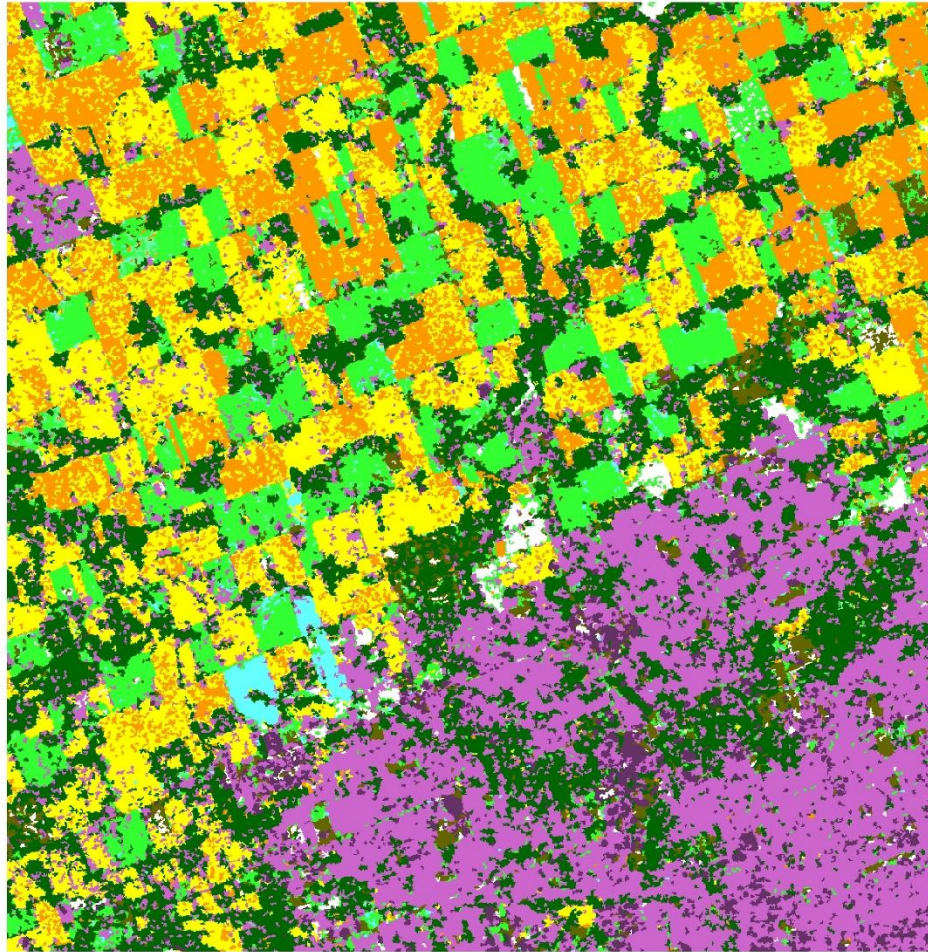


Figure C.2 classification map for Gaussian MLC using Pauli3 elements from 504, 528, 621,715 images

Table C.5 Error matrix for Gaussian MLC using Freeman Durden elements from 528, 621,715 images

Reference Data										
class	Hay	wheat	peas	soybeans	corn	built-ups	CS	forest	lawn	UA
Hay	56	109	0	0	4	12	20	15	9	25%
wheat	20	578	0	2	0	87	45	5	19	76%
peas	0	0	69	0	0	3	0	13	0	81%
soybeans	0	14	0	1511	615	2	1	34	1	69%
corn	0	4	0	333	1507	2	1	2	1	81%
built-ups	0	11	4	1	7	1516	14	132	9	89%
CS	0	0	0	12	6	0	84	0	0	82%
forest	0	18	0	0	4	184	0	737	1	78%
lawn	6	21	0	0	0	46	14	4	173	66%
PA	68%	77%	95%	81%	70%	82%	47%	78%	81%	
OA	0.77		KP	0.71						

528_621_715 Freeman MLC LU/LC Sieve Map



0 1.5 3 6 9 12 Km

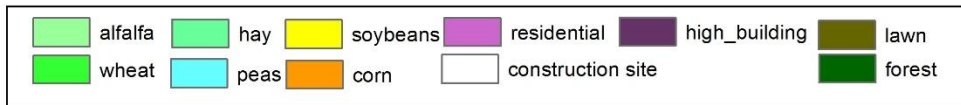
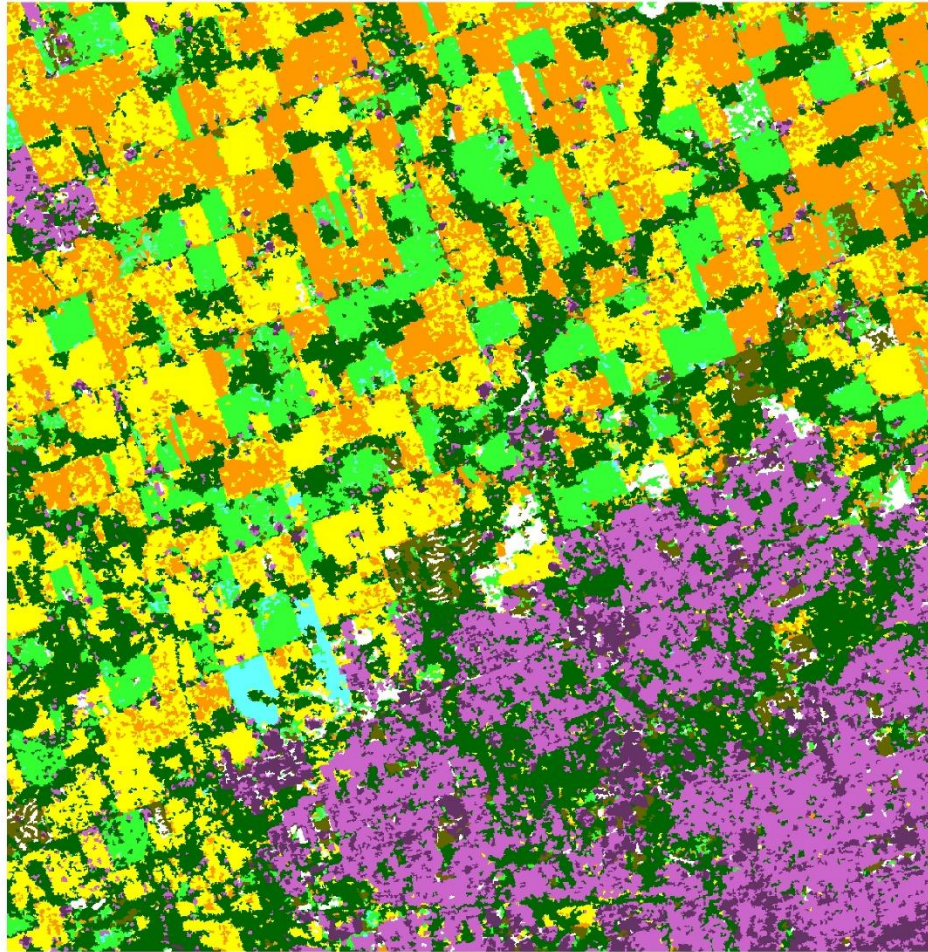


Figure C.3 classification map for Gaussian MLC using Freeman-Durden decomposition parameters from 528, 621,715 images

Table C.6 Error matrix for Gaussian MLC using H/Alpha/A elements from 504, 528, 621,715 images

Reference Data										
class	Hay	wheat	peas	soybeans	corn	built-ups	CS	forest	lawn	UA
Hay	62	2	0	0	0	0	0	3	6	85%
wheat	2	754	0	0	6	17	13	0	0	95%
peas	0	0	72	0	0	0	0	0	0	100%
soybeans	6	0	0	1575	619	0	0	28	14	70%
corn	0	0	0	264	1493	0	0	0	0	85%
built-ups	0	0	0	0	0	1534	4	3	10	99%
CS	5	0	0	1	0	0	154	0	1	96%
forest	0	4	0	3	8	256	9	900	8	76%
lawn	6	0	0	0	0	39	0	0	179	80%
PA	77%	99%	100%	85%	70%	83%	86%	96%	82%	
OA	0.83		KP	0.79						

528_621_715 HAlphaA MLC LU/LC Sieve Map



0 1.5 3 6 9 12 Km

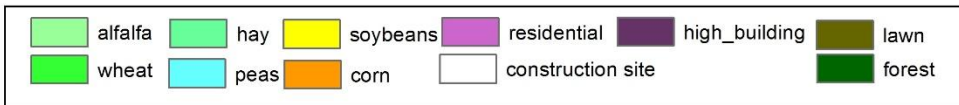


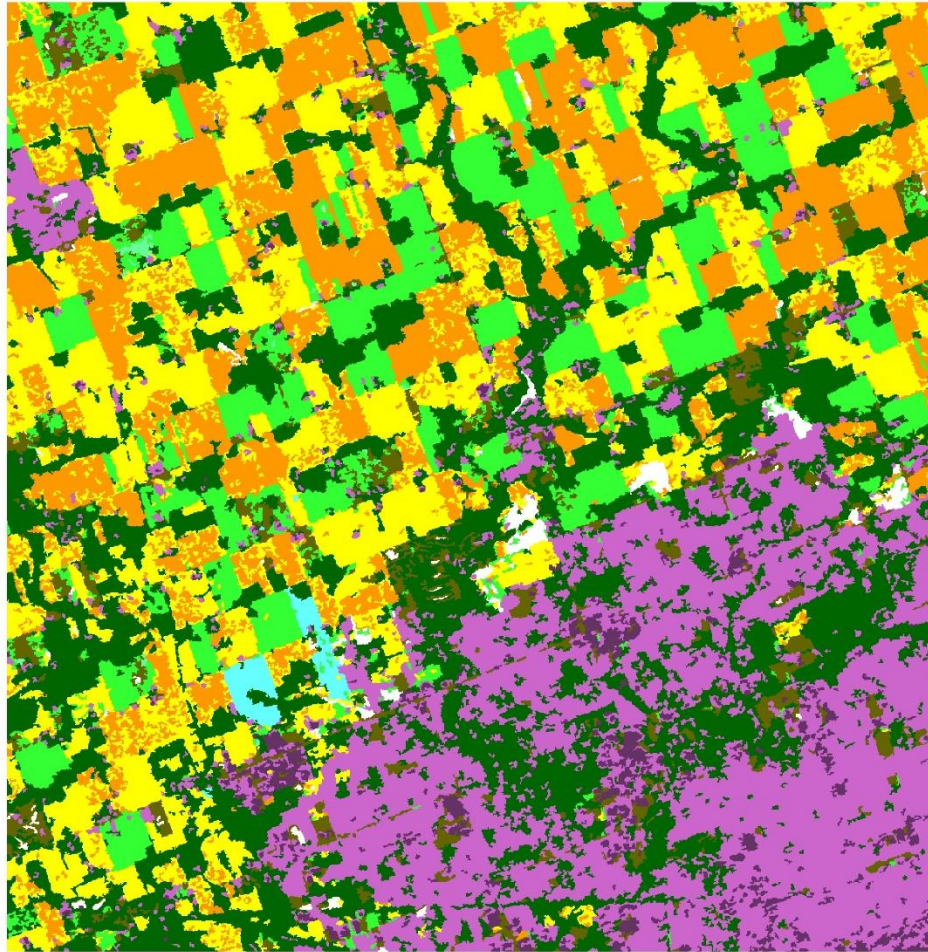
Figure C.4 classification map for Gaussian MLC using H/Alpha/A decomposition parameters from 528, 621,715 images

C.3 Time Combinations

Table C.7 Error matrix for Gaussian MLC Pauli elements from 504, 528, 621,715,901 five- date images

Reference Data										
class	Hay	wheat	peas	soybeans	corn	built-ups	CS	forest	lawn	UA
Hay	31	0	0	0	0	0	0	0	0	100%
wheat	25	740	12	0	4	5	24	0	7	91%
peas	0	0	56	0	0	0	0	0	0	100%
soybeans	4	0	0	1646	211	6	4	24	6	87%
corn	0	0	0	126	1827	0	0	3	2	93%
built-ups	0	0	0	0	4	1577	11	20	9	97%
CS	2	0	0	0	0	0	131	0	0	98%
forest	0	0	0	0	5	138	1	844	5	85%
lawn	11	0	0	0	0	24	0	0	180	84%
PA	42%	100%	82%	93%	89%	90%	77%	95%	86%	
OA	0.91		KP	0.89						

504_528_621_715_901 Pauli3 LU/LC Sieve Map



0 1.5 3 6 9 12 Km

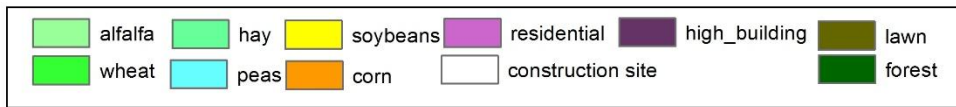


Figure C.5 classification map using Pauli3 from 504, 528, 621,715,901 images

Table C.8 Error matrix for Gaussian MLC Pauli elements from 504, 528, 715,901 four- date images

Reference Data										
class	Hay	wheat	peas	soybeans	corn	built-ups	CS	forest	lawn	UA
Hay	33	0	0	0	0	0	0	0	3	92%
wheat	13	740	13	0	1	1	7	0	0	95%
peas	0	0	55	0	0	0	0	0	0	100%
soybeans	3	0	0	1617	269	0	21	27	9	83%
corn	1	0	0	155	1768	0	13	0	0	91%
built-ups	0	0	0	0	7	1540	8	11	4	98%
CS	2	0	0	0	1	0	121	0	0	98%
forest	0	0	0	0	5	184	1	853	9	81%
lawn	21	0	0	0	0	25	0	0	184	80%
PA	45%	100%	81%	91%	86%	88%	71%	96%	88%	
OA	0.89		KP	0.87						

504_528_715_901 Pauli3 LU/LC Sieve Map



0 1.5 3 6 9 12 Km

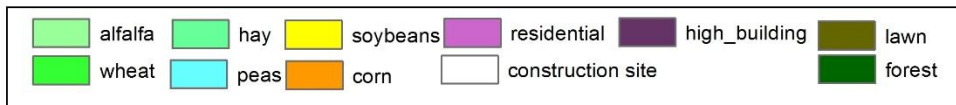
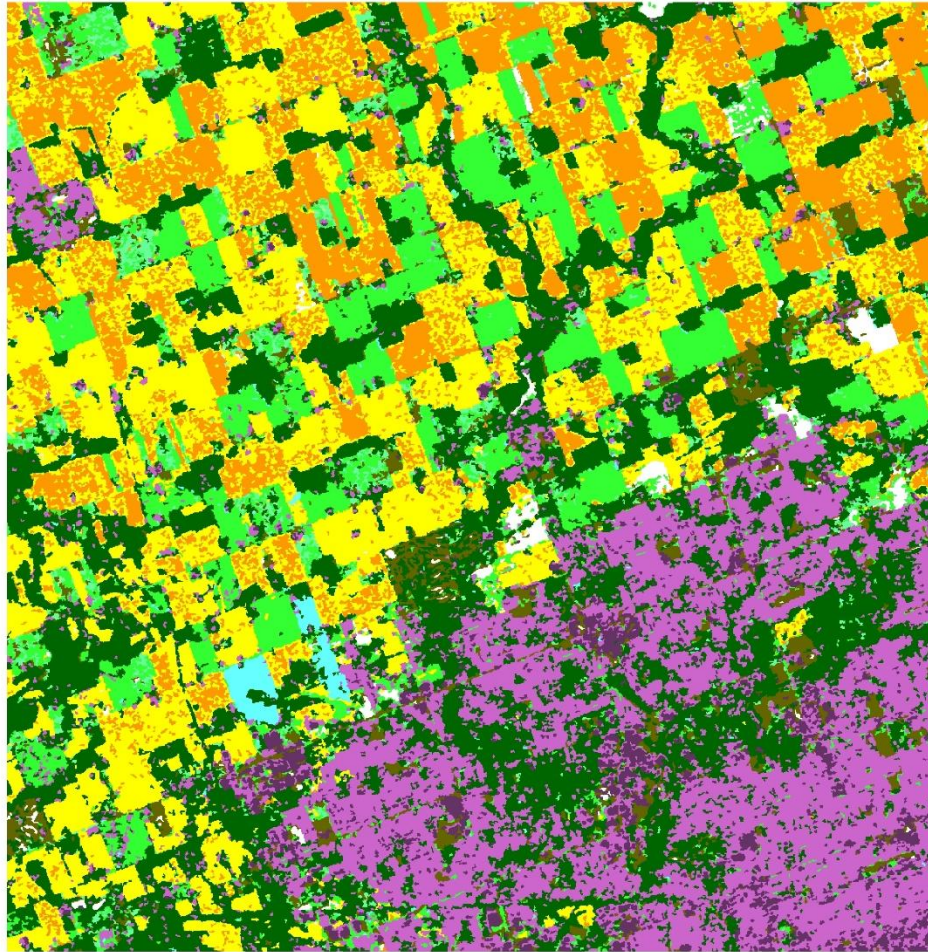


Figure C.6 classification map using Pauli3 from 504, 528, 621,715 images

Table C.9 Error matrix for Gaussian MLC Pauli elements from 528, 715,901 three-date images

Reference Data										
class	Hay	wheat	peas	soybeans	corn	built-ups	CS	forest	lawn	UA
Hay	43	0	0	0	0	0	0	2	7	83%
wheat	4	732	0	0	5	5	23	0	0	95%
peas	0	0	68	0	0	0	0	0	0	100%
soybeans	8	0	0	1553	396	0	17	27	15	77%
corn	0	0	0	219	1636	0	3	0	0	88%
built-ups	0	0	0	0	2	1479	4	7	3	99%
CS	5	0	0	0	1	0	121	0	0	95%
forest	0	2	0	0	11	226	3	855	6	78%
lawn	13	6	0	0	0	40	0	0	178	75%
PA	59%	99%	100%	88%	80%	85%	71%	96%	85%	
OA	0.86		KP	0.83						

528_715_901 Pauli3 LU/LC Sieve Map



0 1.5 3 6 9 12 Km

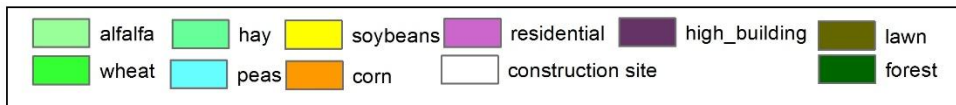


Figure C.7 classification map using Pauli3 from 528, 715,901 images

Table C.10 Error matrix for Gaussian MLC Pauli elements from 528, 715 two-date images

Reference Data										
class	Hay	wheat	peas	soybeans	corn	built-ups	CS	forest	lawn	UA
Hay	58	9	0	0	0	0	0	0	10	75%
wheat	9	706	0	0	0	0	10	0	0	97%
peas	0	9	72	0	0	0	0	0	0	89%
soybeans	0	0	0	1556	711	0	6	21	15	67%
corn	0	0	0	287	1681	0	0	0	0	85%
built-ups	0	0	0	0	0	988	0	0	0	100%
CS	0	0	0	15	3	0	143	0	0	89%
forest	0	6	0	1	0	80	0	677	0	89%
lawn	12	35	0	0	0	11	0	0	136	70%
PA	73%	92%	100%	84%	70%	92%	90%	97%	84%	
OA	0.83		KP	0.78						

528_715 Pauli3 MLC LU/LC Sieve Map

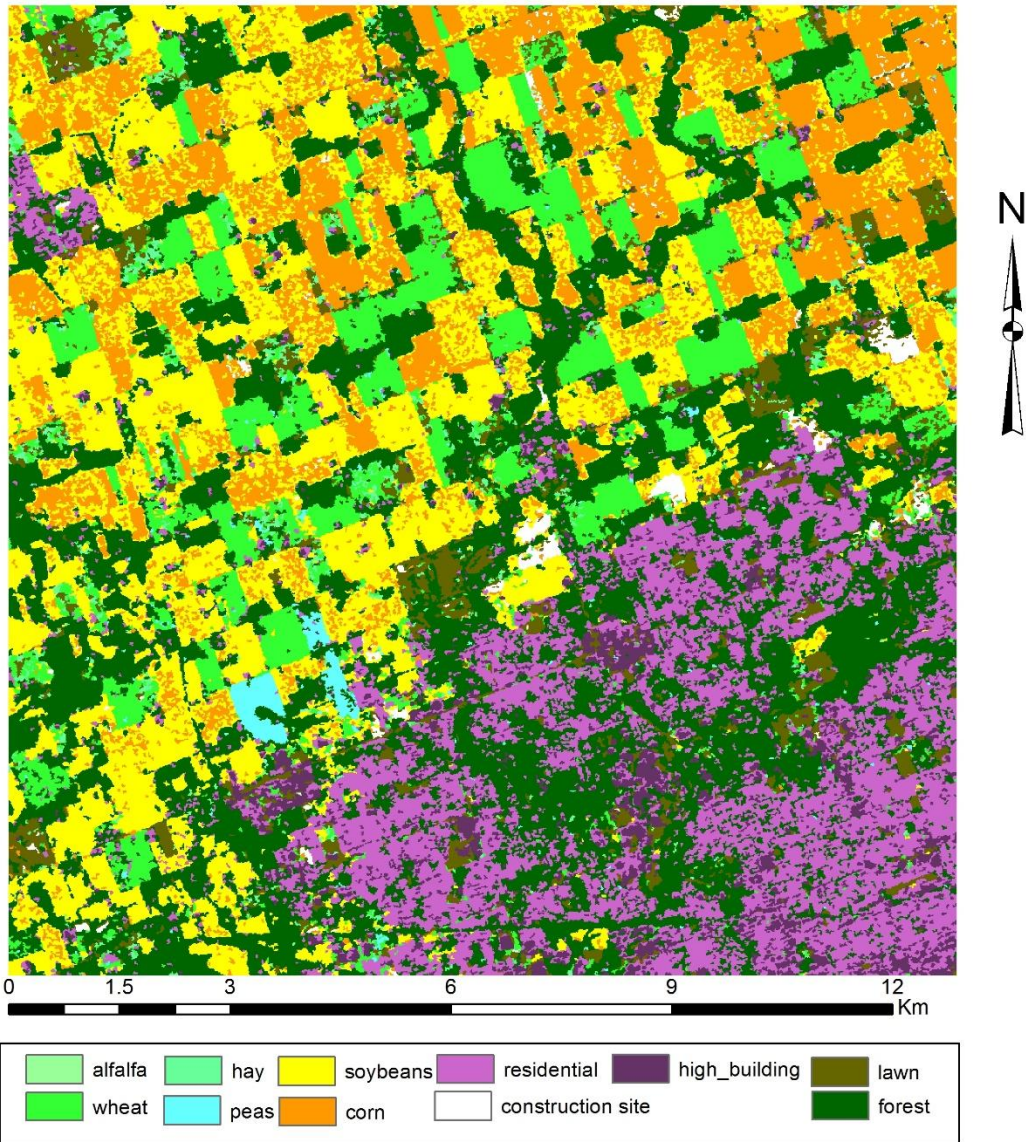


Figure C.8 classification map using Pauli3 from 528, 715 images

Table C.11 Error matrix for Gaussian MLC Pauli elements from 528 one-date image

Reference Data										
class	Hay	wheat	peas	soybeans	corn	built-ups	CS	forest	lawn	UA
Hay	46	14	0	197	126	4	7	2	50	10%
wheat	8	711	0	4	0	79	0	0	6	88%
peas	0	0	57	0	0	57	0	452	0	10%
soybeans	4	0	0	1332	932	0	80	19	1	56%
corn	0	0	0	220	981	0	45	2	0	79%
built-ups	0	0	0	2	0	903	0	29	0	97%
CS	5	0	0	88	350	0	27	0	0	6%
forest	0	0	15	0	0	29	0	194	0	82%
lawn	16	40	0	16	6	7	0	0	104	55%
PA	58%	93%	79%	72%	41%	84%	17%	28%	65%	
OA	0.60		KP	0.51						

528 Pauli3 LU/LC Sieve Map



0 1.5 3 6 9 12 Km

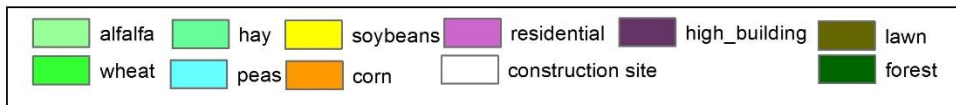


Figure C.9 classification map using Pauli3 from 528, 715 images

C.4 Post-classification Processing

Table C.12 Error matrix for five-date images results without post-classification processing

Reference Data										
class	Hay	wheat	peas	soybeans	corn	built-ups	CS	forest	lawn	UA
Hay	30	2	0	0	0	0	0	0	0	94%
wheat	17	682	11	0	0	11	20	0	6	91%
peas	0	0	50	0	0	0	0	0	0	100%
soybeans	2	0	1	1429	340	0	0	21	3	80%
corn	0	1	0	211	1841	0	0	1	0	90%
built-ups	0	0	0	0	0	868	10	36	0	95%
CS	4	0	0	2	0	2	107	0	0	93%
forest	1	1	0	0	0	54	0	552	4	90%
lawn	7	1	0	0	0	13	0	0	120	85%
PA	49%	99%	81%	87%	84%	92%	78%	90%	90%	
OA	0.88		KP	0.84						

528_621_715 Pauli3 MLC LU/LC primary Map

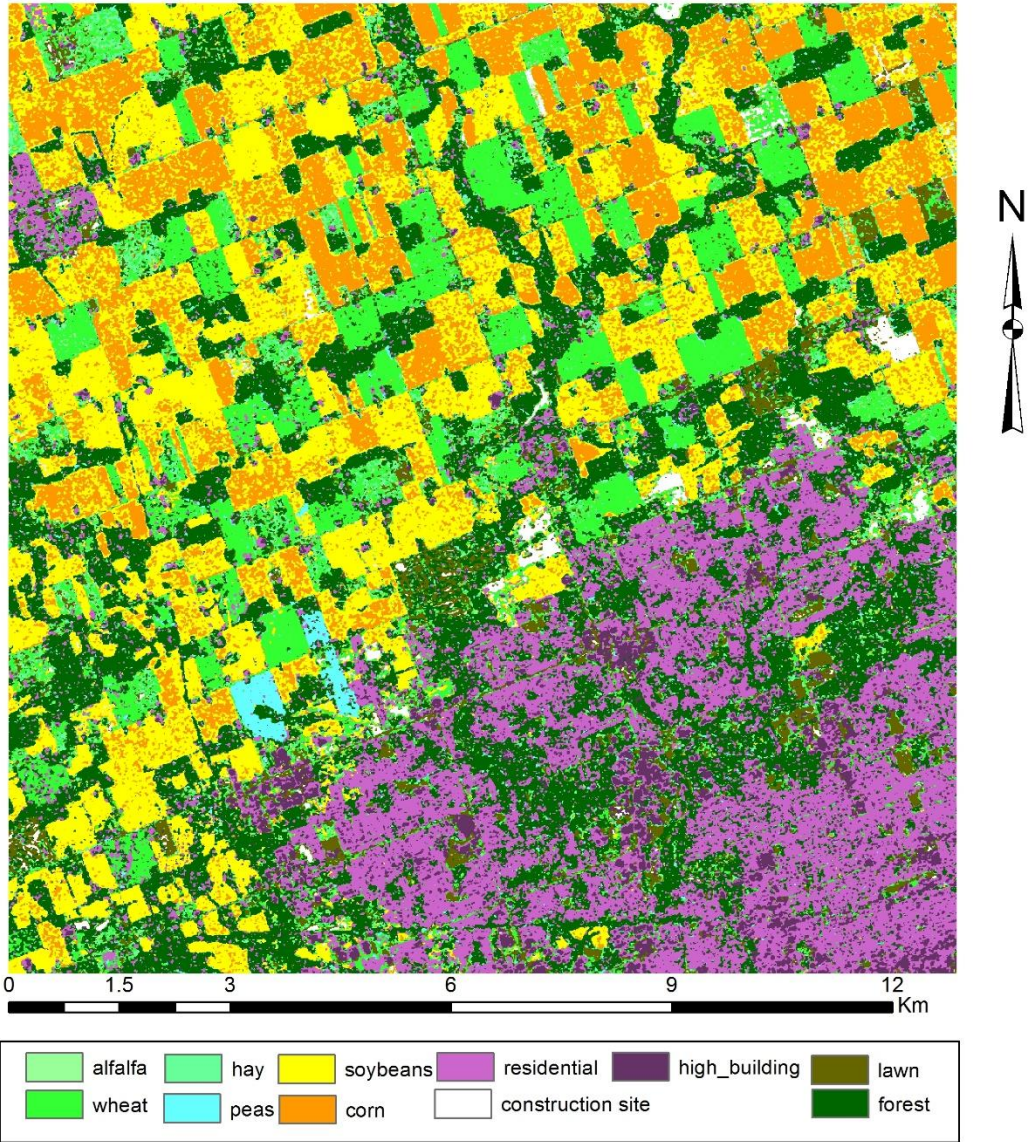


Figure C.10 classification map 528, 621, 715 images without any post-classification processing

Table C.13 Error matrix for five-date images results after sieve filtering

Reference Data										
class	Hay	wheat	peas	soybeans	corn	built-ups	CS	forest	lawn	UA
Hay	31	0	0	0	0	0	0	0	0	100%
wheat	25	740	12	0	4	5	24	0	7	91%
peas	0	0	56	0	0	0	0	0	0	100%
soybeans	4	0	0	1646	211	6	4	24	6	87%
corn	0	0	0	126	1827	0	0	3	2	93%
built-ups	0	0	0	0	4	1577	11	20	9	97%
CS	2	0	0	0	0	0	131	0	0	98%
forest	0	0	0	0	5	138	1	844	5	85%
lawn	11	0	0	0	0	24	0	0	180	84%
PA	42%	100%	82%	93%	89%	90%	77%	95%	86%	
OA	0.91		KP	0.89						

528_621_715 Pauli3 MLC LU/LC Sieve Map

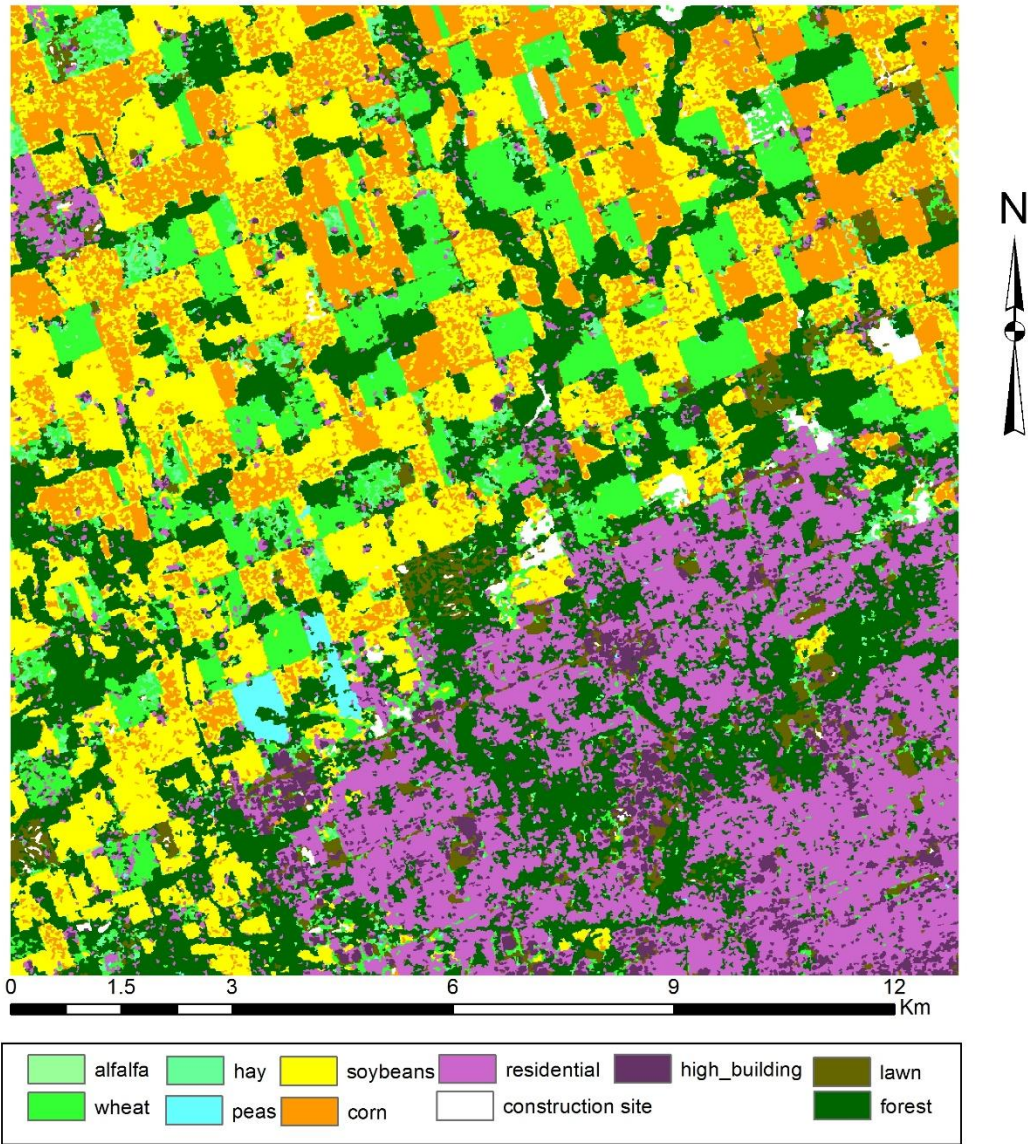


Figure C.11 classification map 528, 621, 715 images after sieving

Table C.14 Error matrix for five-date images results after segmentation

Reference Data										
class	Hay	wheat	peas	soybeans	corn	built-ups	CS	forest	lawn	UA
Hay	4	0	0	0	0	0	0	0	0	100%
wheat	62	760	0	0	3	0	15	0	0	90%
peas	0	0	72	0	0	0	0	0	0	100%
soybeans	0	0	0	1721	137	0	1	26	16	91%
corn	0	0	0	113	1985	0	0	0	0	95%
built-ups	0	0	0	0	0	1670	4	16	4	99%
CS	5	0	0	0	0	0	160	0	0	97%
forest	0	0	0	9	1	160	0	892	12	83%
lawn	10	0	0	0	0	16	0	0	186	88%
PA	5%	100%	100%	93%	93%	90%	89%	96%	85%	
OA	0.92		KP	0.90						

528_621_715 Pauli3 MLC LU/LC Segmentation Map

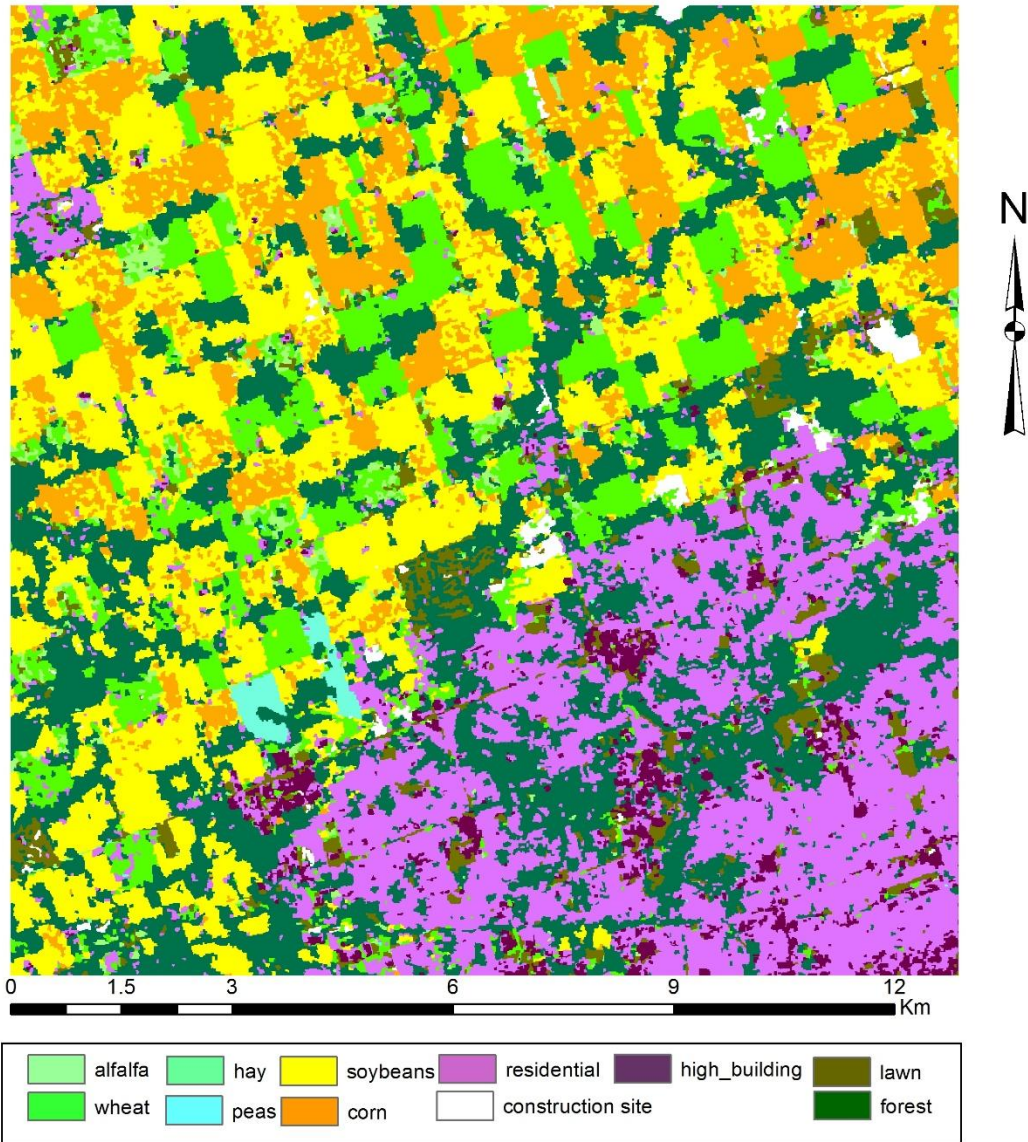


Figure C.12 classification map 528, 621, 715 images after segmentation

Curriculum Vitae

Name: Qin Ma

**Post-secondary
Education and
Degrees:** Nanjing University
Nanjing, Jiangsu, China
2007-2011
B.Sc. Geography

The University of Western Ontario
London, Ontario, Canada
2011-2013 M.Sc. Geography (GIS and Remote Sensing)

**Honors and
Awards:** Western Graduate Research Scholarship,
UWO 2011-2013

**Related Work
Experience** Teaching Assistant, Research Assistant
The University of Western Ontario, Department of Geography
2011-2013